

Vulnerable Connectivity Caused by Local Communities in Spatial Networks

Yingzhou MOU* and Yukio HAYASHI¹

¹Japan Advanced Institute of Science and Technology, Nomi-city,
Ishikawa 923-1292, Japan.

Contributing authors: mouyingzhou@outlook.com;

Abstract

It has been shown that randomly formed communities in topological networks reduce the robustness of connectivity. However, in spatial networks, where community structures are not random but constrained by physical and geographical factors, the effect of these structures on the robustness is unclear. This paper investigates the emergence of local communities in road and communication networks, whose nodes are located by population data of major urban areas in Japan, and connected shortly with low cost. We show that, as the strength of community increases, the spatial networks become more vulnerable to both intentional attacks and random failures. As an application point of view, this result suggests that the densely setting nodes of equipments should be avoided under short links in constructing a spatial network. These findings contribute to understanding the important relation between local communities and the robustness of connectivity against attacks and disasters especially in spatial networks.

Keywords: Robustness of Connectivity, Community, Spatial Networks, Proximity Graphs, Population Distribution

1 Introduction

Many real networks in biological, technological, and social systems have commonly scale-free (SF) topological structure with a high heterogeneous degree distribution.

Unfortunately, this provides extreme vulnerability against intentional attacks [1]. Moreover, community structures (also known as modular) are widely observed in these networks [2] [3]. Since the existing implies relatively dense intra-links in communities than inter-links between communities, the inter-links often serve as critical bridges for communities. Therefore, once these critical bridge links are removed by attacks or disasters, the entire network tends to fragment into multiple disconnected parts [4]. The vulnerability by randomly added communities has been indeed shown in SF networks and Erdős-Rényi random graphs [4][5].

In spatial networks, community structures are not randomly formed but rather constrained by physical and geographical factors. Particularly, in infrastructural networks embedded on the surface of Earth, locations of nodes are geographically constrained. Their distributions are usually mixing of sparse and dense depending on population density. In densely populated areas, road networks tend to have more intersections [6], while wireless communication networks need more base stations to maintain service quality [7]. The existing community structure has been investigated in transportation networks on geographical spaces [8] [9] [10]. Moreover, it has been pointed out that, *in a topological structure affected by geographical constraints on linking, the connectivity is weakened by constructing local stubs with small cycles.* [11]. However, the reason was unclear without considering communities. Since community structures have negative effects on the robustness of connectivity at least topologically [4] [5], we should also elucidate the relation between communities and the robustness of connectivity especially in spatial networks.

On the other hand, road and communication networks tend to have short links because of construction costs and geographical constraints. These spatial constraints are applied for modeling as proximity graphs. For example, relative neighbor graph (RNG) approximates a road network [12] [13], while gabriel graph (GG) approximates

fiber-optic and ad-hoc networks [14] [15]. Building upon these network characteristics, our study investigates the robustness of spatial networks such as transportation or communication systems whose node's distributions are based on population data. We show that, by locating nodes either in densely populated areas for better service accessibility or in sparsely populated areas for low construction costs, they have critical difference in robustness compared to uniformly distributed networks particularly against targeted attacks on nodes between communities.

The remainder of this paper is organized as follows. In Section 2, we introduce the proximity graphs of RNG and GG with short links for constructing spatial networks based on population distribution data that determine the locations of nodes. We consider three node removal strategies (1) recalculated betweenness attacks (RB) [16] by removing high betweenness centrality nodes, (2) initial degree attacks (ID) [17] by removing high degree nodes, and (3) random failure (RF) [1] by removing nodes randomly. We focus on RB since betweenness centrality-based attacks are the most effective for fragmenting the largest connected component (LCC) in networks with communities, while ID and RF are typical node removals for comparing with the above damages. In Section 3, we reveal the relation between community structures and the robustness of connectivity. In particular, we conclude that spatial networks with strong community structures have low robustness against both intentional attacks and random failures.

2 Methods

We introduce the models of road and communication networks by considering four types of node's location with different strengths of communities, whose spatial distribution affects the robustness of connectivity against node removals.

2.1 Models of Spatial Networks

Real networks such as road or communication systems tend to be planar on a geographical space. These networks usually have short links because of low construction costs. Recognizing this, we introduce relative neighborhood graph (RNG) and Gabriel graph (GG) as our fundamental models, which are used to construct spatial networks in our simulation. These models have unique advantages for network analysis, particularly related to real-world population data as mentioned later. Note that RNG is a subgraph of GG and both of them are planar in proximity graphs with short links.

RNG [18] and GG [19] are defined as follows. For a given set of nodes on a geographical space, two nodes are connected if no other node exists within a neighboring area of them. As shown in Figures 1 (a) (b), each shaded area is the intersection of two circles centered at two nodes with a radius equal to the distance between them.

RNG can be used to model road networks, because these links almost coincide with road segments in urban cities [12] [13]. GG has been used for modeling optical or ad-hoc wireless networks, because it resembles the structure of physical networks [19] [14] [15]. In particular, directional antennas are used in wireless networks with better beam power for linking [20]. In Figure 2, blue and orange shades represent strong area of directional beams, while the center circle represents the interference area. If other base station is located in this area with interference, connecting those two points is prohibited.

2.2 Node's Locations and Removal Strategies

Some studies focus on the strong correlation between population densities in cities and node's locations [9] [10]. Areas with higher population densities require more nodes, since they maintain adequate signal coverage, such as in a community network [21] [22] [23]. In road networks, each cross point can be considered as a node, areas with higher population densities tend to have more nodes [6].

Taking into account the correlation between population density and node's locations, we set three types of node's locations: Population (Pop.), Inverse Population (Inv.) and Uniform (Uni). For Pop., the nodes are located according to densely populated points ranking from highest to lowest. In contrast, for Inv., the nodes are located according to sparsely populated points ranking from the lowest to the highest, taking advantage of lower land prices in less populated regions. Here, the location of points are determined by the centers of meshes as mentioned in the next section. For Uni, the nodes are located according to a uniformly at random distribution. In most cities, population density is uneven, there is mixing of sparse and dense node's locations in both Pop. and Inv.. The mixtures also occur in Uni. because of the spatial point process (SPP) theory [24]. Based on the SPP theory, the number of nodes in a given area follows a Poisson distribution, therefore there are mixtures of sparse and dense node's locations. These mixtures give community structures as shown later. By connecting nodes on the locations of Pop., Inv., and Uni., spatial networks are constructed according to the previously described constraints of short links in RNG and GG shown in Figure 1. Moreover, to investigate how node's locations influence the robustness of connectivity in these networks, we consider the fourth type of node's locations on a 2D square lattice (2DL) [25], where nodes are set on the 2DL as completely uniform without mixtures of dense and sparse node's locations. According to the degree distributions $P(k)$ obtained from Pop., Inv., and Uni. networks (whose distributions show slight differences as discussed later), we randomly assign the corresponding number of links to each node on the 2DL. We assume that the other end of a link is free (unconnected) to perform the following two steps of trials for linking. The first trial is established by connecting free-ends between neighbor nodes on the lattice. When free-ends are remaining but its neighbor nodes have no available free-ends, the second trial is performed for connecting more distant nodes with free-ends available.

On the other hand, to investigate the robustness of connectivity in these networks against node removals, we consider three typical strategies: recalculated betweenness (RB) attacks [16], initial degree (ID) [17] attacks, and random failures (RF) [1]. In these strategies, nodes (and links connected to them) are removed one by one until q/N nodes are removed, where q and N denote the fraction of removed nodes and network size, respectively. Removed nodes are selected in decreasing order of degrees for ID attacks or betweenness centrality for RB attacks. Note that RB attacks recalculate betweenness centrality, while ID attacks select nodes according to the initial degree. Besides, RF is considered to investigate the difference between intentional attacks and random failures. We emphasize that RB has a strong affect on global fragmentation in networks with communities.

3 Results

This section shows the numerical results for the robustness in spatial networks by our simulation. In subsection 3.1, we show the emergence of spatial communities in RNG and GG as modeling road and communication networks whose nodes are located by Pop., Inv., and Uni.. In subsection 3.2, we investigate the robustness of connectivity against node removals. We confirm that community structures based on the spatial node's locations affect on the robustness against both intentional attacks and random failures.

3.1 Emergence of Spatial Communities

Our study uses statistical population data in seven major Japanese areas to set node's locations in spatial networks. These areas are Fukuoka, Hiroshima, Kyoto-Osaka (referred to as Keihan), Nagoya, Tokyo, Sendai, and Sapporo [26]. Each of them is divided into $500m \times 500m$ block meshes with totaling $(8 \times 10 \times 2 \times 3)^2 = 230,400$ blocks, while nodes are located at the centers of meshes. We select N nodes whose

locations are based on Pop., Inv. and Uni., respectively, as mentioned in subsection 2.2 previously. To ensure that \sqrt{N} is an integer when constructing a 2DL for later comparison, we set $N = 100, 484, 1024, 5041$ and 10000 . Links between nodes are created by connection rules of RNG and GG as shown in Figure 1. Local communities emerge in such spatial networks.

To measure the strength of community structure, we introduce modularity Q [27] defined as:

$$Q = \frac{1}{2M} \sum_{ij} \left[A_{ij} - \frac{k_i k_j}{2M} \right] \delta(c_i, c_j),$$

where A_{ij} denotes the i, j element of adjacency matrix: $A_{ij} = 1$ if there is a link between nodes i and j , 0 otherwise. k_i and k_j are the degrees of them, respectively. M is the total number of links, c_i represents the community identifier to which node i belongs, $\delta(c_i, c_j)$ is an indicator function equal to 1 if nodes i and j belong to a same community, and 0 otherwise. We estimate c_i by using Louvain method [28]. A higher value of Q indicates a stronger community structure, where there are many intra-links but a few inter-links.

We explain the typical results of communities for Tokyo $N = 1024$ node networks as an example. For other sizes N and cities, the results are shown in Appendix from Figures A1 to A68. Figures 3 and 4 show the communities for node's location based on Pop. and Inv. with short links created by RNG and GG. Since RNG is a subgraph of GG, the numbers of links in Figures 3 and 4 (a) are less than them in Figures 3 and 4 (b). Thus, the results of communities in RNG and GG networks are different. Moreover, Figures 5 and 6 show the examples of communities for node's location based on Pop. and Inv. after 10% nodes (and links connected to them) removals against RB attacks. The removal of nodes causes the network to break into disconnected components, particularly at the boundaries between different communities. This fragmentation is the most noticeable in densely populated areas. Table 1 shows both Pop.

and Inv. have slightly higher Q values compared to Uni. as shown in Appendix from Table A15 to A18 for several sizes N and seven Japanese areas, these results suggest that Pop. and Inv. networks have slightly stronger community structures than that of Uni.. The differences of node's locations in Pop., Inv., and Uni. affect the strength of communities in networks. Although Uni. has a slightly lower Q value than that of Pop. and Inv., it still maintains community structure obviously. Remember that from the SPP theory in subsection 2.2, there is a mixture of sparse and dense node's locations, and contributes to the emergence of community structures even in Uni. networks.

3.2 Robustness of Connectivity Against Recalculated Betweenness attacks

Robustness of connectivity plays a crucial role in complex networks for quantifying a network's ability to maintain the functionality when subjected to intentional attacks or random failures, such as RB, ID and RF mentioned in subsection 2.2. As the measures, we use the robustness index R [29] and the critical fraction q_c [30]. Here, the robustness index R is the area under the curve of the LCC's relative size $S^{1st}(q)/N$ against the fraction q of removed nodes. A higher R value indicates greater overall robustness of connectivity. The critical fraction q_c is the value of q at which the relative size $S^{2nd}(q)/N$ of the second LCC reaches its peak. It captures the critical point of structural change in a network. A higher q_c value suggests that the network can withstand more removals of nodes before substantial fragmentation. However, R is a more precise measure because different R values are possible for stupid and gradual curves of $S^{1st}(q)/N$ even with a same q_c . The combination of these two measures provides us with ways to observe not only how well a network maintains its connectivity against attacks but also when it reaches its breaking point.

Taking Tokyo 1024 nodes' networks as an example, Figure 7 shows one of the important results for the robustness of connectivity against RB attacks as follows:

Firstly, comparing RNG (Figures 7ac) and GG (Figures 7bd), we confirm that all curves in GG exhibit a rightward shift compared to their corresponding curves for RNG with same colors and line types. This rightward shift indicates higher robustness for GG as shown by both larger areas under the $S^{1st}(q)/N$ curves (higher R values) and delayed peaks in $S^{2nd}(q)/N$ curves (higher q_c values). Remember that RNG has fewer links than GG as the subgraph. By comparing Figures 7ac, and Figures 7bd, we can observe a well-known relation between $S^{1st}(q)/N$ and $S^{2nd}(q)/N$ curves: When $S^{2nd}(q)/N$ reaches its peak at q_c , the corresponding $S^{1st}(q)/N$ curve is rapidly decreased.

Secondly, to investigate the effect of community structures on the robustness, we compare green, red, and blue (RGB) solid lines for the original networks with RGB dashed lines for the randomized networks under the same degree distributions $P(k)$ in Figure 8 for each of Pop., Inv., and Uni. in each of Figure 7abcd. Green and red dashed lines (randomized Inv.) show a significant rightward shift compared to the corresponding solid lines (the original Pop., Inv.), indicating that the weakest community structure enhances the robustness. Similarly, blue dashed lines (randomized Uni.) show the improvement of robustness to its solid counterparts. In each of Figure 7abcd for the original networks (RGB solid lines), both green (Pop.) and red (Inv.) solid lines exhibit leftward shifts compared to blue lines (Uni.). It indicates that Uni. networks have higher robustness. These comparisons consistently show that stronger community structures (higher modularity) lead to lower robustness, also as evidenced by increasing modularity Q values (Tables 1 and 2). In other words, the limited number of inter-links create potential vulnerabilities during attacks. However, this relation becomes slightly complex in randomized networks with some exceptions: For RNG (Figure 7a), the green dashed lines (randomized Pop.) exhibit higher robustness than the blue dashed lines (randomized Uni.), while the red dashed lines (randomized Inv.) show lower robustness. For GG (Figure 7b), both green and red dashed lines have lower

robustness than the blue dashed lines. With the exception of randomized RNG networks, most cases suggest that a uniform distribution of nodes contributes to improved the robustness.

Thirdly, we investigate the spatial effect in networks constructed on 2D lattice with completely homogeneous node's locations to compare the original RNG or GG of Pop., Inv., and Uni. under each of the same $P(k)$. Remember that even the cases of Uni. have mixtures of dense and sparse node's locations in a Poisson distribution from SPP theory [24]. Cyan-Yellow-Magenta (CYM) solid lines in each of Figure 7abcd show how node's locations affect the robustness. In these networks, although nodes are located in completely identical positions on the lattice, the degree distributions $P(k)$ is set to each of them obtained from the original RNG or GG of Pop., Inv., and Uni. respectively. We observe that the cyan solid lines (2DL-Uni.) show higher robustness than the blue solid lines (the original Uni.), as evidenced by both larger area under the $S^{1st}(q)/N$ curves (higher R value) and delayed peak in $S^{2nd}(q)/N$ curve (higher q_c value). Similar improvements of robustness are also observed when comparing the yellow solid lines (2DL-Pop.) with the green solid lines (the original Pop.), and the magenta solid lines (2DL-Inv.) with the red solid lines (the original Inv.). It is important to note that community structures exist in all these networks. As shown in Tables 1, 2 and 3, the original networks with Pop., Inv., and Uni. node's locations show the strongest community structures, while 2DL networks show weaker community which affects for all cases. When comparing across these networks, we observe a clear hierarchy in robustness: In order to investigate the pure effect of $P(k)$ on the robustness, under the same $P(k)$ to each of Pop., Inv., and Uni., randomized networks (RGB dashed lines) without communities show the highest robustness, followed by 2DL networks (CYM solid lines), while the original networks (RGB solid lines) with communities have the lowest robustness. For instance, the blue dashed lines (randomized Uni.) show to be higher robust than the cyan solid lines (2DL-Uni.), which show to be even more

robust than the blue solid lines (the original Uni.). Similar results can be observed in the comparisons between solid-green and dashed-yellow lines (Pop.), and between solid-red and dashed-magenta lines (Inv.). These comparisons indicate that weaker community structure arising from spatial node’s locations improve the robustness. Moreover, uniform node distribution enhances the robustness (as shown by 2DL curves’ rightward shifts compared to that in the original networks), the weakest community structure through randomization has the highest robustness against RB attacks.

Figures 9 and 10 show the important relation between modularity Q and the robustness measures R and q_c . As Q increases, both R and q_c decrease. Figure 11 confirms that these relation exist not only in Tokyo 1024-node networks but also in the networks for other Japanese areas. Figures A171, A172, A173, A174 in Appendix provide additional evidences of similar relations in the networks with several sizes N for all seven major Japanese areas. These relations can be explained by the nature of community structure in networks. In other words, as higher Q values indicate stronger community structures, the robustness becomes more vulnerable in the spatial network because of the limited number of inter-links (especially against RB attacks whose targets are the end-nodes of such bridges between communities).

3.3 Robustness of Connectivity Against Initial Degree attacks and Random Failures

On the other hand, we further investigate the robustness of connectivity against typical Initial Degree (ID) attacks and Random Failures (RF). For Uni. networks, we confirm that q_c values are almost identical to the analytical values [31] as shown in Tables 5 and 7. Tables 4 and 5 present the robustness index R and critical fraction q_c against ID attacks, respectively. Similarly, Tables 6 and 7 show the corresponding R and q_c values against RF. Note that a clear hierarchy exists as following the relation

$R^{RB} < R^{ID} < R^{RF}$ and $q_c^{RB} < q_c^{ID} < q_c^{RF}$ (see Table A5, A6 in Appendix for detailed comparison) in network robustness across different attack strategies.

In both ID attacks and RF, networks whose nodes are located according to Pop. and Inv. generally show lower R and q_c values than those to Uni. networks as similar to the results against RB attacks. However, several exceptions exist. As values with upper-triangles (\triangle) in Tables 4, 5, 6, and 7, some networks based on Pop. and Inv. have higher robustness than those on Uni.. The reason may be caused by two factors: (1) Higher average degree $\langle k \rangle$ in RNG Pop. networks as shown in Table 8, which may provide additional alternative paths after node removals; (2) The presence of regular grid-like parts in certain regions of Pop. networks contributes to enhance the robustness against RF as shown in Figure 12. The effect of grid-like parts is explained as follows. In our study, all nodes are located limitedly in the centers of mesh blocks (500m \times 500m), rather than having arbitrary positions in a geographical space. This constraint on node's locations leads to a particular network characteristic. When nodes are densely distributed in neighboring mesh blocks, as often occurs in Pop. networks, they tend to form grid-like parts. We quantify these grid-like parts by calculating the proportion of nodes that have degree 4 with four neighbors of degree 4, which represents a typical local grid formation. As shown in Table 9, Pop. networks show notably higher proportions of such grid-like parts (ranging from 2.05% to 15.14% in RNG and 2.25% to 15.33% in GG) compared to Inv. networks (mostly 0% in RNG and below 1.17% in GG) and Uni. networks (0% in RNG and 0.79% in GG) as values with upper-triangles (\triangle). According to percolation theory [32], a 2D square lattice network maintains its connectivity until the fraction 0.4073 (percolation threshold $p_c = 0.5927$) of randomly removed nodes. This critical fraction 0.4073 is larger than the analytical values 0.205 in RNG and 0.365 in GG shown in Table 7. The presence of these grid-like parts increases the critical fraction than the above values in RNG and GG on free node's locations at random.

4 Summary

Our study investigates the relations between community structure and the robustness of connectivity in spatial networks whose node's locations are according to the order of real population (Pop.), inverse population (Inv.), and uniformly at random (Uni.), while the links between nodes are short by using proximity graphs of RNG and GG as modeling road and communication systems, respectively. Remember that Pop., Inv., and Uni. are considered to investigate the effect of difference in spatial node densities on the robustness. We show that, for the measures of robustness index R and critical fraction q_c , Pop. and Inv. have lower robustness than that of Uni. against intentional attacks and random failures in both RNG and GG, because Pop. and Inv. have stronger community structure than Uni.. We summarize that networks with more evenly distributed node's locations have higher robustness, as shown in Figure 7. In particular, both R and q_c decrease with increasing modularity Q , as shown in Figures 9, 10 and 11. Therefore, we conclude that the emergence of local communities in spatial networks such as road and communication systems is caused by two factors (1) the mixture of sparse and dense of node's locations, and (2) the short link between nodes.

List of Abbreviations

RGB Red-Green-Blue (color scheme)

CYM Cyan-Yellow-Magenta (color scheme)

GG Gabriel Graph

RNG Relative Neighborhood Graph

2DL Two-Dimensional Square Lattice

Pop. Population

Inv. Inverse Population

Uni. Uniform

RB Recalculated Betweenness (attack strategy)

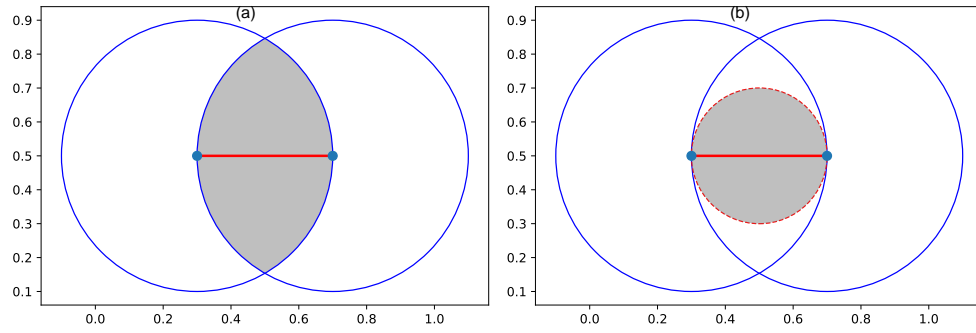


Fig. 1 Illustration of connection constraints for (a) RNG and (b) GG. A link colored by red is established between two nodes colored by blue, when no other node exists within the shaded area.

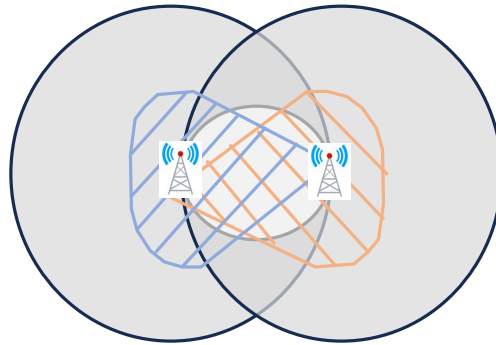


Fig. 2 Coverage diagram of radio waves between two base stations in wireless communication. The ranges of strong beams are shown by blue and orange shades. The center circle represents the signal interference area. If other base stations exist within it, the two stations cannot be connected.

ID Initial Degree (attack strategy)

RF Random Failures

SF Scale-Free

SPP Spatial Point Process

LCC Largest Connected Component

References

- [1] Albert, R., Jeong, H., Barabási, A.-L.: Error and attack tolerance of complex networks. *Nature* **406**(6794), 378–382 (2000) <https://doi.org/10.1038/35019019>

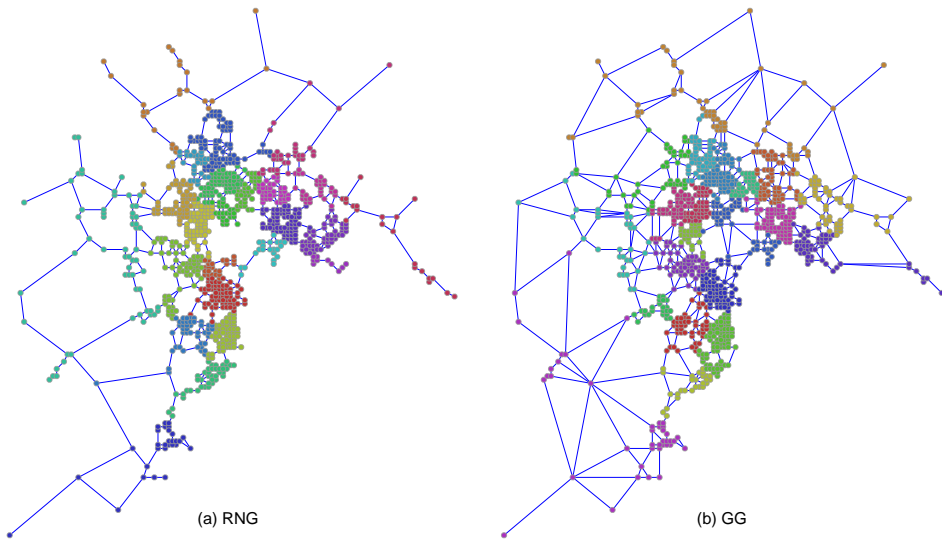


Fig. 3 Visualization of community structures in Tokyo before node removal. $N = 1024$ nodes are located by the decreasing order of population (Pop.). Different colors represent different communities estimated by Louvain algorithm. There are clear community formations particularly in densely populated areas.

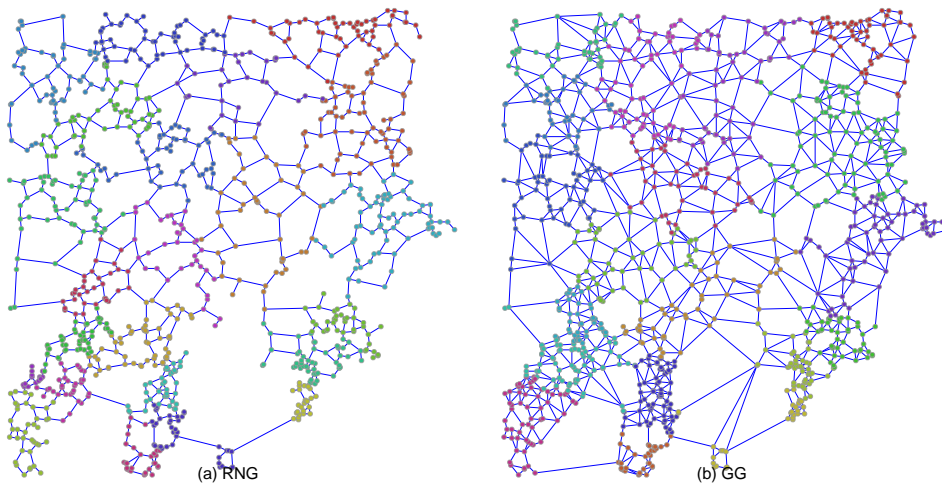


Fig. 4 Visualization of community structures in Tokyo before node removal. $N = 1024$ nodes are located by the inverse order of population (Inv.). Different colors represent different communities estimated by Louvain algorithm. There are different community formations compared to Figure 3.

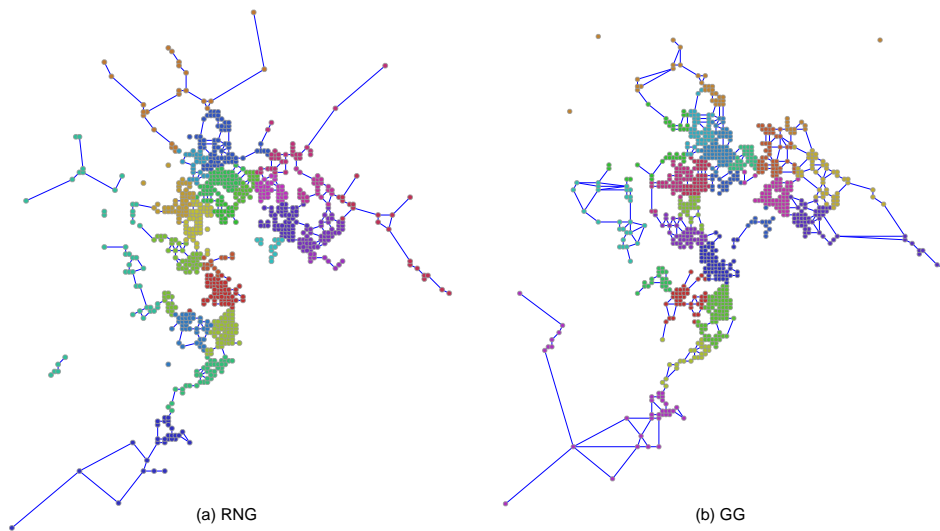


Fig. 5 Tokyo networks with $N = 1024$ nodes after 10% node removals by recalculated betweenness (RB) attacks. The locations of nodes are selected by decreasing order of population (Pop.). The fragmentation is observed by removing links between communities especially in densely populated areas

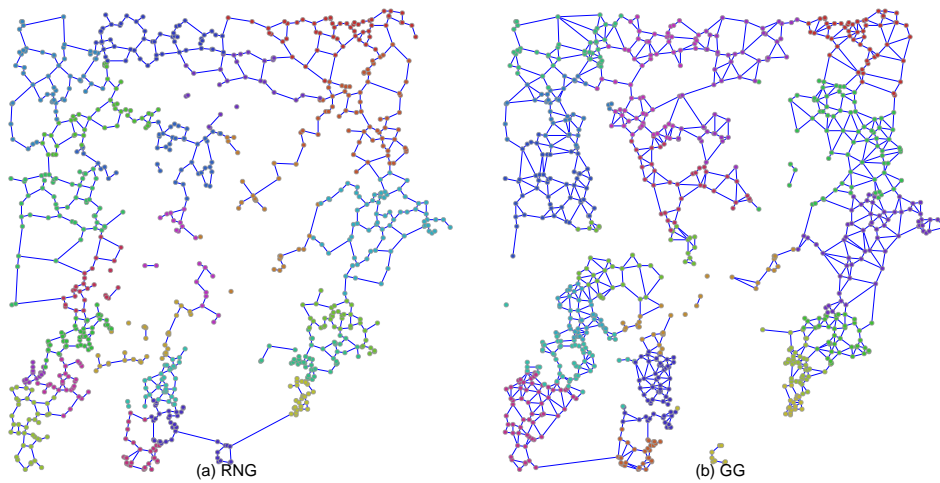


Fig. 6 Tokyo networks with $N = 1024$ nodes after 10% node removals by recalculated betweenness (RB) attacks. The locations of nodes are selected by inverse order of population (Inv.). The fragmentation is observed by removing links between communities which are different as compared to Figure 5.

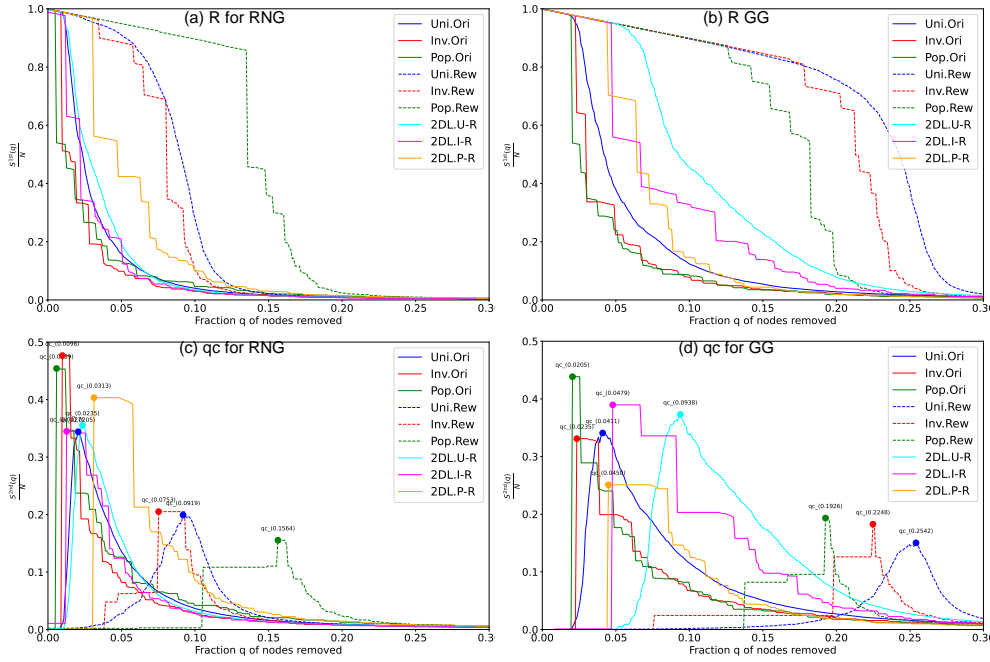


Fig. 7 Robustness against recalculated betweenness (RB) attacks for Tokyo networks with $N = 1024$ nodes. For both Rew (Randomized networks) and 2DL lines, the rewiring process preserves the original degree distributions. Two measures are applied: (a) (b) the relative size $S^{1st}(q)/N$ of largest connected component, and (c) (d) the critical fraction q_c at the peak of the relative size $S^{2nd}(q)/N$ of second largest component.

- [2] Newman, M.E.: Modularity and community structure in networks. Proceedings of the National Academy of Sciences in USA **103**(23), 8577–8582 (2006) <https://doi.org/10.1073/pnas.0601602103>
- [3] Girvan, M., Newman, M.E.: Community structure in social and biological networks. Proceedings of the National Academy of Sciences in USA **99**(12), 7821–7826 (2002) <https://doi.org/10.1073/pnas.122653799>
- [4] Shai, S., Kenett, D.Y., Kenett, Y.N., Faust, M., Dobson, S., Havlin, S.: Critical tipping point distinguishing two types of transitions in modular network structures. Physical Review E **92**(6), 062805 (2015) <https://doi.org/10.1103/PhysRevE.92.062805>

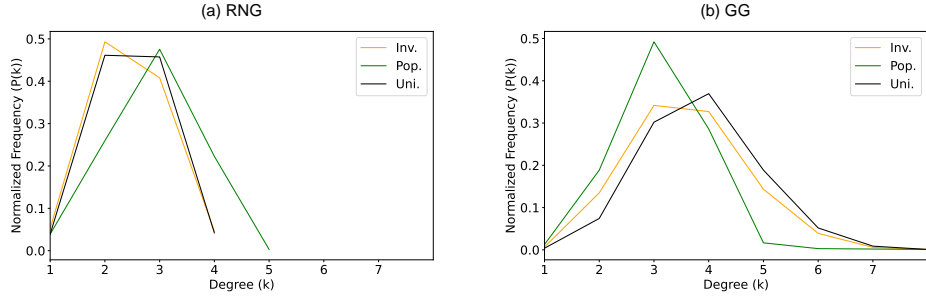


Fig. 8 Similar degree distributions of bell-shapes for Pop., Inv., and Uni. in Tokyo networks with $N = 1024$ nodes.

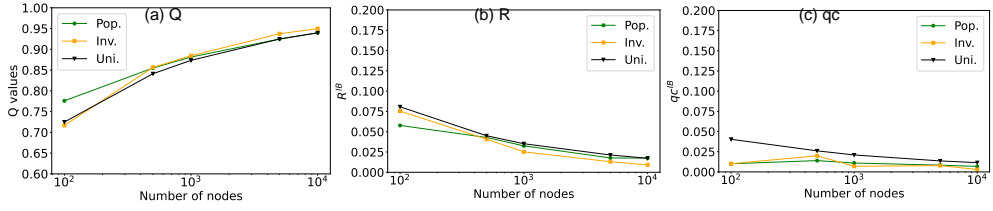


Fig. 9 Increasing modularity Q vs. decreasing robustness index R^{RB} or critical fraction q_c^{RB} for varying the size N in Tokyo RNG networks.

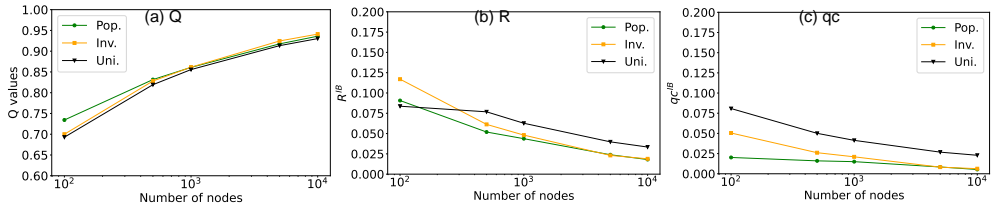


Fig. 10 Increasing modularity Q vs. decreasing robustness index R^{RB} or critical fraction q_c^{RB} for varying the size N in Tokyo GG networks.

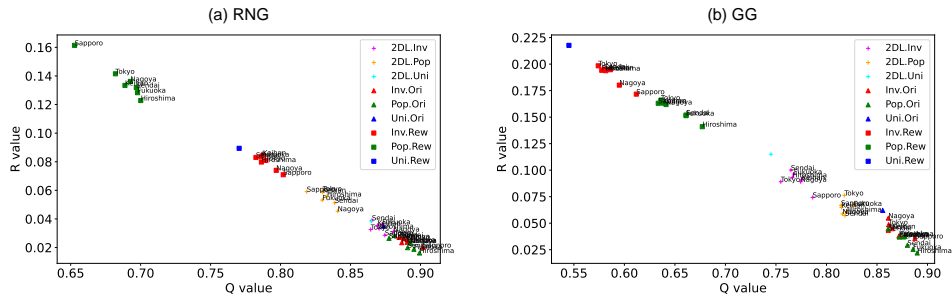


Fig. 11 Relation between robustness index R^{RB} and modularity Q in networks with $N = 1024$ nodes

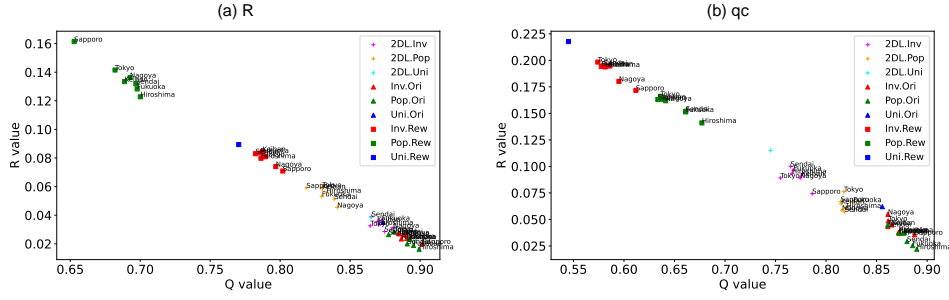


Fig. 12 Scatter plots show relation between network robustness measures (a for R and b for q_c) and the proportion of grid-like parts against random failures (RF). Networks with $N = 1024$ nodes are considered, where Pop. networks (green) show notably higher proportions of grid-like parts compared to Inv. (red) and Uni. (blue) networks. See the text at the end of subsection 3.3 for the detail.

Cities	RNG		GG	
	Inv.	Pop.	Inv.	Pop.
Fukuoka	0.8905 Δ	0.8953 Δ	0.8728 Δ	0.8857 Δ
Hiroshima	0.8866 Δ	0.8993 Δ	0.8717 Δ	0.8898 Δ
Keihan	0.8903 Δ	0.8924 Δ	0.8651 Δ	0.8777 Δ
Nagoya	0.8880 Δ	0.8929 Δ	0.8612 Δ	0.8764 Δ
Tokyo	0.8846 Δ	0.8814 Δ	0.8615 Δ	0.8610 Δ
Sendai	0.8853 Δ	0.8908 Δ	0.8612 Δ	0.8801 Δ
Sapporo	0.9017 Δ	0.8775 Δ	0.8875 Δ	0.8722 Δ
Uniform	0.8735		0.8557	

Table 1 Modularity Q in the original networks with 1024 nodes for seven major Japanese areas. Higher values indicate stronger community structures. Values with upper-triangles (Δ) indicate where the cases of Pop. and Inv. have higher modularity than the case of Uni. for both RNG and GG.

- [5] Nguyen, Q., Vu, T.V., Dinh, H.-D., Cassi, D., Scotognella, F., Alfieri, R., Bellingeri, M.: Modularity affects the robustness of scale-free model and real-world social networks under betweenness and degree-based node attack. *Applied Network Science* **6**, 1–21 (2021) <https://doi.org/10.1007/s41109-021-00426-y>
- [6] Boeing, G.: Urban spatial order: Street network orientation, configuration, and entropy. *Applied Network Science* **4**(1), 1–19 (2019) <https://doi.org/10.1007/s41109-019-0189-1>
- [7] Boccaletti, S., Latora, V., Moreno, Y., Chavez, M., Hwang, D.-U.: Complex

Cities	RNG		GG	
	Inv.	Pop.	Inv.	Pop.
Fukuoka	0.786 [△]	0.6978 [▽]	0.5776 [△]	0.661 [△]
Hiroshima	0.7863 [△]	0.7001 [▽]	0.5815 [△]	0.6771 [△]
Keihan	0.7874 [△]	0.6888 [▽]	0.5861 [△]	0.6383 [△]
Nagoya	0.7969 [△]	0.6927 [▽]	0.595 [△]	0.6412 [△]
Tokyo	0.7895 [△]	0.682 [▽]	0.5741 [△]	0.6362 [△]
Sendai	0.7824 [△]	0.6969 [▽]	0.58 [△]	0.6611 [△]
Sapporo	0.8019 [△]	0.6528 [▽]	0.6118 [△]	0.6335 [△]
Uniform	0.7704		0.5451	

Table 2 Modularity Q in networks with 1024 nodes for seven major Japanese areas after randomization. $P(k)$ is maintained as same to that in the original networks. Higher values indicate stronger community structures. Values with upper-triangles (Δ) indicate where the cases of Pop. and Inv. have higher modularity than the case of Uni., while values with lower-triangles (∇) indicate lower modularity than the case of Uni. for both RNG and GG.

Cities	RNG		GG	
	Inv.	Pop.	Inv.	Pop.
Fukuoka	0.8726 [△]	0.8298 [▽]	0.7677 [△]	0.8269 [△]
Hiroshima	0.8704 [△]	0.8332 [▽]	0.7662 [△]	0.8203 [△]
Keihan	0.8693 [△]	0.8302 [▽]	0.7756 [△]	0.8149 [△]
Nagoya	0.8807 [△]	0.8408 [▽]	0.7744 [△]	0.8158 [△]
Tokyo	0.8644 [▽]	0.8301 [▽]	0.7548 [△]	0.8177 [△]
Sendai	0.8653 [△]	0.8387 [▽]	0.7648 [△]	0.8184 [△]
Sapporo	0.8745 [△]	0.8187 [▽]	0.7863 [△]	0.8144 [△]
Uniform	0.8649		0.745	

Table 3 Modularity Q in networks with 1024 nodes for seven major Japanese areas after nodes relocation on a 2DL. $P(k)$ is maintained as same to that in the original networks. Higher values indicate stronger community structures. Values with upper-triangles (Δ) indicate where the cases of Pop. and Inv. have higher modularity than the case of Uni., while values with lower-triangles (∇) indicate lower modularity than the case of Uni. for both RNG and GG.

networks: Structure and dynamics. Physics Reports **424**(4-5), 175–308 (2006)

<https://doi.org/10.1016/j.physrep.2005.10.009>

- [8] Gastner, M., Newman, M.: The spatial structure of networks. The European Physical Journal B **2**(49), 247–252 (2006) <https://doi.org/10.1140/epjb/e2006-00046-8>

Cities	RNG		GG	
	Inv.	Pop.	Inv.	Pop.
Fukuoka	0.1264	0.2541 Δ	0.2171	0.2693 Δ
Hiroshima	0.1162	0.1319 Δ	0.2332	0.1606
Keihan	0.1531 Δ	0.1765 Δ	0.1998	0.1758
Nagoya	0.1404 Δ	0.1943 Δ	0.2238	0.2084
Tokyo	0.1363 Δ	0.2191 Δ	0.2250	0.2083
Sendai	0.1240	0.1801 Δ	0.2132	0.1257
Sapporo	0.1055	0.1646 Δ	0.1890	0.2042
Uniform	0.132		0.247	

Table 4 Robustness index R^{ID} against Initial Degree (ID) attacks in the original networks with $(N) = 1024$ nodes for seven major Japanese areas. Higher values indicate greater robustness. Values with upper-triangles (Δ) indicate where the cases of Pop. and Inv. have stronger robustness (higher R^{ID}) than the case of the Uni. network.

Cities	RNG		GG	
	Inv.	Pop.	Inv.	Pop.
Fukuoka	0.0901	0.2172 Δ	0.1832	0.2202
Hiroshima	0.0821	0.0981	0.2032	0.1051
Keihan	0.1692 Δ	0.0751	0.1712	0.1782
Nagoya	0.1552 Δ	0.1772 Δ	0.2392	0.0631
Tokyo	0.1361 Δ	0.2412 Δ	0.2362	0.1512
Sendai	0.0591	0.1061	0.1882	0.0170
Sapporo	0.0851	0.1441 Δ	0.1301	0.1522
Analytical	0.12		0.263	
Uniform	0.1351		0.2643	

Table 5 Critical fraction q_c^{ID} against Initial Degree (ID) attacks in the original networks with $(N) = 1024$ nodes for seven major Japanese areas. Until the values of q_c^{ID} , the connectivity is remaining without global fragmentation. Higher values indicate greater resilience. Values with upper-triangles (Δ) indicate cases where Pop. and Inv. have greater resilience (higher q_c^{ID}) than the case of the Uni. network.

[9] Guimera, R., Mossa, S., Turtschi, A., Amaral, L.N.: The worldwide air transportation network: Anomalous centrality, community structure, and cities' global roles. *Proceedings of the National Academy of Sciences* **102**(22), 7794–7799 (2005)
<https://doi.org/10.1073/pnas.0407994102>

[10] Kaluza, P., Kölsch, A., Gastner, M.T., Blasius, B.: The complex network of

Cities	RNG		GG	
	Inv.	Pop.	Inv.	Pop.
Fukuoka	0.1573	0.1338	0.282	0.1902
Hiroshima	0.1476	0.1227	0.2627	0.151
Keihan	0.204 Δ	0.2001 Δ	0.2486	0.2421
Nagoya	0.1711	0.206 Δ	0.2752	0.2068
Tokyo	0.1721	0.2146 Δ	0.2998	0.2614
Sendai	0.1771	0.1407	0.265	0.1806
Sapporo	0.1253	0.2053 Δ	0.2126	0.2345
Uniform	0.1972		0.3083	

Table 6 Robustness index R^{RF} against random failure (RF) in the original networks with $(N) = 1024$ nodes for seven major Japanese areas. Higher values indicate greater robustness. Values with upper-triangles (Δ) indicate cases where Pop. and Inv. have stronger robustness (higher R^{RF}) than the case of the Uni. network.

Cities	RNG		GG	
	Inv.	Pop.	Inv.	Pop.
Fukuoka	0.1191	0.0911	0.3724 Δ	0.1682
Hiroshima	0.1832	0.032	0.3093	0.0601
Keihan	0.1522	0.2382 Δ	0.3844 Δ	0.2773
Nagoya	0.1692	0.0881	0.2653	0.3093
Tokyo	0.1031	0.2873 Δ	0.2332	0.2513
Sendai	0.1131	0.033	0.2843	0.0541
Sapporo	0.1391	0.033	0.2302	0.4014
Analytical	0.205		0.365	
Uniform	0.2112		0.3694	

Table 7 Critical fraction q_c^{RF} against random failure (RF) in the original networks with $(N) = 1024$ nodes for seven major Japanese areas. Until values of q_c^{RF} , the connectivity is remaining without global fragmentation. Higher values indicate greater resilience. Values with upper-triangles (Δ) indicate cases where Pop. and Inv. have greater resilience (higher q_c^{RF}) than the case of the Uni. network.

global cargo ship movements. Journal of the Royal Society Interface **7**(48), 1093–1103 (2010) <https://doi.org/10.1098/rsif.2009.0495>

- [11] Hayashi, Y., Matsukubo, J.: Improvement of the robustness on geographical networks by adding shortcuts. Physica A: Statistical Mechanics and its Applications **380**, 552–562 (2007) <https://doi.org/10.1016/j.physa.2007.02.080>
- [12] Watanabe, D.: A study on analyzing road network patterns using proximity

Cities	RNG		GG	
	Inv.	Pop.	Inv.	Pop.
Fukuoka	2.4492	2.8223 [△]	3.584	2.9844
Hiroshima	2.4414	2.7852 [△]	3.5996	2.9199
Keihan	2.4395	2.8535 [△]	3.5469	3.1367
Nagoya	2.3945	2.8535 [△]	3.4785	3.1367
Tokyo	2.4473	2.8906 [△]	3.6113	3.1191
Sendai	2.459	2.834 [△]	3.582	3.0195
Sapporo	2.3789	3.0684 [△]	3.3105	3.1563
Uniform	2.5017		3.864	

Table 8 Average degree $\langle k \rangle$ in networks with $N = 1024$ nodes for seven major Japanese areas. Values with upper-triangles (Δ) indicate cases where Pop. and Inv. show higher $\langle k \rangle$ than the case of Uni.

Cities	RNG		GG	
	Inv.	Pop.	Inv.	Pop.
Fukuoka	0	0.0771 [△]	0.0039	0.0771 [△]
Hiroshima	0	0.0205 [△]	0.0078	0.0205 [△]
Keihan	0	0.0391 [△]	0.0078	0.0479 [△]
Nagoya	0	0.0391 [△]	0.0088 [△]	0.0479 [△]
Tokyo	0	0.0205 [△]	0.0068	0.0225 [△]
Sendai	0	0.0459 [△]	0.0117 [△]	0.0498 [△]
Sapporo	0	0.1514 [△]	0.001	0.1533 [△]
Uniform	0		0.0079	
Lattice	0.7656			

Table 9 Proportion of grid-like parts in networks with $N = 1024$ nodes for seven major Japanese areas. A grid-like structure is identified when a node has degree 4 with the neighbors of degree 4. Values with upper-triangles (Δ) indicate cases where the proportions exceed that of Uni. networks. Note that 2D lattice shows the highest proportion (76.56%) because of its completely ordered grid arrangement.

graphs. Journal of the City Planning Institute of Japan **40.3**, 133–138 (2005)

<https://doi.org/10.11361/journalcpj.40.3.133>

- [13] Watanabe, D.: A study on analyzing the grid road network patterns using relative neighborhood graph. In: The Ninth International Symposium on Operations Research and Its Applications, pp. 112–119 (2010). Lecture Notes in Operations Research. Beijing, China: World Publishing ...

- [14] Bose, P., Morin, P., Stojmenović, I., Urrutia, J.: Routing with guaranteed delivery in ad hoc wireless networks. In: Proceedings of the 3rd International Workshop on Discrete Algorithms and Methods for Mobile Computing and Communications. DIALM '99, pp. 48–55. Association for Computing Machinery, New York, NY, USA (1999). <https://doi.org/10.1145/313239.313282> . <https://doi.org/10.1145/313239.313282>
- [15] Karp, B., Kung, H.T.: Gpsr: greedy perimeter stateless routing for wireless networks. In: Proceedings of the 6th Annual International Conference on Mobile Computing and Networking. MobiCom '00, pp. 243–254. Association for Computing Machinery, New York, NY, USA (2000). <https://doi.org/10.1145/345910.345953> . <https://doi.org/10.1145/345910.345953>
- [16] Holme, P., Kim, B.J., Yoon, C.N., Han, S.K.: Attack vulnerability of complex networks. *Physical Review E* **65**(5), 056109 (2002) <https://doi.org/10.1103/PhysRevE.65.056109>
- [17] Barabási, A.-L., Albert, R.: Emergence of scaling in random networks. *Science* **286**(5439), 509–512 (1999) <https://doi.org/10.1126/science.286.5439.509>
- [18] Toussaint, G.T.: The relative neighbourhood graph of a finite planar set. *Pattern Recognition* **12**(4), 261–268 (1980) [https://doi.org/10.1016/0031-3203\(80\)90066-7](https://doi.org/10.1016/0031-3203(80)90066-7)
- [19] Gabriel, K.R., Sokal, R.R.: A new statistical approach to geographic variation analysis. *Systematic Zoology* **18**(3), 259–278 (1969) <https://doi.org/10.2307/2412323>
- [20] Anderson, E., Phillips, C., Sicker, D., Grunwald, D.: Modeling environmental

- effects on directionality in wireless networks. In: 2009 7th International Symposium on Modeling and Optimization in Mobile, Ad Hoc, and Wireless Networks, pp. 1–7 (2009). <https://doi.org/10.1109/WIOPT.2009.5291577>
- [21] Singh, J., Kaur, G., Kaur, G.: Determining best setup sites for cellular towers using fuzzy logic. In: 2015 International Conference on Futuristic Trends on Computational Analysis and Knowledge Management (ABLAZE), pp. 256–260 (2015). <https://doi.org/10.1109/ABLAZE.2015.7155002> . IEEE
- [22] Onim, A., Kihato, P., Musyoki, S.: Optimization of base station location in 3g networks using fuzzy clustering and mesh adaptive direct search. In: Proceedings of Sustainable Research and Innovation Conference, pp. 30–35 (2014)
- [23] Office for National Statistics: Population density, Census 2021. [Online; accessed 01-August-2024] (2021). <https://www.ons.gov.uk/census/maps/choropleth/population/population-density/population-density/persons-per-square-kilometre>
- [24] Keeler, H.P.: Notes on the poisson point process. Weierstrass Inst., Berlin, Germany, Technical Report (2016)
- [25] Kittel, C., McEuen, P.: Introduction to Solid State Physics, 8th edn. John Wiley & Sons, Hoboken, NJ (2018)
- [26] Statistics Bureau of Japan: 2010 Census of Japan. <https://www.stat.go.jp/english/data/kokusei/2010/summary.html>. [Online; accessed 2024-08-05] (2010)
- [27] Newman, M.E.J., Girvan, M.: Finding and evaluating community structure in networks. *Physical Review E* **69**(2), 026113 (2004) <https://doi.org/10.1103/PhysRevE.69.026113>

- [28] Blondel, V.D., Guillaume, J.-L., Lambiotte, R., Lefebvre, E.: Fast unfolding of communities in large networks. *Journal of Statistical Mechanics: Theory and Experiment* **2008**(10), 10008 (2008) <https://doi.org/10.1088/1742-5468/2008/10/P10008>
- [29] Schneider, C.M., Moreira, A.A., Andrade Jr, J.S., Havlin, S., Herrmann, H.J.: Mitigation of malicious attacks on networks. *Proceedings of the National Academy of Sciences in USA* **108**(10), 3838–3841 (2011) <https://doi.org/10.1073/pnas.1009440108>
- [30] Callaway, D.S., Newman, M.E., Strogatz, S.H., Watts, D.J.: Network robustness and fragility: Percolation on random graphs. *Physical Review Letters* **85**(25), 5468 (2000) <https://doi.org/10.1103/PhysRevLett.85.5468>
- [31] Norrenbrock, C., Melchert, O., Hartmann, A.K.: Fragmentation properties of two-dimensional proximity graphs considering random failures and targeted attacks. *Physical Review E* **94**(6), 062125 (2016) <https://doi.org/10.1103/PhysRevE.94.062125>
- [32] Stauffer, D., Aharony, A.: *Introduction To Percolation Theory: Second Edition*, 2nd edn., p. 192. Taylor & Francis, London (1992). <https://doi.org/10.1201/9781315274386>

Declarations

Availability of data and materials

The population data used in this study are available from the “Regional Mesh Statistics: First Regional Division, 2010 Population Census (World Geodetic System)” provided by the Statistical Information Institute for Consulting and Analysis (SINFONICA). The data were purchased under license from SINFONICA (located

at Nogaku Shorin Building 5F, 3-6 Kanda-Jinbocho, Chiyoda-ku, Tokyo 101-0051, Japan). These data are subject to usage restrictions. Researchers interested in accessing these data should contact SINFONICA (<https://www.sinfonica.or.jp/>) for purchase and licensing information.

The code used to generate the results is also available from the corresponding author upon reasonable request.

Competing interests

The authors declare that they have no competing interests.

Funding

JSPS KAKENHI Grant Number JP.21H03425

Authors' contributions

YM analyzed the data, performed the simulations, and wrote the manuscript. YH supervised the research, provided guidance on methodology, and contributed to manuscript revision. All authors read and approved the final manuscript.

Acknowledgements

This research is supported in part by JSPS KAKENHI Grant Number JP.21H03425

Authors' information

1. Yingzhou MOU (Corresponding author)

Japan Advanced Institute of Science and Technology, Nomi-city,
Ishikawa 923-1292, Japan

E-mail: mouyingzhou@outlook.com

2. Yukio HAYASHI

Japan Advanced Institute of Science and Technology, Nomi-city,

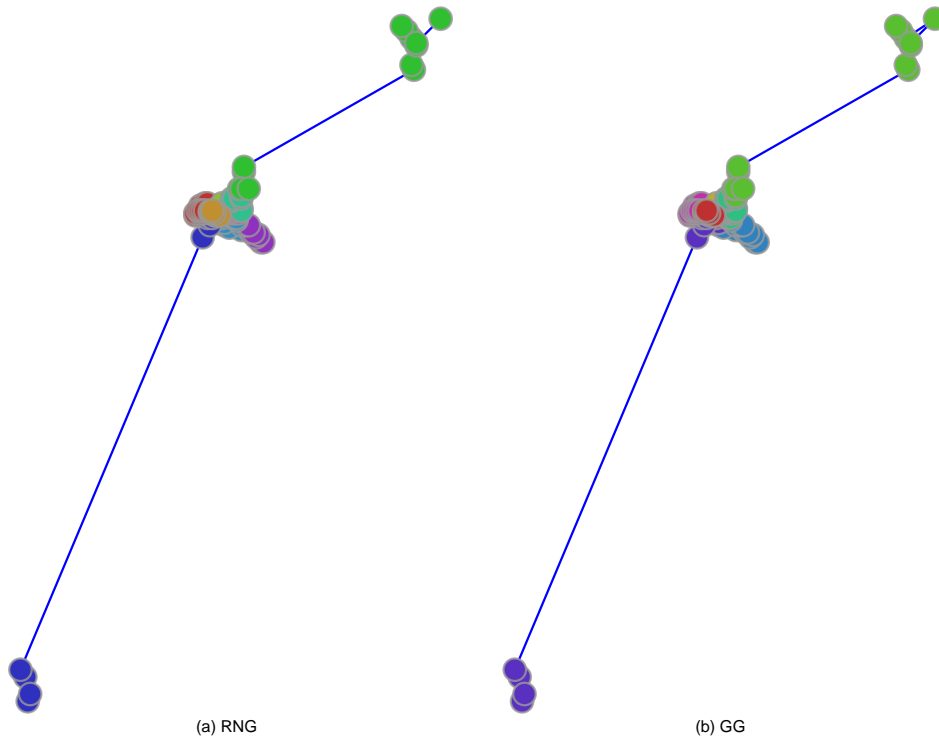


Fig. A1 Visualization of community structures in Fukuoka before node removal. $N = 100$ nodes are located by the decreasing order of population (Pop.). Different colors represent different communities estimated by Louvain algorithm. There are clear community formations particularly in densely populated areas.

Ishikawa 923-1292, Japan

E-mail: yhayashi@jaist.ac.jp

Appendix

.1 Visualization maps. before attacks

3

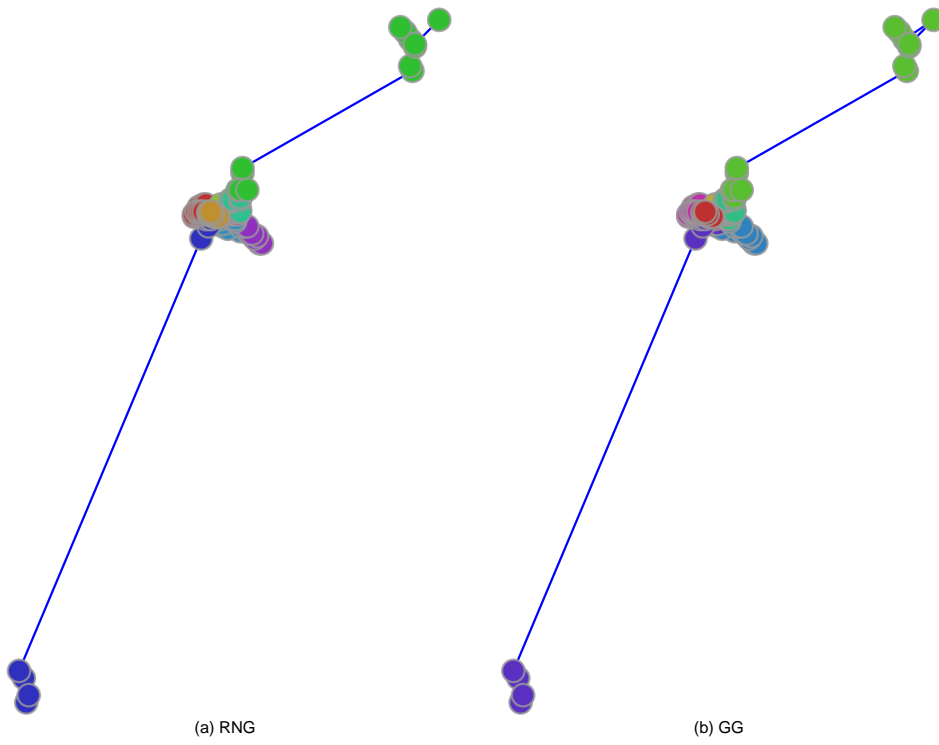


Fig. A2 Visualization of community structures in Fukuoka before node removal. $N = 100$ nodes are located by the inverse order of population (Inv.). Different colors represent different communities estimated by Louvain algorithm. There are different community formations compared to Figure A1.

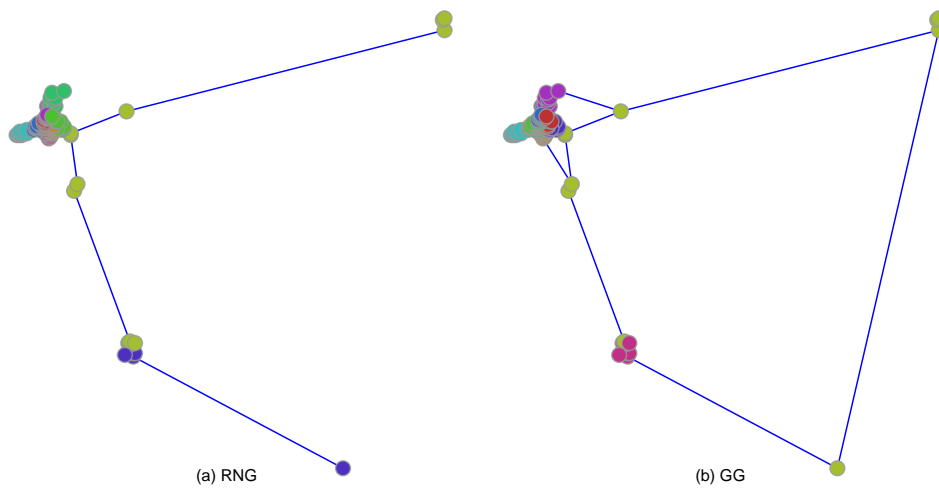


Fig. A3 Visualization of community structures in Hiroshima before node removal. $N = 100$ nodes are located by the decreasing order of population (Pop.). Different colors represent different communities estimated by Louvain algorithm. There are clear community formations particularly in densely populated areas.

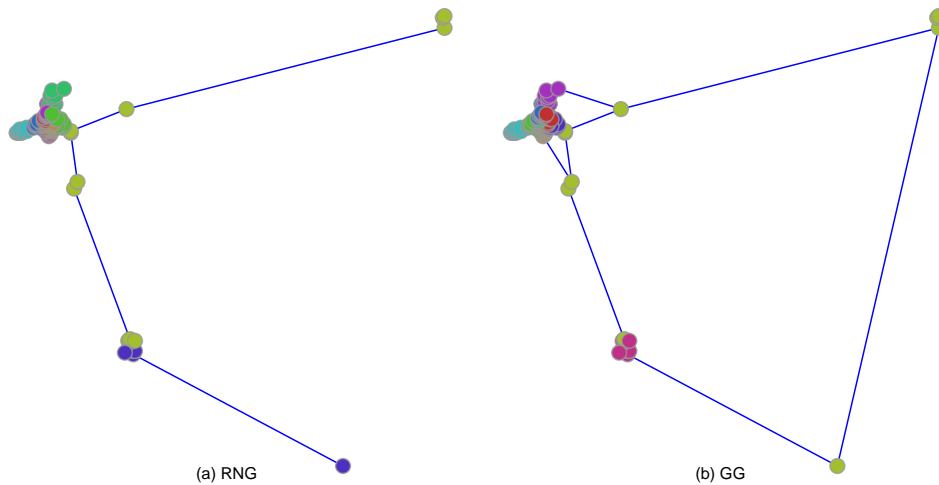


Fig. A4 Visualization of community structures in Hiroshima before node removal. $N = 100$ nodes are located by the inverse order of population (Inv.). Different colors represent different communities estimated by Louvain algorithm. There are different community formations compared to Figure A3.

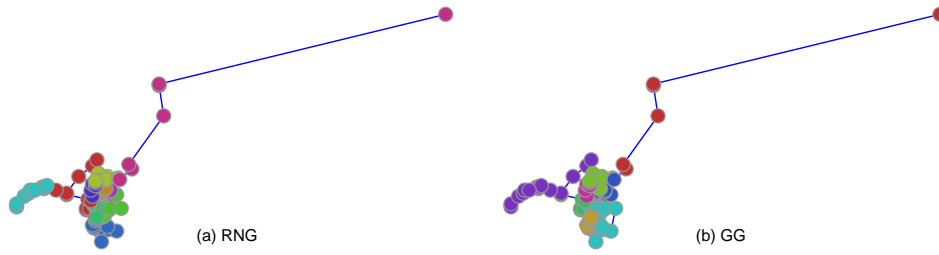


Fig. A5 Visualization of community structures in Keihan before node removal. $N = 100$ nodes are located by the decreasing order of population (Pop.). Different colors represent different communities estimated by Louvain algorithm. There are clear community formations particularly in densely populated areas.

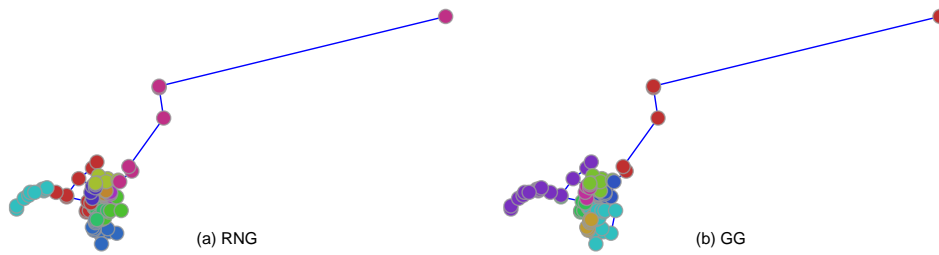


Fig. A6 Visualization of community structures in Keihan before node removal. $N = 100$ nodes are located by the inverse order of population (Inv.). Different colors represent different communities estimated by Louvain algorithm. There are different community formations compared to Figure A5.

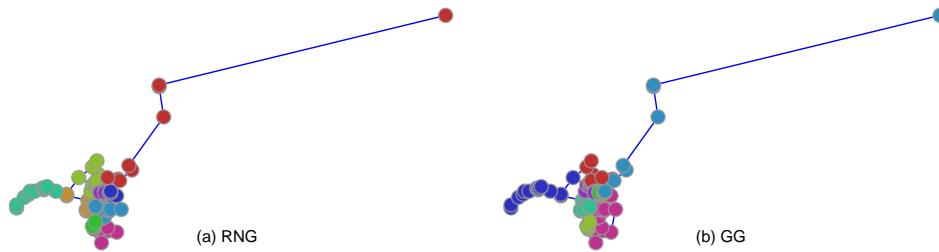


Fig. A7 Visualization of community structures in Nagoya before node removal. $N = 100$ nodes are located by the decreasing order of population (Pop.). Different colors represent different communities estimated by Louvain algorithm. There are clear community formations particularly in densely populated areas.

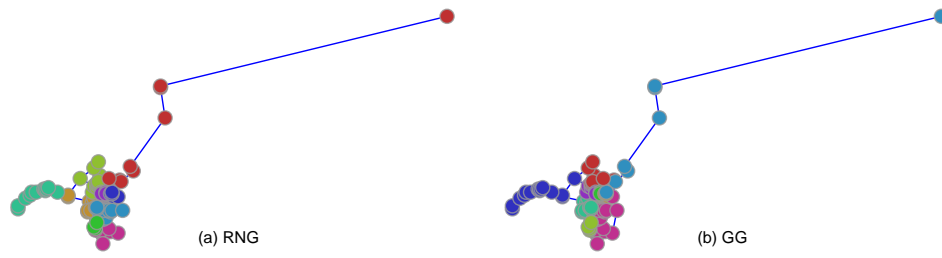


Fig. A8 Visualization of community structures in Nagoya before node removal. $N = 100$ nodes are located by the inverse order of population (Inv.). Different colors represent different communities estimated by Louvain algorithm. There are different community formations compared to Figure A7.

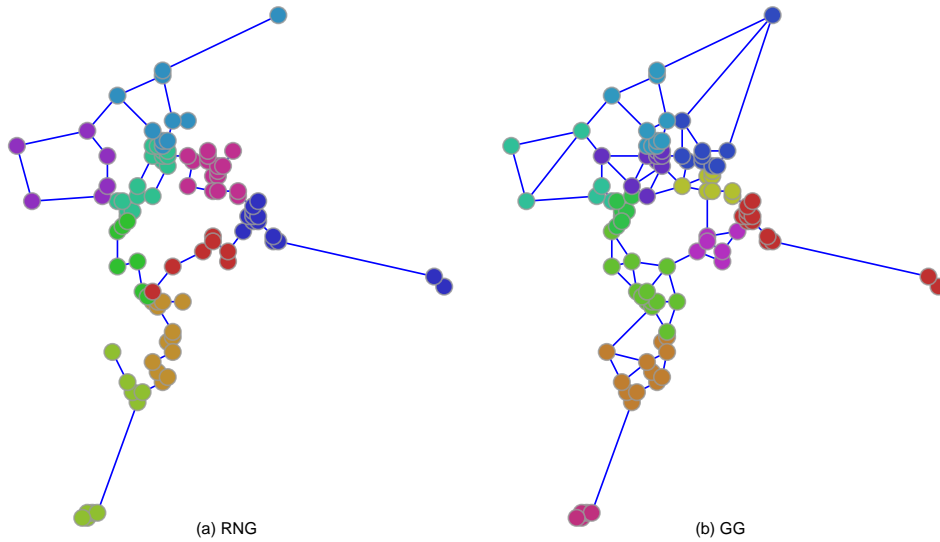


Fig. A9 Visualization of community structures in Tokyo before node removal. $N = 100$ nodes are located by the decreasing order of population (Pop.). Different colors represent different communities estimated by Louvain algorithm. There are clear community formations particularly in densely populated areas.

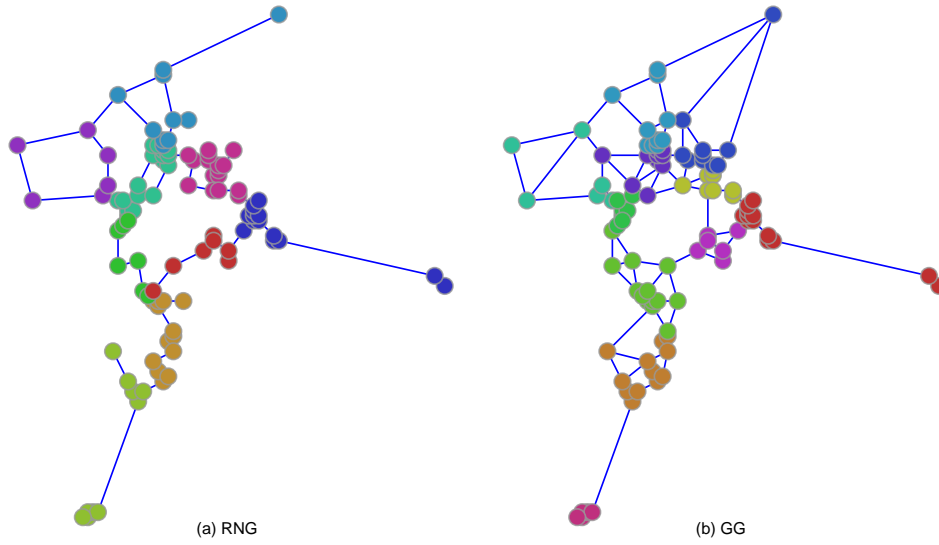


Fig. A10 Visualization of community structures in Tokyo before node removal. $N = 100$ nodes are located by the inverse order of population (Inv.). Different colors represent different communities estimated by Louvain algorithm. There are different community formations compared to Figure A9.

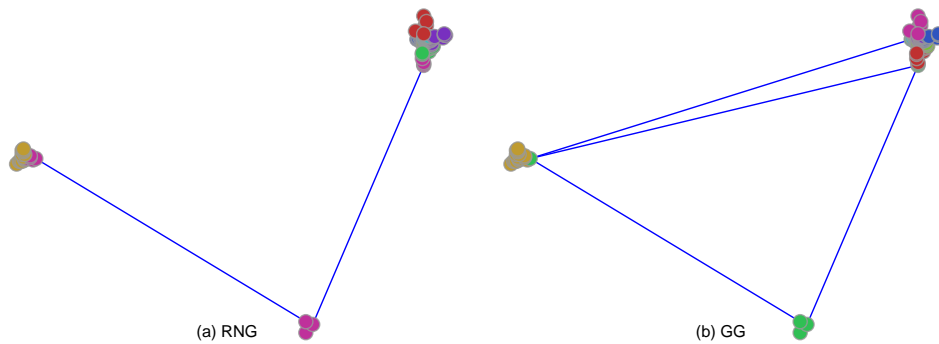


Fig. A11 Visualization of community structures in Sendai before node removal. $N = 100$ nodes are located by the decreasing order of population (Pop.). Different colors represent different communities estimated by Louvain algorithm. There are clear community formations particularly in densely populated areas.

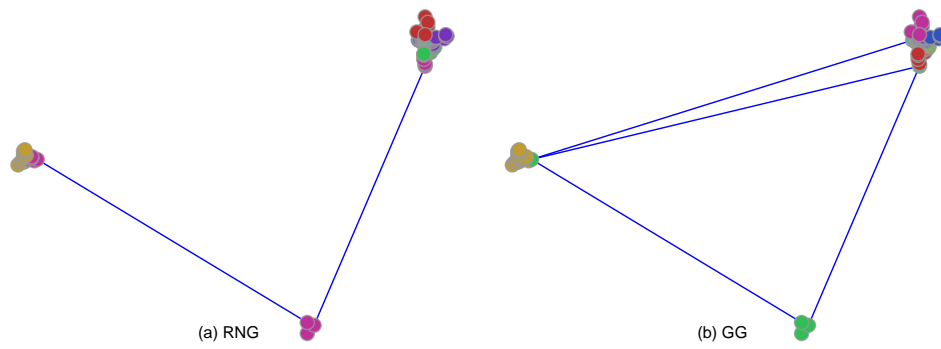


Fig. A12 Visualization of community structures in Sendai before node removal. $N = 100$ nodes are located by the inverse order of population (Inv.). Different colors represent different communities estimated by Louvain algorithm. There are different community formations compared to Figure A11.

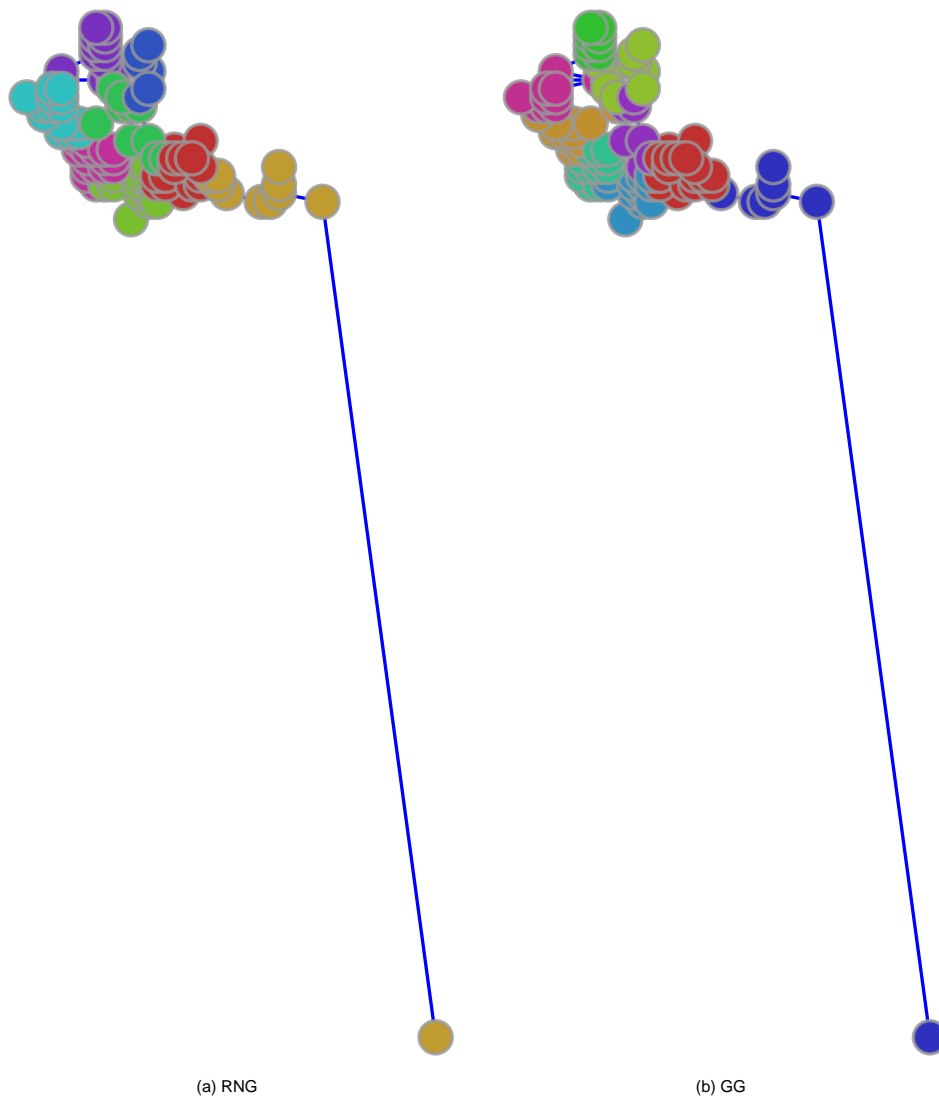


Fig. A13 Visualization of community structures in Sapporo before node removal. $N = 100$ nodes are located by the decreasing order of population (Pop.). Different colors represent different communities estimated by Louvain algorithm. There are clear community formations particularly in densely populated areas.

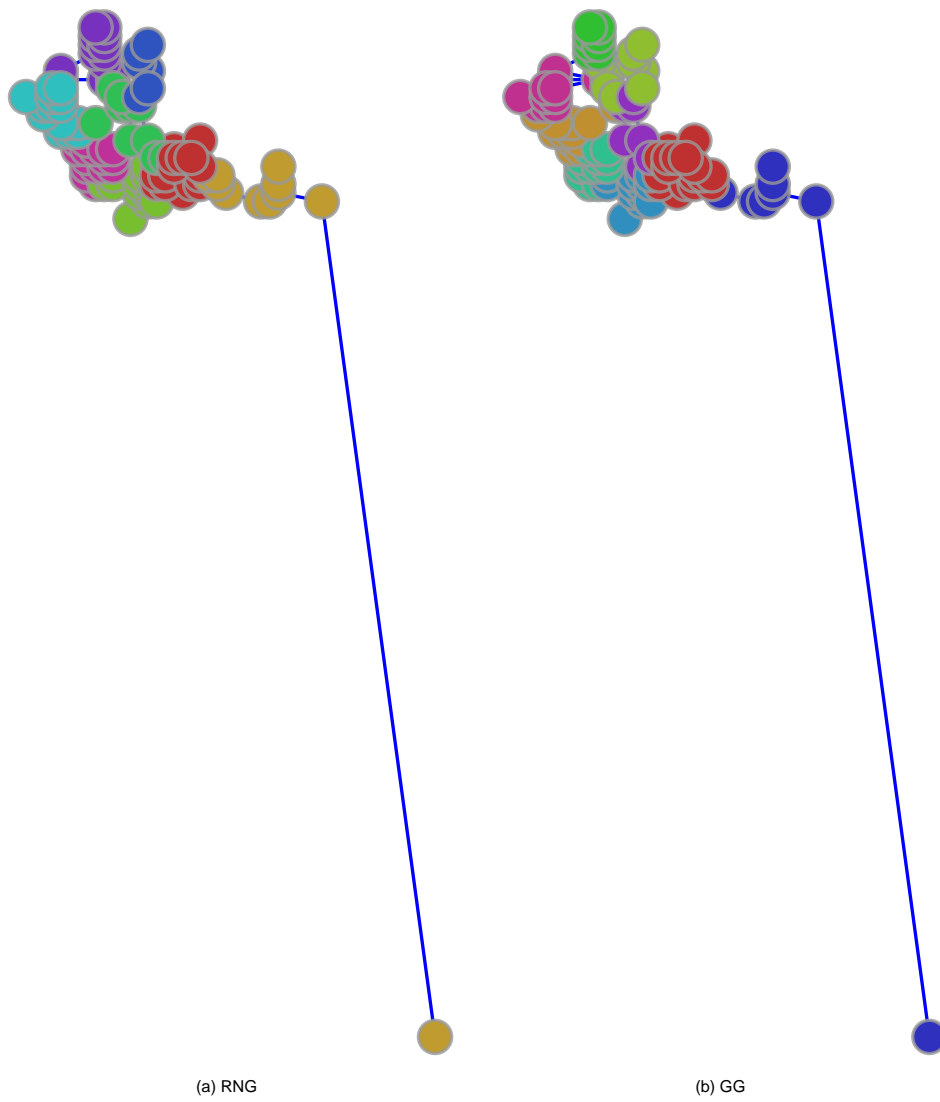


Fig. A14 Visualization of community structures in Sapporo before node removal. $N = 100$ nodes are located by the inverse order of population (Inv.). Different colors represent different communities estimated by Louvain algorithm. There are different community formations compared to Figure A13.

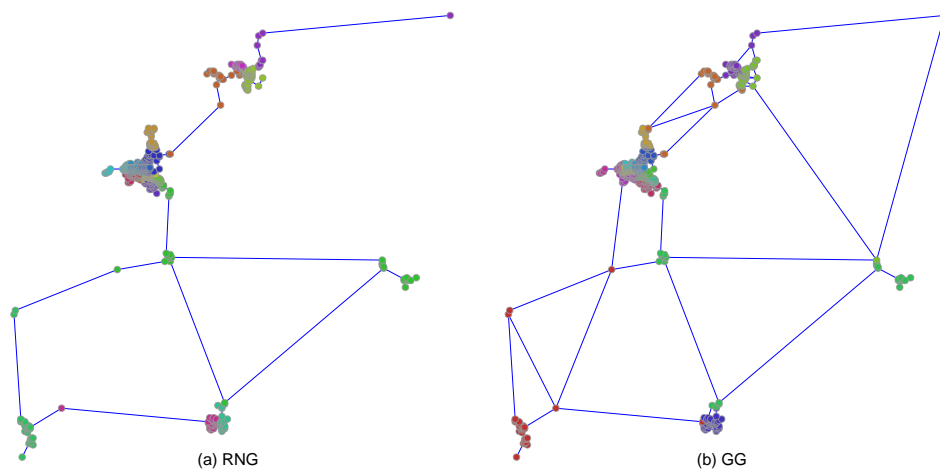


Fig. A15 Visualization of community structures in Fukuoka before node removal. $N = 484$ nodes are located by the decreasing order of population (Pop.). Different colors represent different communities estimated by Louvain algorithm. There are clear community formations particularly in densely populated areas.

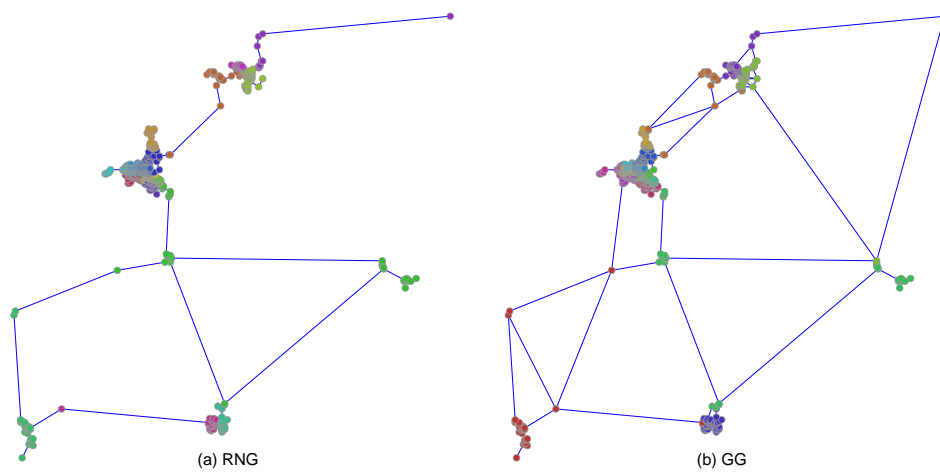


Fig. A16 Visualization of community structures in Fukuoka before node removal. $N = 484$ nodes are located by the inverse order of population (Inv.). Different colors represent different communities estimated by Louvain algorithm. There are different community formations compared to Figure A15.

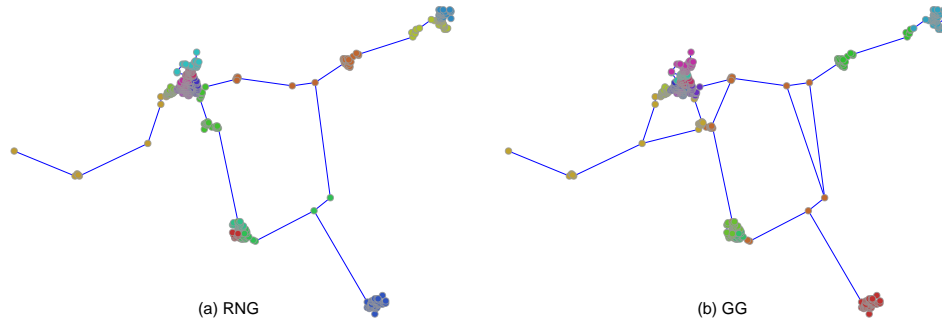


Fig. A17 Visualization of community structures in Hiroshima before node removal. $N = 484$ nodes are located by the decreasing order of population (Pop.). Different colors represent different communities estimated by Louvain algorithm. There are clear community formations particularly in densely populated areas.

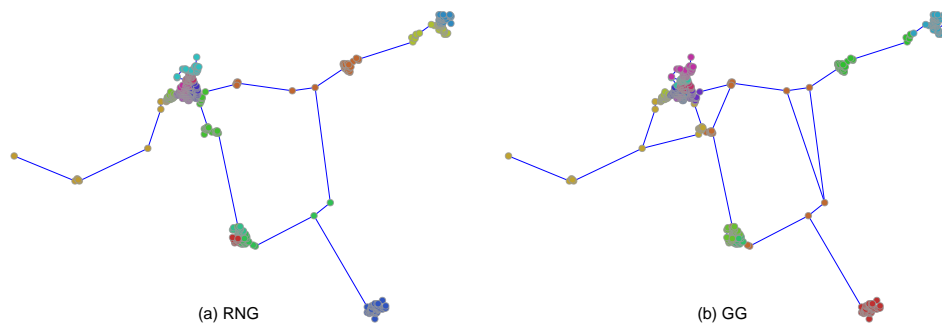


Fig. A18 Visualization of community structures in Hiroshima before node removal. $N = 484$ nodes are located by the inverse order of population (Inv.). Different colors represent different communities estimated by Louvain algorithm. There are different community formations compared to Figure A17.

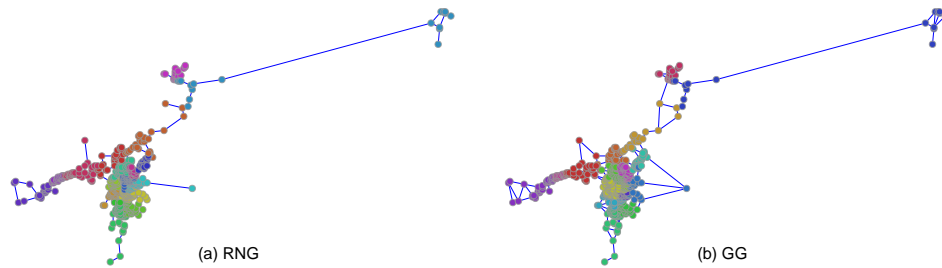


Fig. A19 Visualization of community structures in Keihan before node removal. $N = 484$ nodes are located by the decreasing order of population (Pop.). Different colors represent different communities estimated by Louvain algorithm. There are clear community formations particularly in densely populated areas.

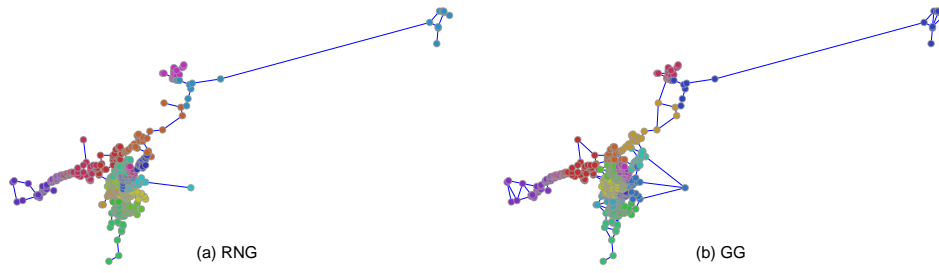


Fig. A20 Visualization of community structures in Keihan before node removal. $N = 484$ nodes are located by the inverse order of population (Inv.). Different colors represent different communities estimated by Louvain algorithm. There are different community formations compared to Figure A19.

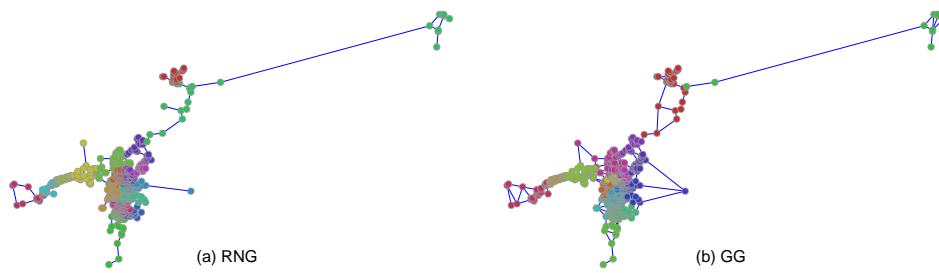


Fig. A21 Visualization of community structures in Nagoya before node removal. $N = 484$ nodes are located by the decreasing order of population (Pop.). Different colors represent different communities estimated by Louvain algorithm. There are clear community formations particularly in densely populated areas.

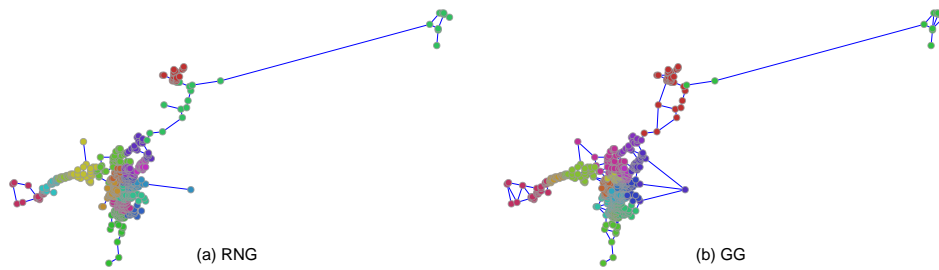


Fig. A22 Visualization of community structures in Nagoya before node removal. $N = 484$ nodes are located by the inverse order of population (Inv.). Different colors represent different communities estimated by Louvain algorithm. There are different community formations compared to Figure A21.

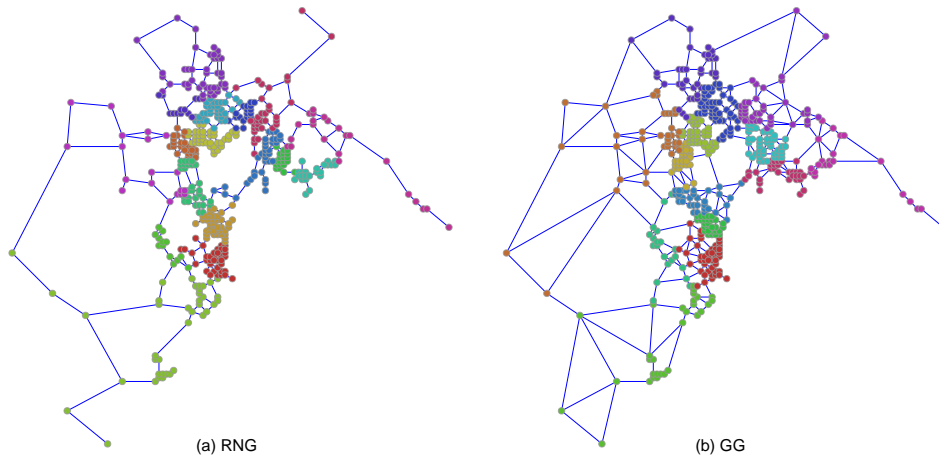


Fig. A23 Visualization of community structures in Tokyo before node removal. $N = 484$ nodes are located by the decreasing order of population (Pop.). Different colors represent different communities estimated by Louvain algorithm. There are clear community formations particularly in densely populated areas.

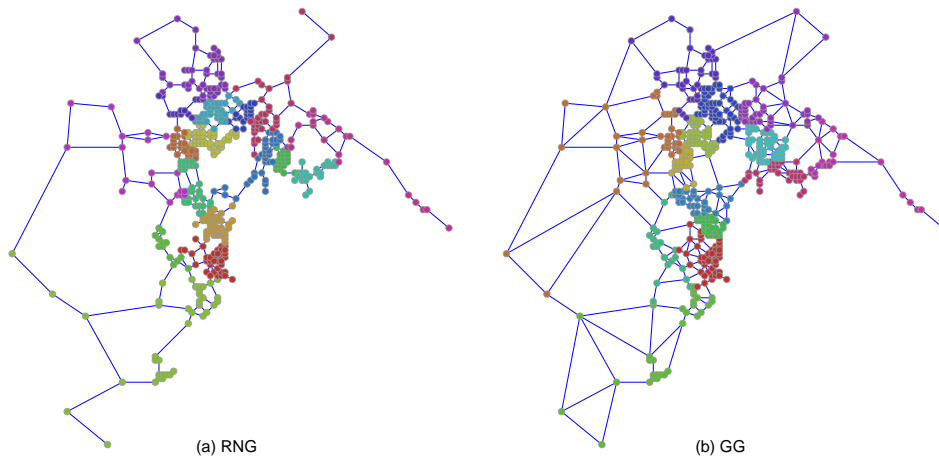


Fig. A24 Visualization of community structures in Tokyo before node removal. $N = 484$ nodes are located by the inverse order of population (Inv.). Different colors represent different communities estimated by Louvain algorithm. There are different community formations compared to Figure A23.

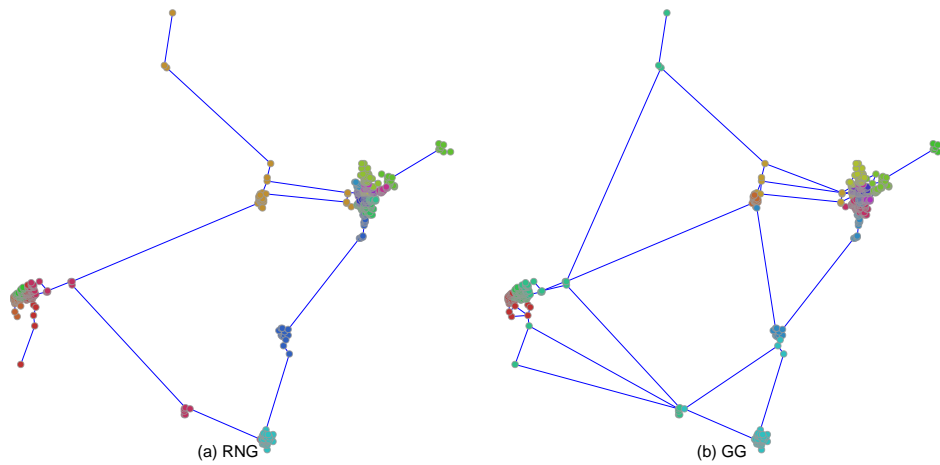


Fig. A25 Visualization of community structures in Sendai before node removal. $N = 484$ nodes are located by the decreasing order of population (Pop.). Different colors represent different communities estimated by Louvain algorithm. There are clear community formations particularly in densely populated areas.

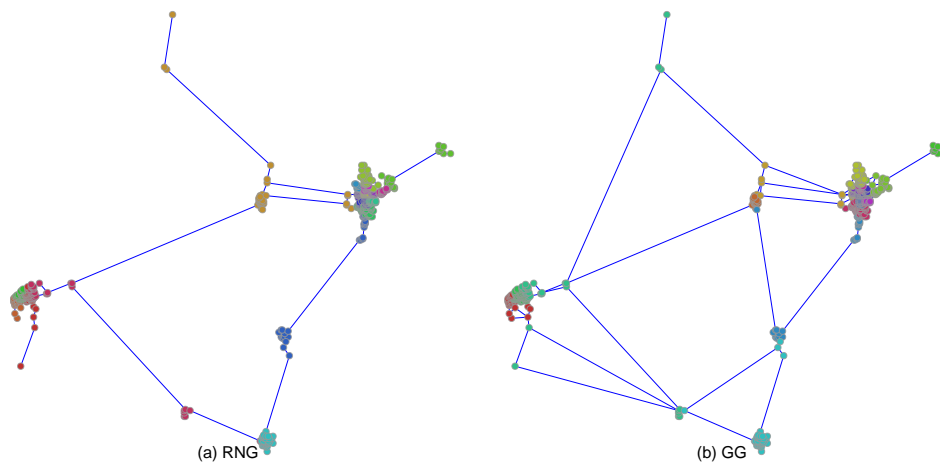


Fig. A26 Visualization of community structures in Sendai before node removal. $N = 484$ nodes are located by the inverse order of population (Inv.). Different colors represent different communities estimated by Louvain algorithm. There are different community formations compared to Figure A25.

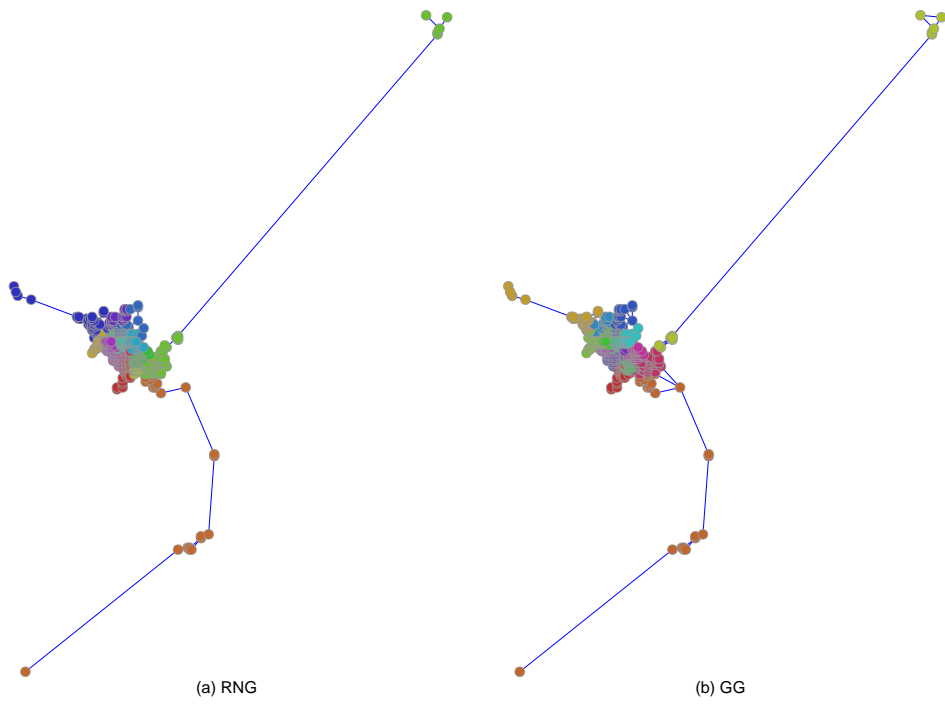


Fig. A27 Visualization of community structures in Sapporo before node removal. $N = 484$ nodes are located by the decreasing order of population (Pop.). Different colors represent different communities estimated by Louvain algorithm. There are clear community formations particularly in densely populated areas.

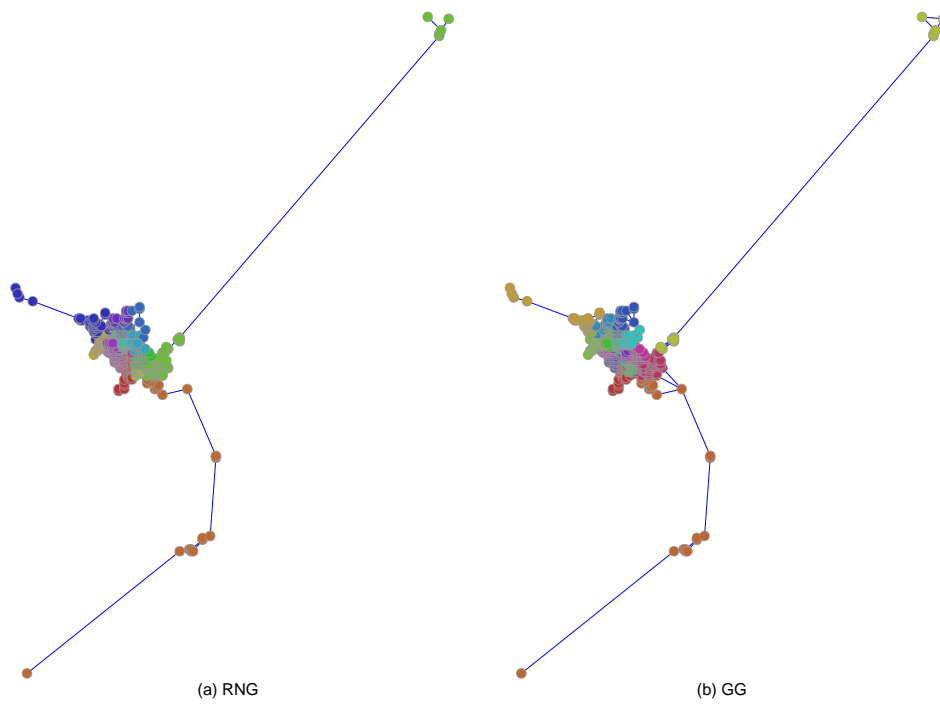


Fig. A28 Visualization of community structures in Sapporo before node removal. $N = 484$ nodes are located by the inverse order of population (Inv.). Different colors represent different communities estimated by Louvain algorithm. There are different community formations compared to Figure A27.

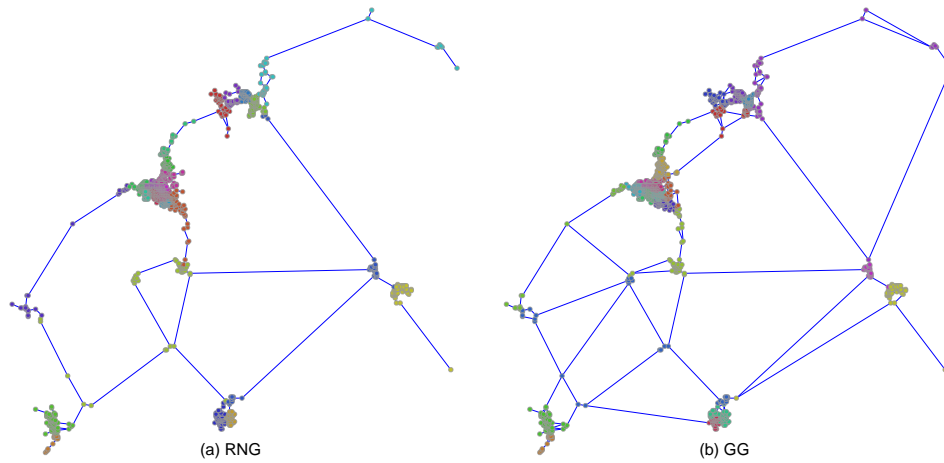


Fig. A29 Visualization of community structures in Fukuoka before node removal. $N = 1024$ nodes are located by the decreasing order of population (Pop.). Different colors represent different communities estimated by Louvain algorithm. There are clear community formations particularly in densely populated areas.

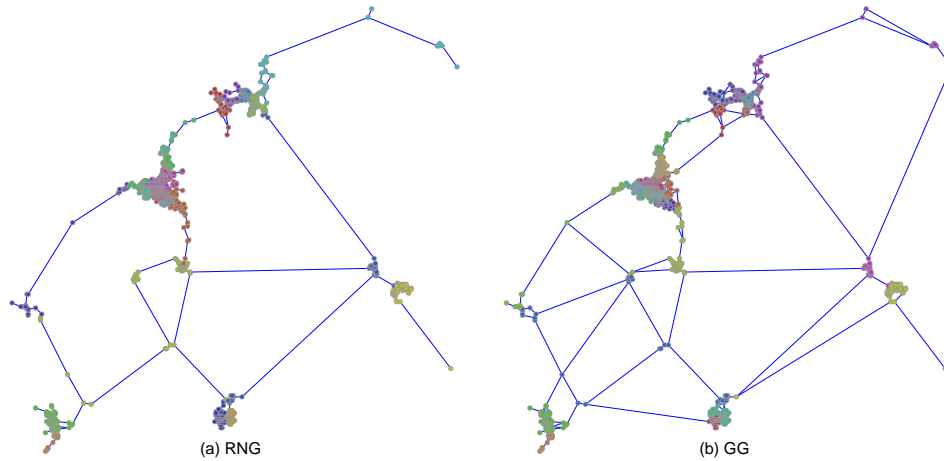


Fig. A30 Visualization of community structures in Fukuoka before node removal. $N = 1024$ nodes are located by the inverse order of population (Inv.). Different colors represent different communities estimated by Louvain algorithm. There are different community formations compared to Figure A29.

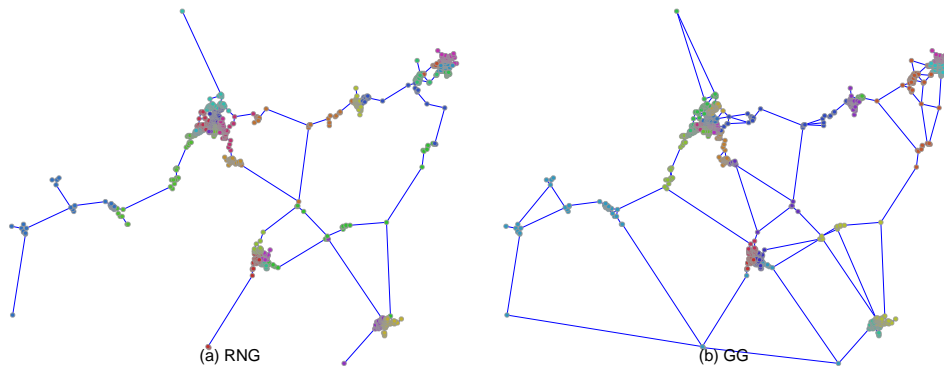


Fig. A31 Visualization of community structures in Hiroshima before node removal. $N = 1024$ nodes are located by the decreasing order of population (Pop.). Different colors represent different communities estimated by Louvain algorithm. There are clear community formations particularly in densely populated areas.

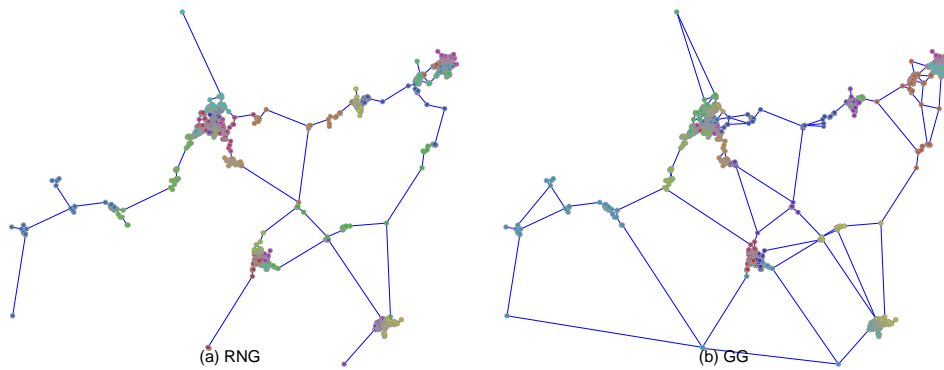


Fig. A32 Visualization of community structures in Hiroshima before node removal. $N = 1024$ nodes are located by the inverse order of population (Inv.). Different colors represent different communities estimated by Louvain algorithm. There are different community formations compared to Figure A31.

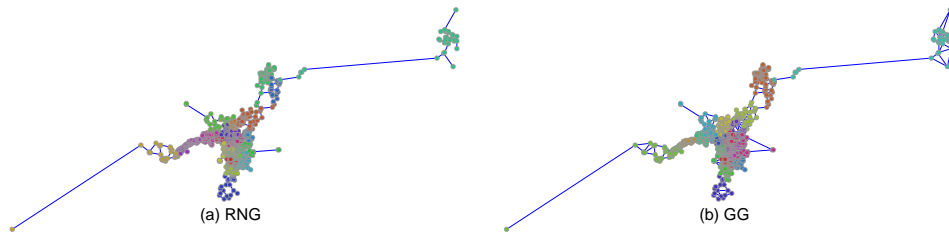


Fig. A33 Visualization of community structures in Keihan before node removal. $N = 1024$ nodes are located by the decreasing order of population (Pop.). Different colors represent different communities estimated by Louvain algorithm. There are clear community formations particularly in densely populated areas.

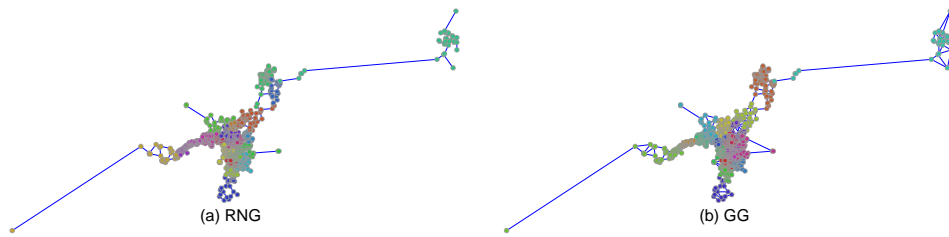


Fig. A34 Visualization of community structures in Keihan before node removal. $N = 1024$ nodes are located by the inverse order of population (Inv.). Different colors represent different communities estimated by Louvain algorithm. There are different community formations compared to Figure A33.

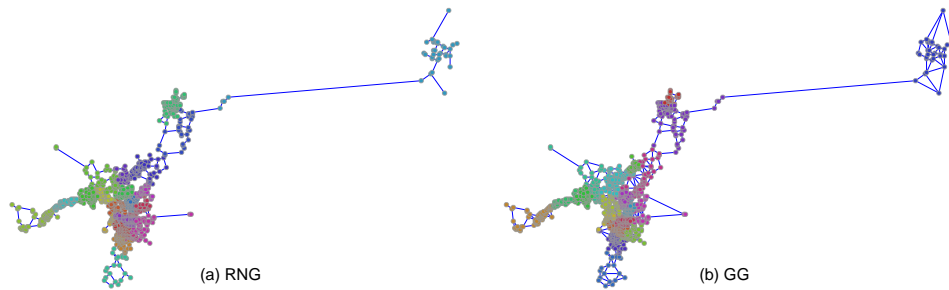


Fig. A35 Visualization of community structures in Nagoya before node removal. $N = 1024$ nodes are located by the decreasing order of population (Pop.). Different colors represent different communities estimated by Louvain algorithm. There are clear community formations particularly in densely populated areas.

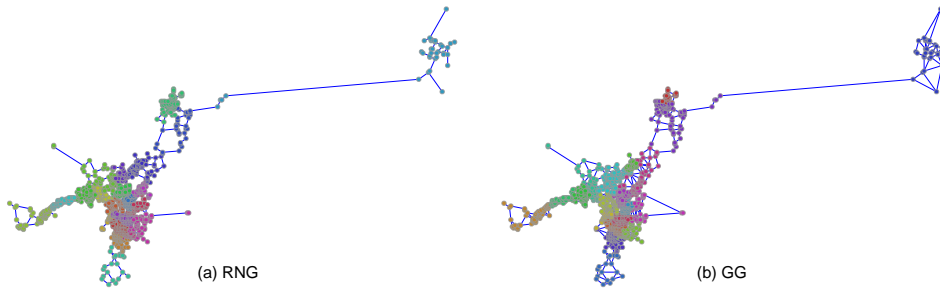


Fig. A36 Visualization of community structures in Nagoya before node removal. $N = 1024$ nodes are located by the inverse order of population (Inv.). Different colors represent different communities estimated by Louvain algorithm. There are different community formations compared to Figure A35.

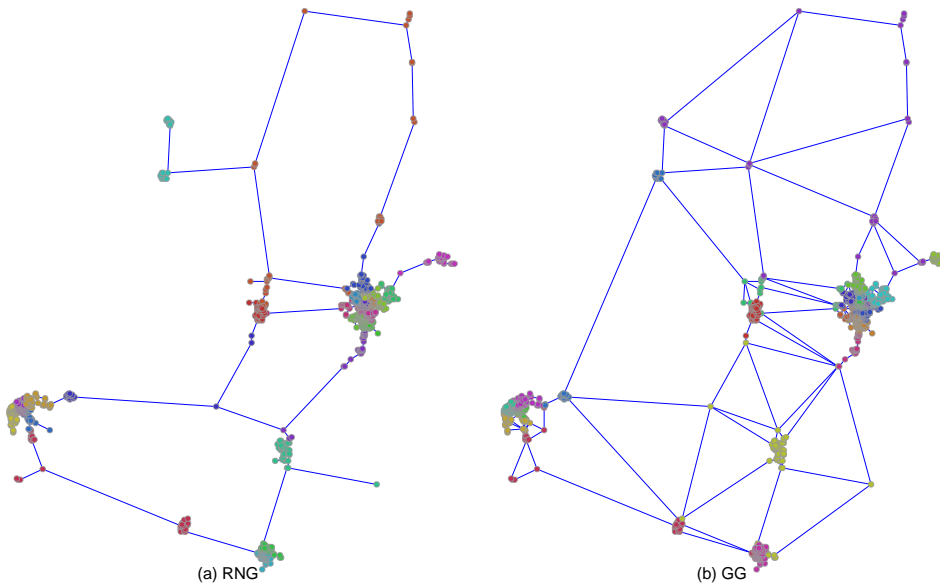


Fig. A37 Visualization of community structures in Sendai before node removal. $N = 1024$ nodes are located by the decreasing order of population (Pop.). Different colors represent different communities estimated by Louvain algorithm. There are clear community formations particularly in densely populated areas.

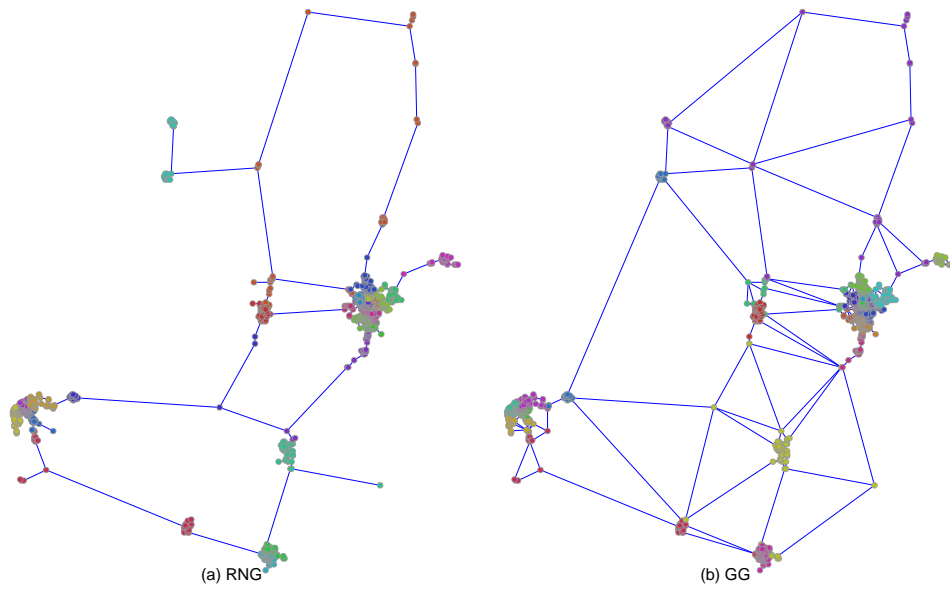


Fig. A38 Visualization of community structures in Sendai before node removal. $N = 1024$ nodes are located by the inverse order of population (Inv.). Different colors represent different communities estimated by Louvain algorithm. There are different community formations compared to Figure A37.

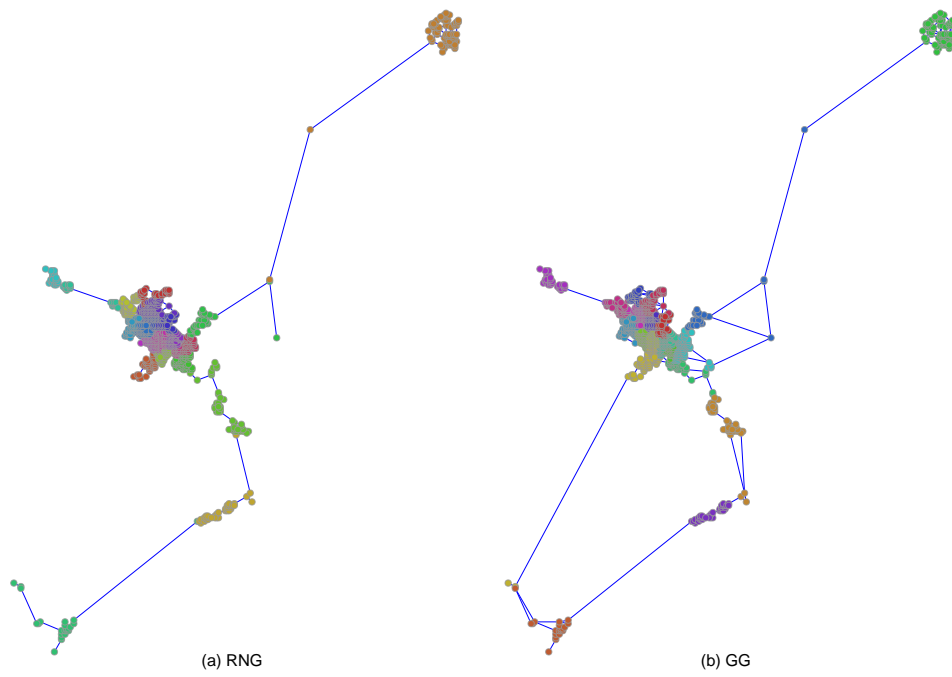


Fig. A39 Visualization of community structures in Sapporo before node removal. $N = 1024$ nodes are located by the decreasing order of population (Pop.). Different colors represent different communities estimated by Louvain algorithm. There are clear community formations particularly in densely populated areas.

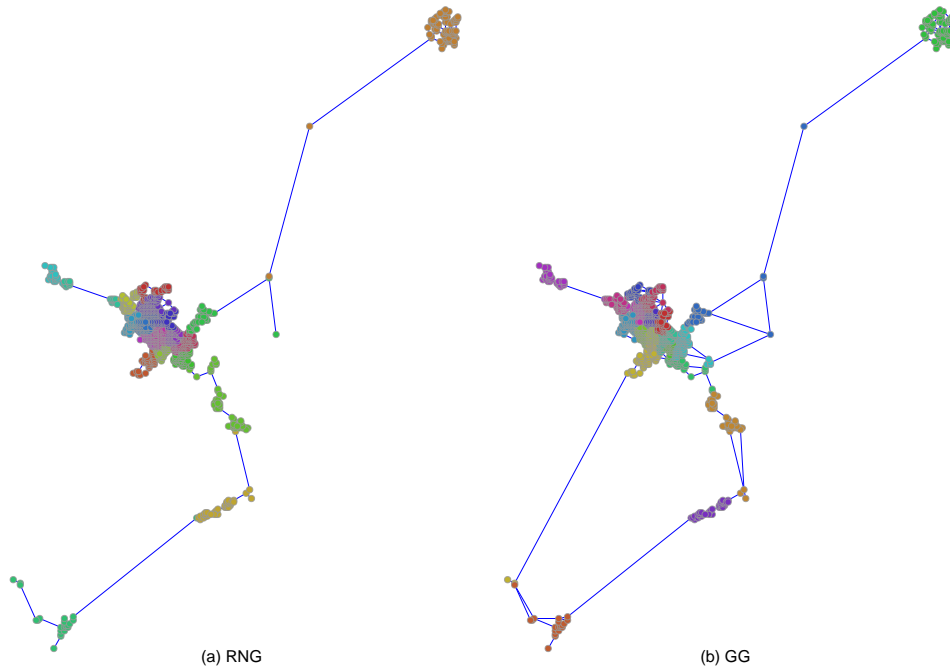


Fig. A40 Visualization of community structures in Sapporo before node removal. $N = 1024$ nodes are located by the inverse order of population (Inv.). Different colors represent different communities estimated by Louvain algorithm. There are different community formations compared to Figure A39.

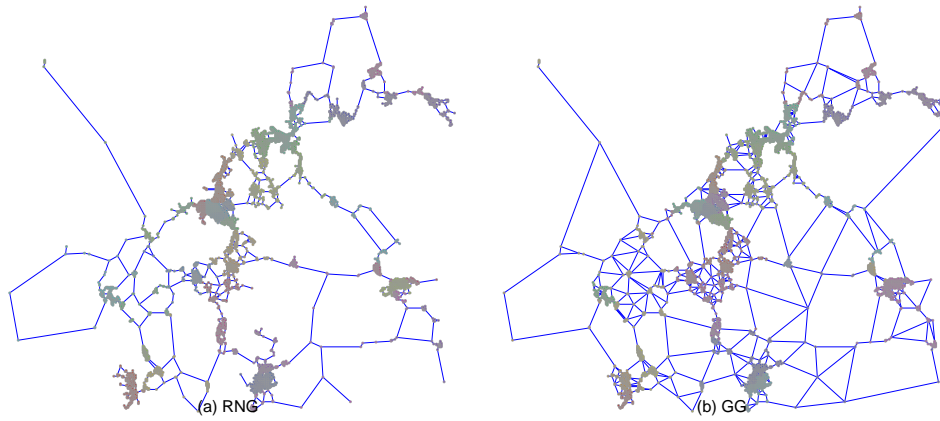


Fig. A41 Visualization of community structures in Fukuoka before node removal. $N = 5041$ nodes are located by the decreasing order of population (Pop.). Different colors represent different communities estimated by Louvain algorithm. There are clear community formations particularly in densely populated areas.

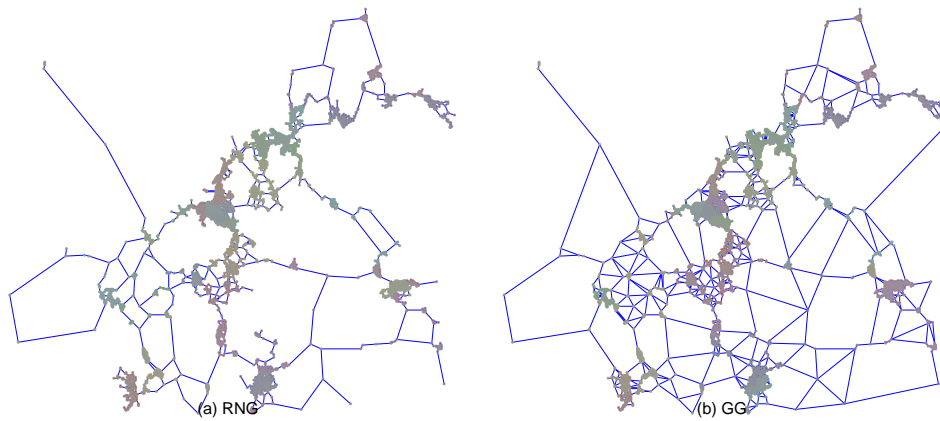


Fig. A42 Visualization of community structures in Fukuoka before node removal. $N = 5041$ nodes are located by the inverse order of population (Inv.). Different colors represent different communities estimated by Louvain algorithm. There are different community formations compared to Figure A41.

.2 Visualization maps, after 10% node removals

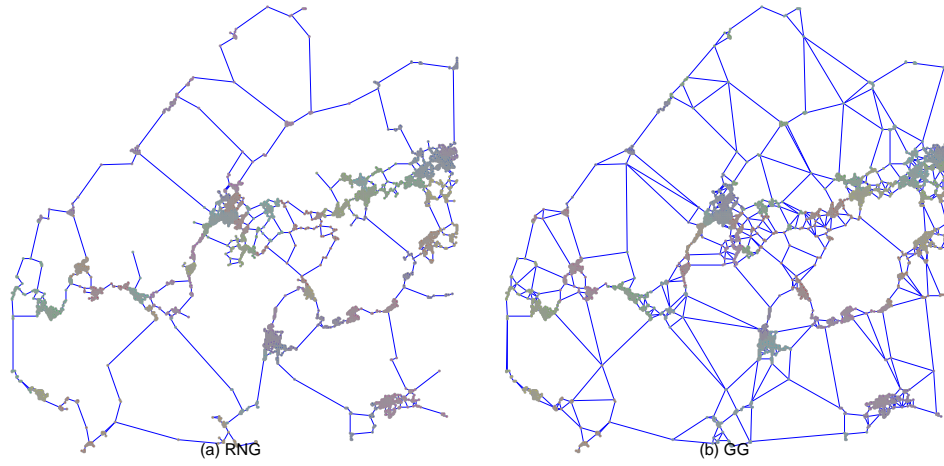


Fig. A43 Visualization of community structures in Hiroshima before node removal. $N = 5041$ nodes are located by the decreasing order of population (Pop.). Different colors represent different communities estimated by Louvain algorithm. There are clear community formations particularly in densely populated areas.

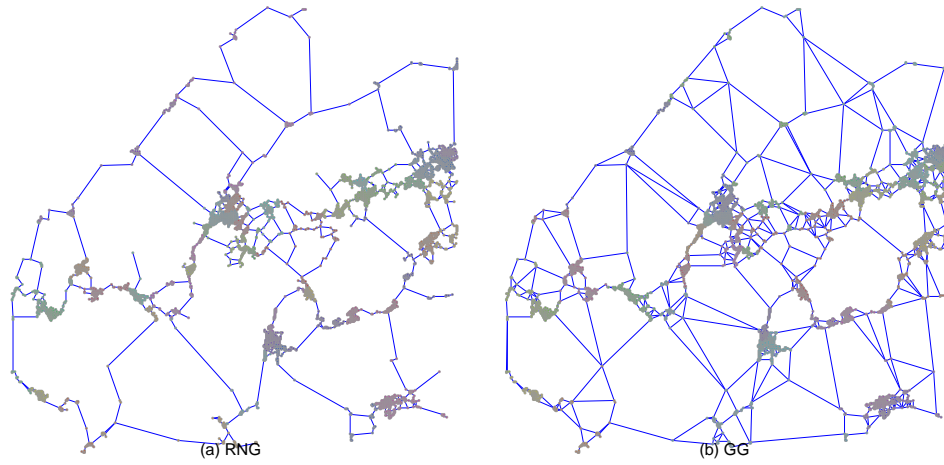


Fig. A44 Visualization of community structures in Hiroshima before node removal. $N = 5041$ nodes are located by the inverse order of population (Inv.). Different colors represent different communities estimated by Louvain algorithm. There are different community formations compared to Figure A43.

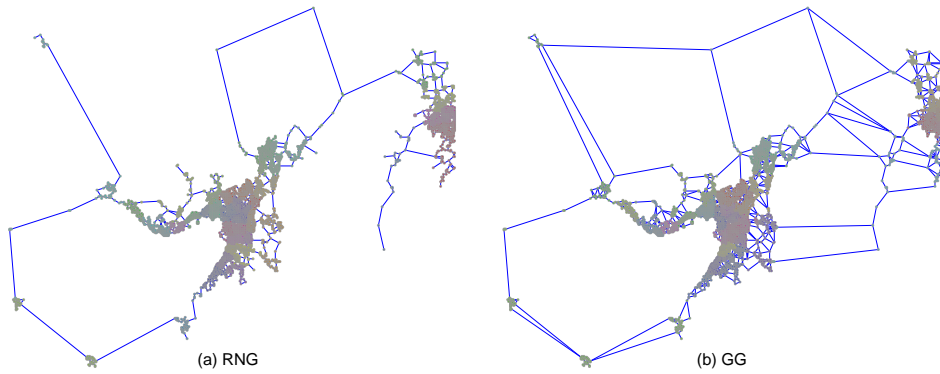


Fig. A45 Visualization of community structures in Keihan before node removal. $N = 5041$ nodes are located by the decreasing order of population (Pop.). Different colors represent different communities estimated by Louvain algorithm. There are clear community formations particularly in densely populated areas.

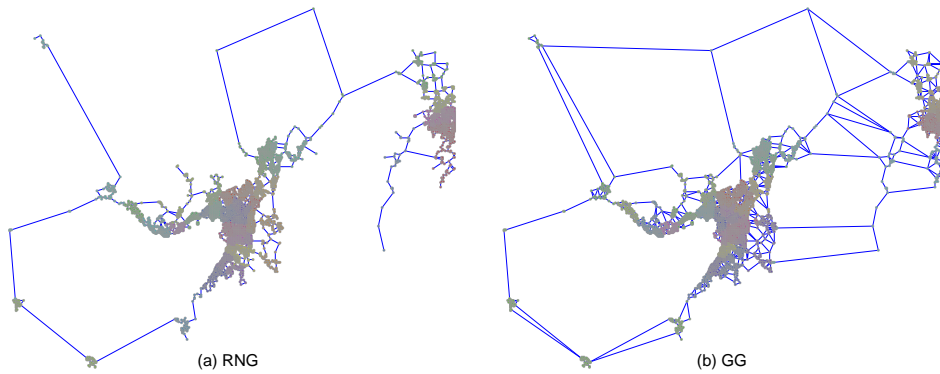


Fig. A46 Visualization of community structures in Keihan before node removal. $N = 5041$ nodes are located by the inverse order of population (Inv.). Different colors represent different communities estimated by Louvain algorithm. There are different community formations compared to Figure A45.

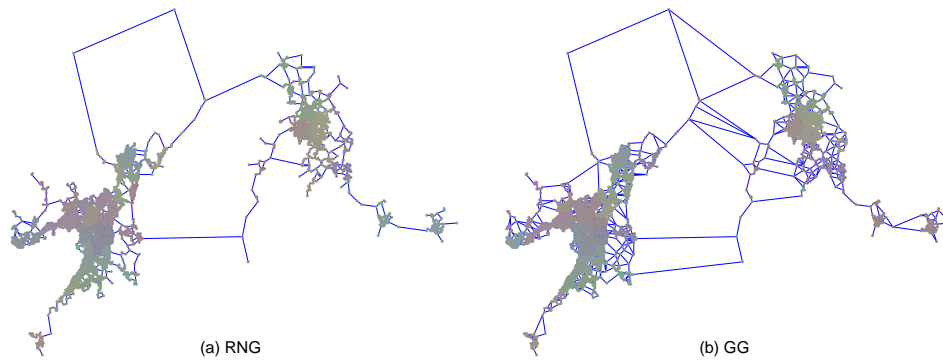


Fig. A47 Visualization of community structures in Nagoya before node removal. $N = 5041$ nodes are located by the decreasing order of population (Pop.). Different colors represent different communities estimated by Louvain algorithm. There are clear community formations particularly in densely populated areas.

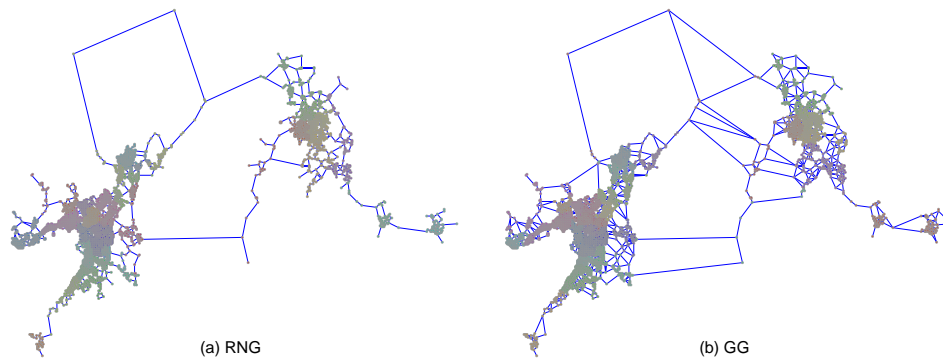


Fig. A48 Visualization of community structures in Nagoya before node removal. $N = 5041$ nodes are located by the inverse order of population (Inv.). Different colors represent different communities estimated by Louvain algorithm. There are different community formations compared to Figure A47.

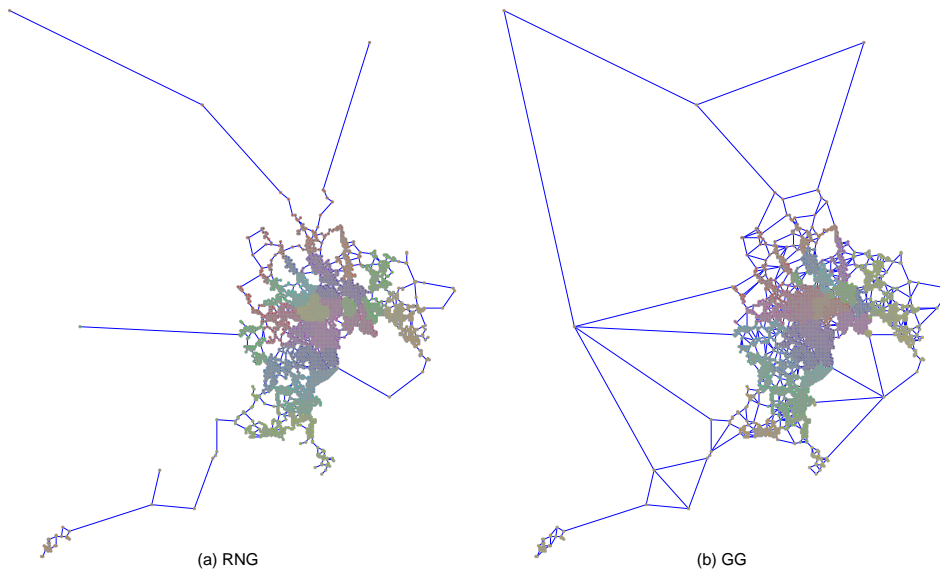


Fig. A49 Visualization of community structures in Tokyo before node removal. $N = 5041$ nodes are located by the decreasing order of population (Pop.). Different colors represent different communities estimated by Louvain algorithm. There are clear community formations particularly in densely populated areas.

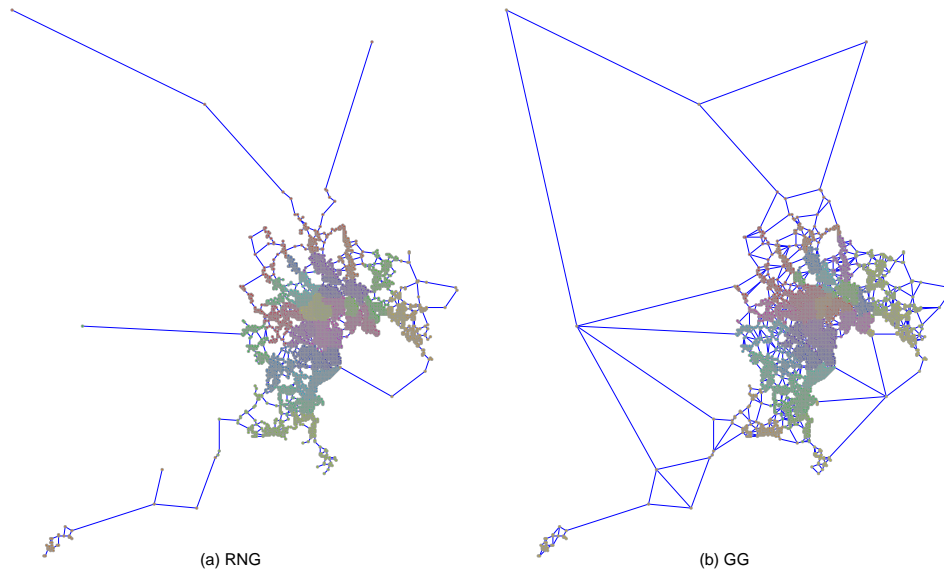


Fig. A50 Visualization of community structures in Tokyo before node removal. $N = 5041$ nodes are located by the inverse order of population (Inv.). Different colors represent different communities estimated by Louvain algorithm. There are different community formations compared to Figure A49.

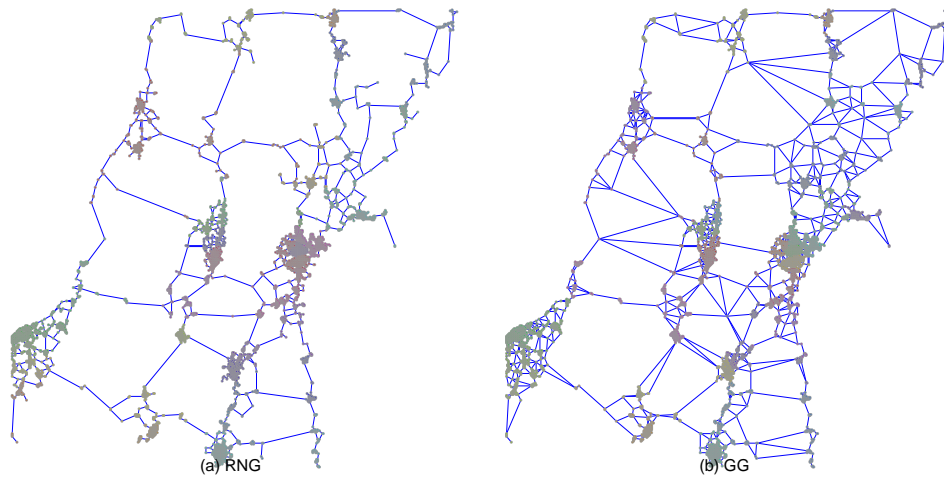


Fig. A51 Visualization of community structures in Sendai before node removal. $N = 5041$ nodes are located by the decreasing order of population (Pop.). Different colors represent different communities estimated by Louvain algorithm. There are clear community formations particularly in densely populated areas.

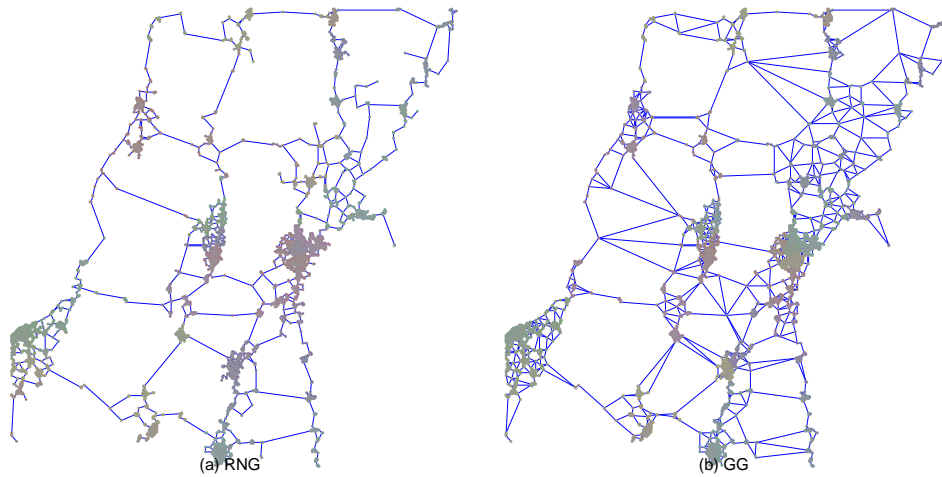


Fig. A52 Visualization of community structures in Sendai before node removal. $N = 5041$ nodes are located by the inverse order of population (Inv.). Different colors represent different communities estimated by Louvain algorithm. There are different community formations compared to Figure A51.

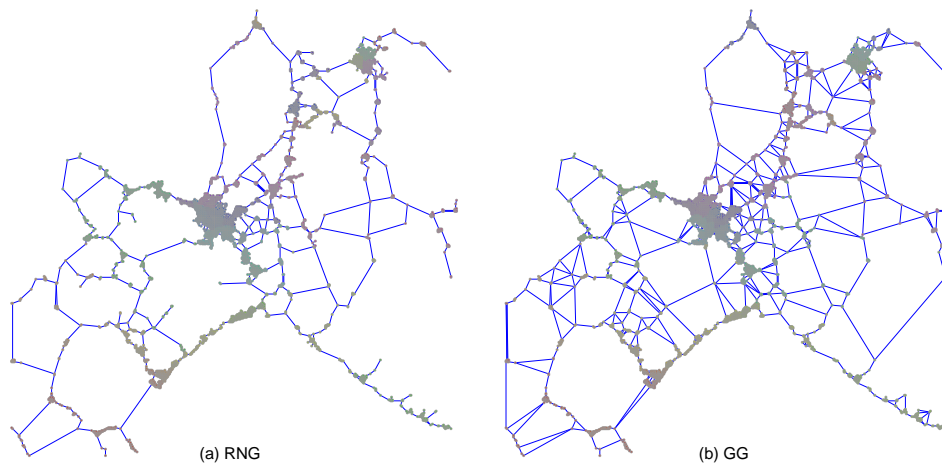


Fig. A53 Visualization of community structures in Sapporo before node removal. $N = 5041$ nodes are located by the decreasing order of population (Pop.). Different colors represent different communities estimated by Louvain algorithm. There are clear community formations particularly in densely populated areas.

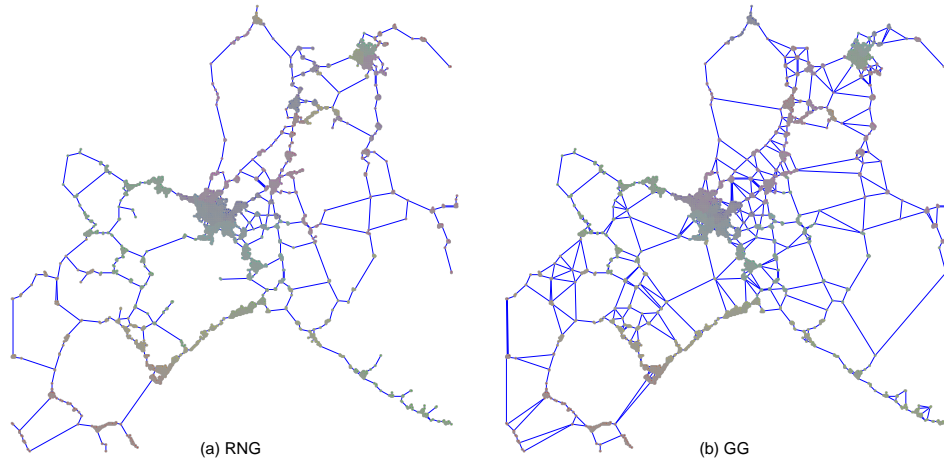


Fig. A54 Visualization of community structures in Sapporo before node removal. $N = 5041$ nodes are located by the inverse order of population (Inv.). Different colors represent different communities estimated by Louvain algorithm. There are different community formations compared to Figure A53.

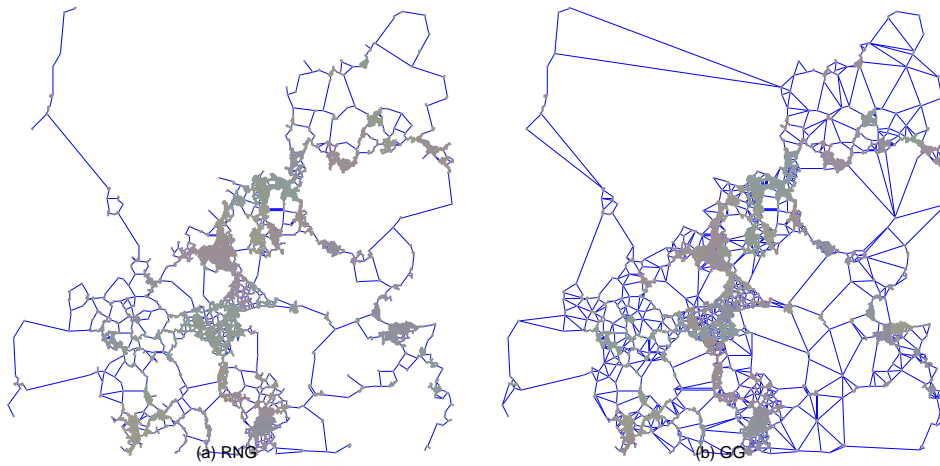


Fig. A55 Visualization of community structures in Fukuoka before node removal. $N = 10000$ nodes are located by the decreasing order of population (Pop.). Different colors represent different communities estimated by Louvain algorithm. There are clear community formations particularly in densely populated areas.

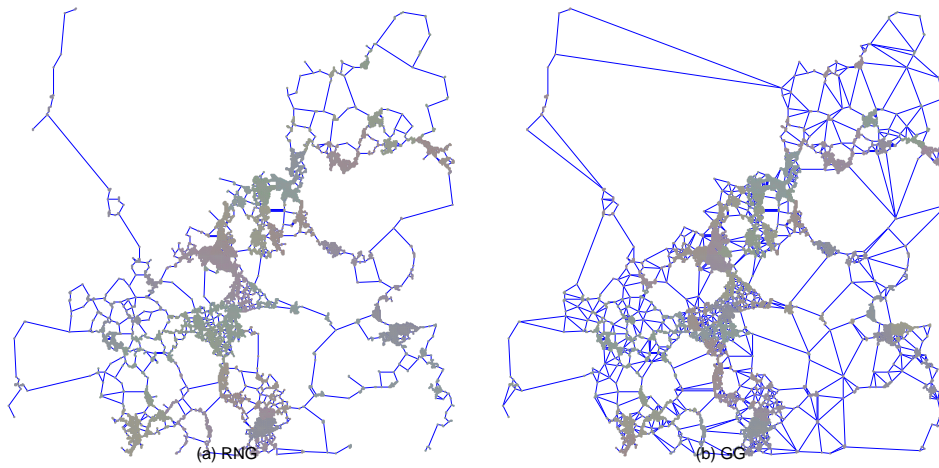


Fig. A56 Visualization of community structures in Fukuoka before node removal. $N = 10000$ nodes are located by the inverse order of population (Inv.). Different colors represent different communities estimated by Louvain algorithm. There are different community formations compared to Figure A55.

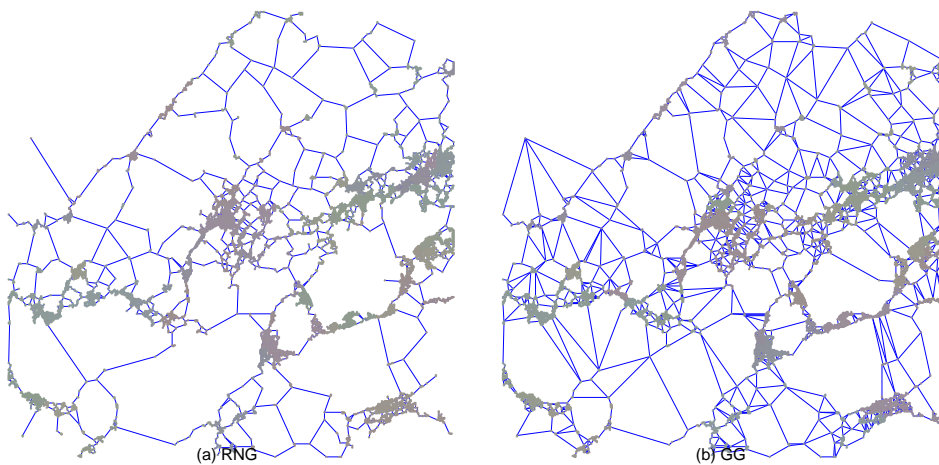


Fig. A57 Visualization of community structures in Hiroshima before node removal. $N = 10000$ nodes are located by the decreasing order of population (Pop.). Different colors represent different communities estimated by Louvain algorithm. There are clear community formations particularly in densely populated areas.

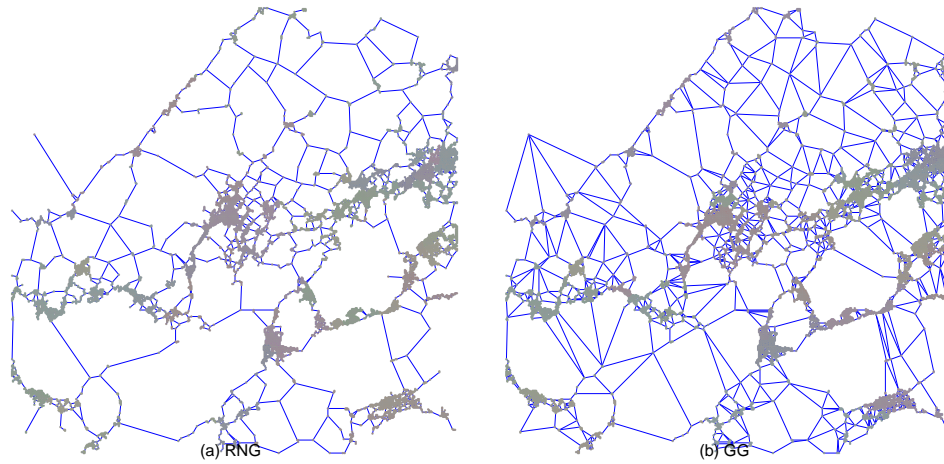


Fig. A58 Visualization of community structures in Hiroshima before node removal. $N = 10000$ nodes are located by the inverse order of population (Inv.). Different colors represent different communities estimated by Louvain algorithm. There are different community formations compared to Figure A57.

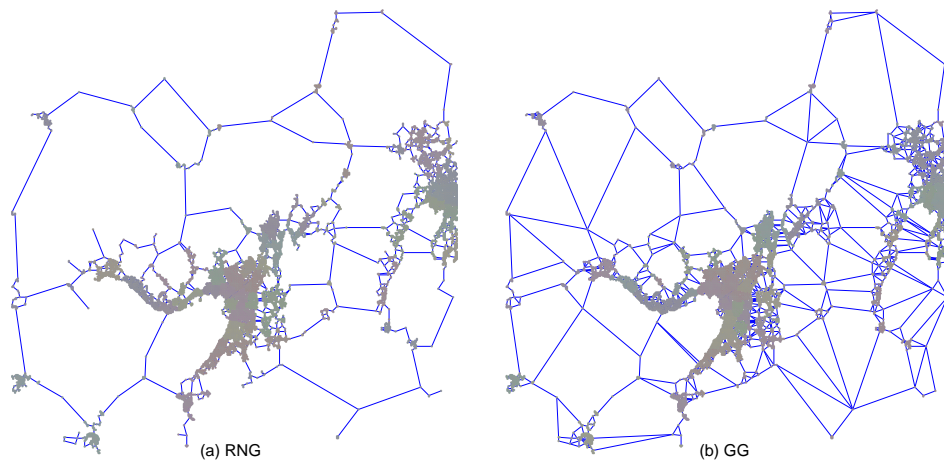


Fig. A59 Visualization of community structures in Keihan before node removal. $N = 10000$ nodes are located by the decreasing order of population (Pop.). Different colors represent different communities estimated by Louvain algorithm. There are clear community formations particularly in densely populated areas.

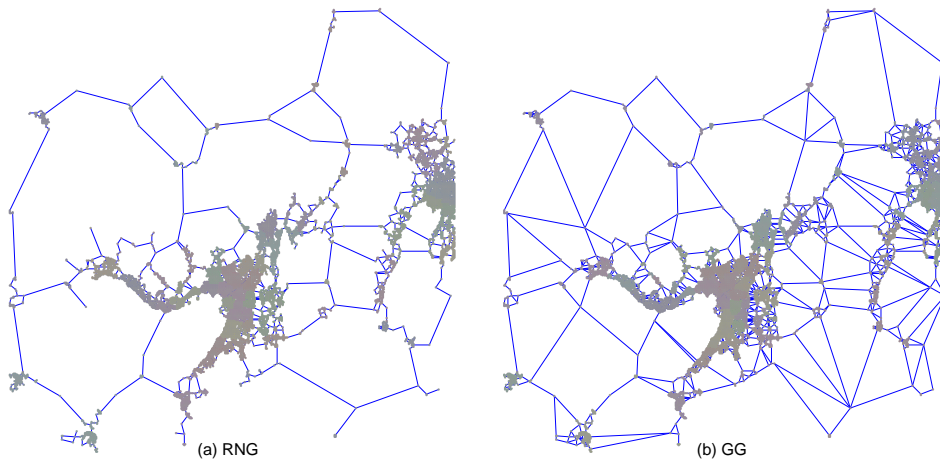


Fig. A60 Visualization of community structures in Keihan before node removal. $N = 10000$ nodes are located by the inverse order of population (Inv.). Different colors represent different communities estimated by Louvain algorithm. There are different community formations compared to Figure A59.

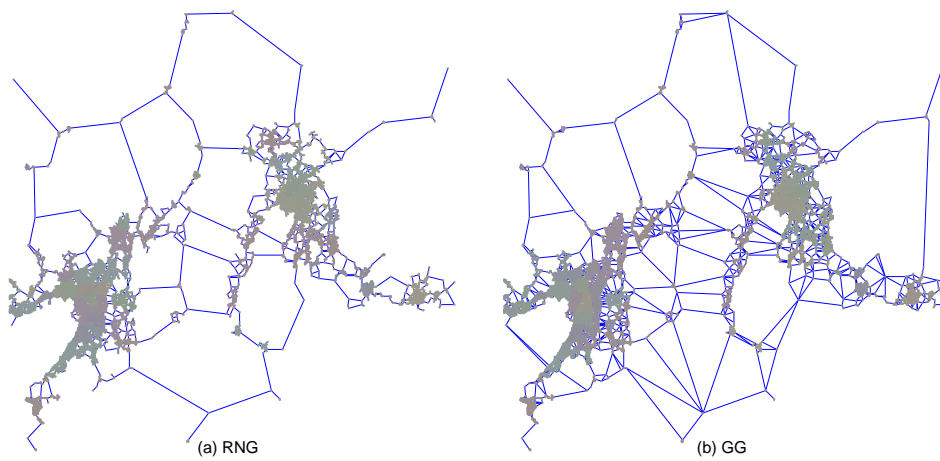


Fig. A61 Visualization of community structures in Nagoya before node removal. $N = 10000$ nodes are located by the decreasing order of population (Pop.). Different colors represent different communities estimated by Louvain algorithm. There are clear community formations particularly in densely populated areas.

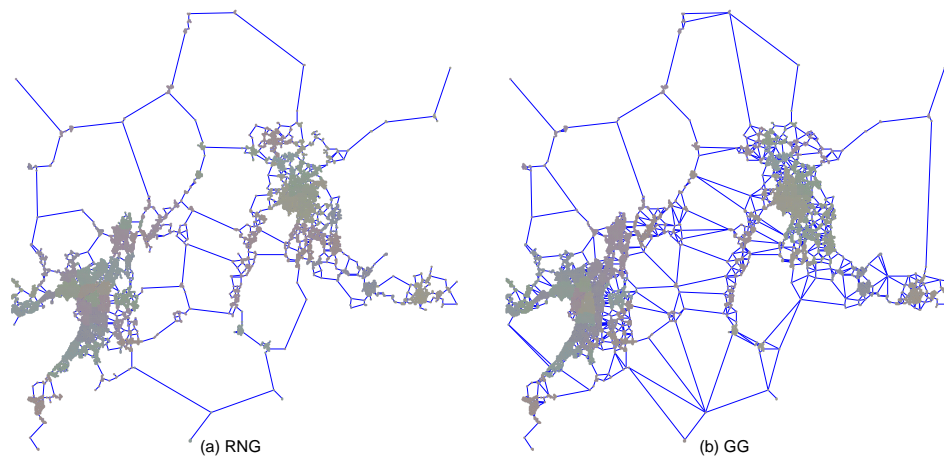


Fig. A62 Visualization of community structures in Nagoya before node removal. $N = 10000$ nodes are located by the inverse order of population (Inv.). Different colors represent different communities estimated by Louvain algorithm. There are different community formations compared to Figure A61.

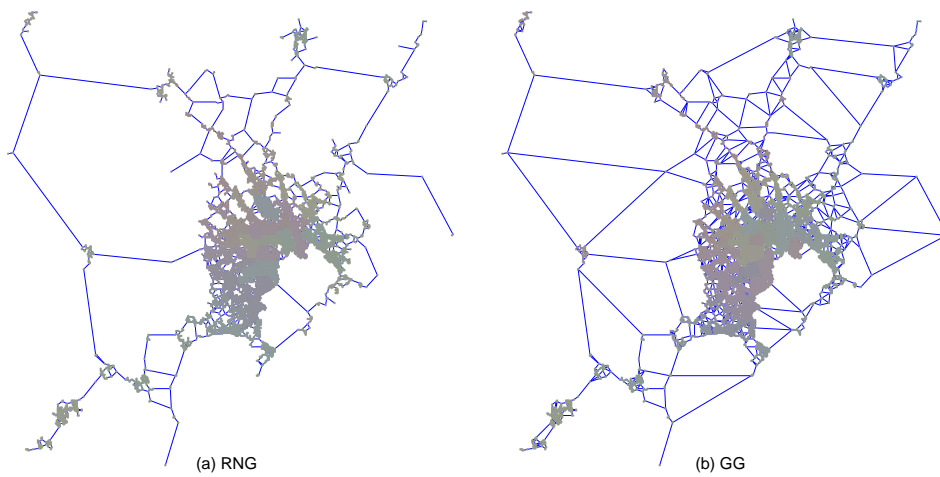


Fig. A63 Visualization of community structures in Tokyo before node removal. $N = 10000$ nodes are located by the decreasing order of population (Pop.). Different colors represent different communities estimated by Louvain algorithm. There are clear community formations particularly in densely populated areas.

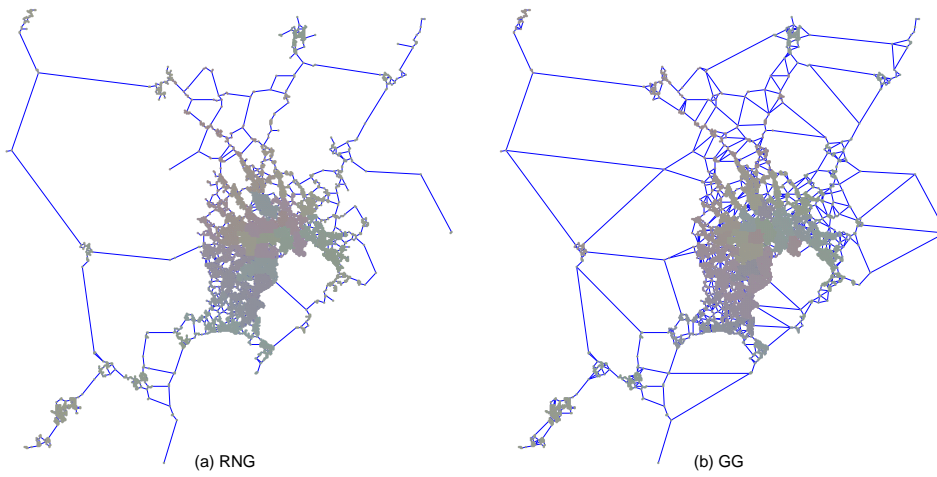


Fig. A64 Visualization of community structures in Tokyo before node removal. $N = 10000$ nodes are located by the inverse order of population (Inv.). Different colors represent different communities estimated by Louvain algorithm. There are different community formations compared to Figure A63.

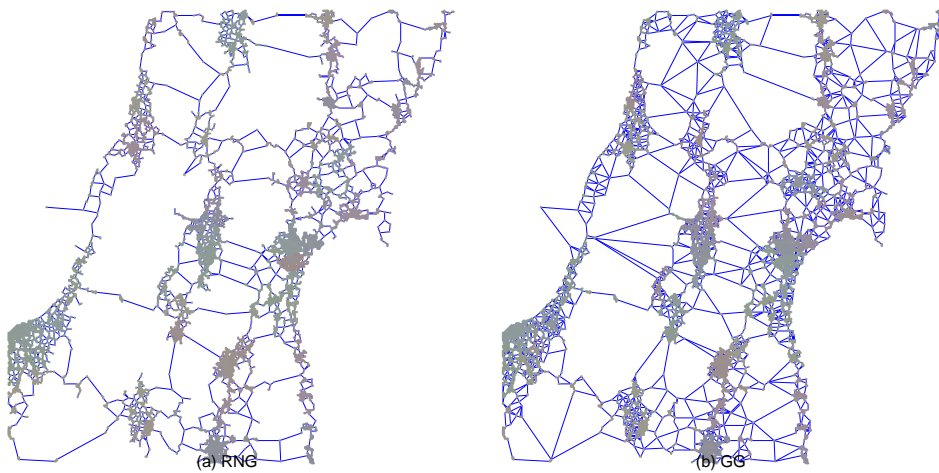


Fig. A65 Visualization of community structures in Sendai before node removal. $N = 10000$ nodes are located by the decreasing order of population (Pop.). Different colors represent different communities estimated by Louvain algorithm. There are clear community formations particularly in densely populated areas.

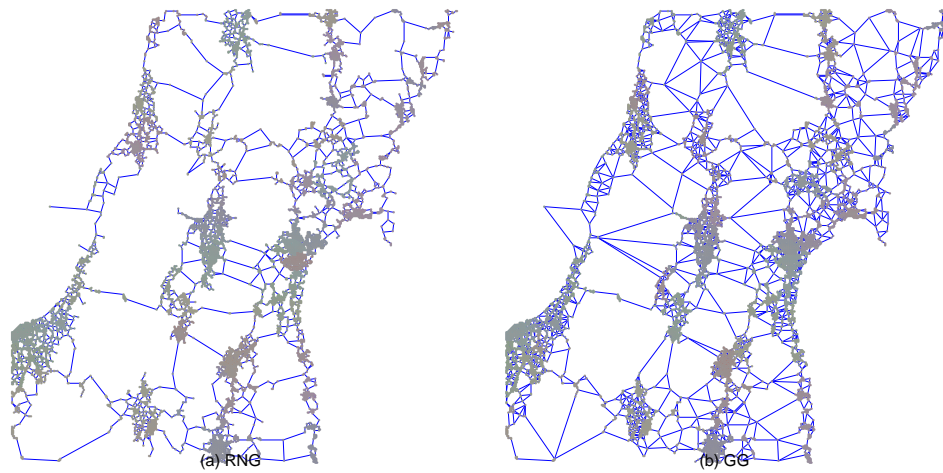


Fig. A66 Visualization of community structures in Sendai before node removal. $N = 10000$ nodes are located by the inverse order of population (Inv.). Different colors represent different communities estimated by Louvain algorithm. There are different community formations compared to Figure A65.

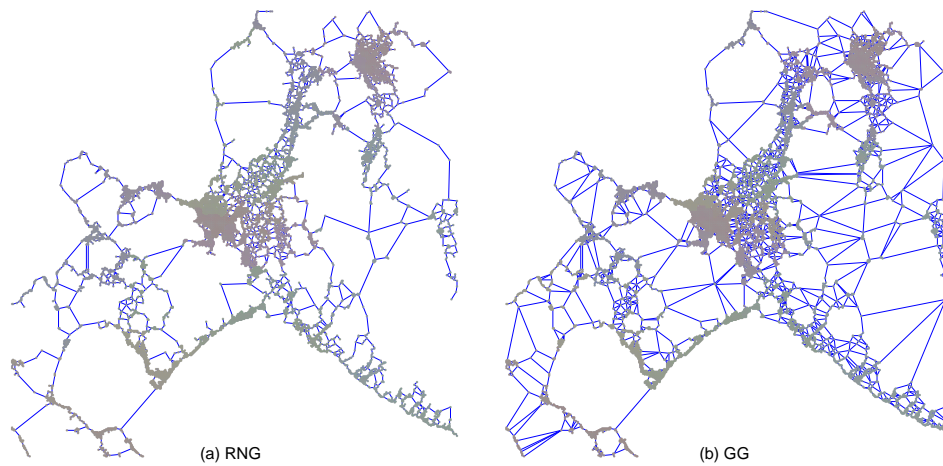


Fig. A67 Visualization of community structures in Sapporo before node removal. $N = 10000$ nodes are located by the decreasing order of population (Pop.). Different colors represent different communities estimated by Louvain algorithm. There are clear community formations particularly in densely populated areas.

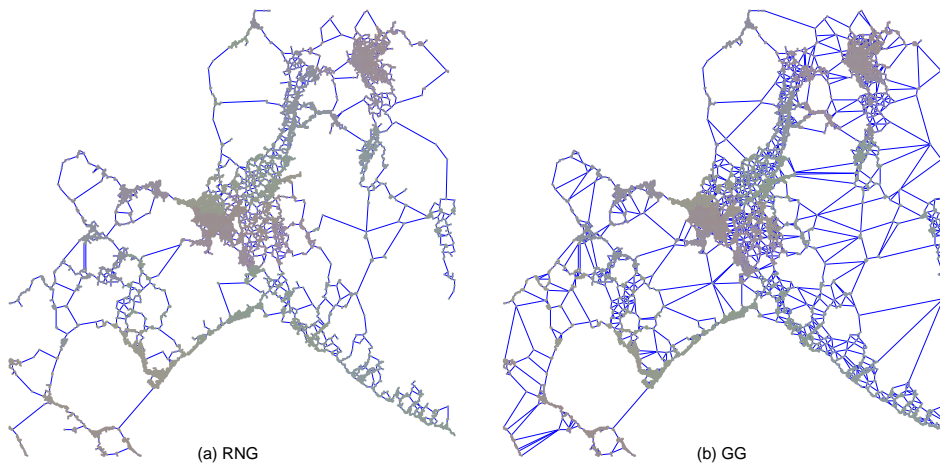


Fig. A68 Visualization of community structures in Sapporo before node removal. $N = 10000$ nodes are located by the inverse order of population (Inv.). Different colors represent different communities estimated by Louvain algorithm. There are different community formations compared to Figure A67.

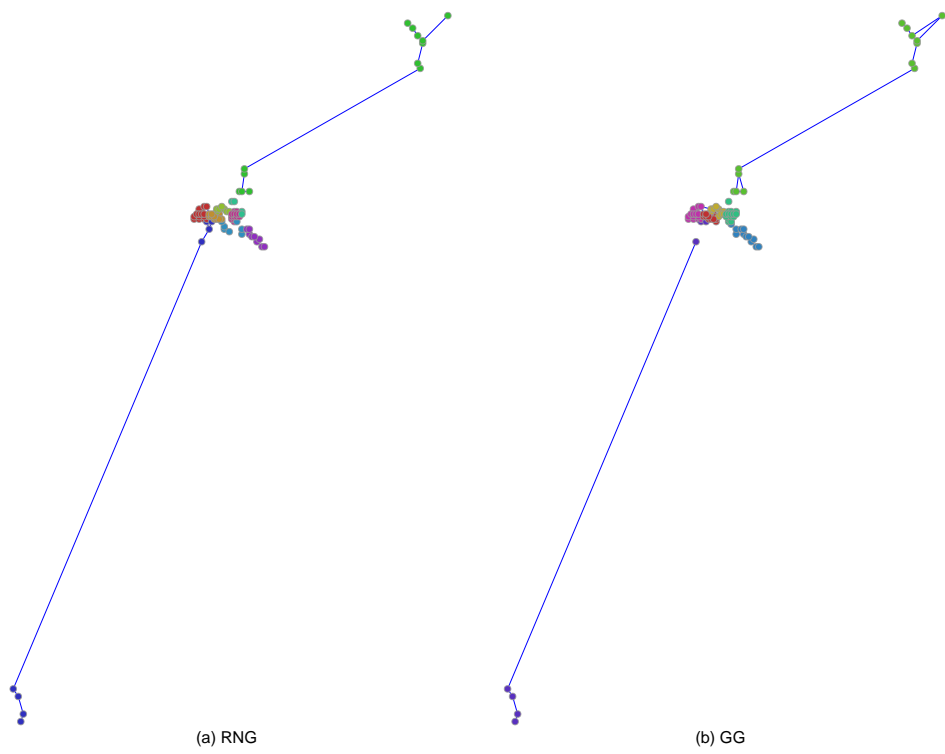


Fig. A69 Fukuoka networks with $N = 100$ nodes after 10% node removals by recalculated betweenness (RB) attacks. The locations of nodes are selected by decreasing order of population (Pop.). The fragmentation is observed by removing links between communities especially in densely populated areas

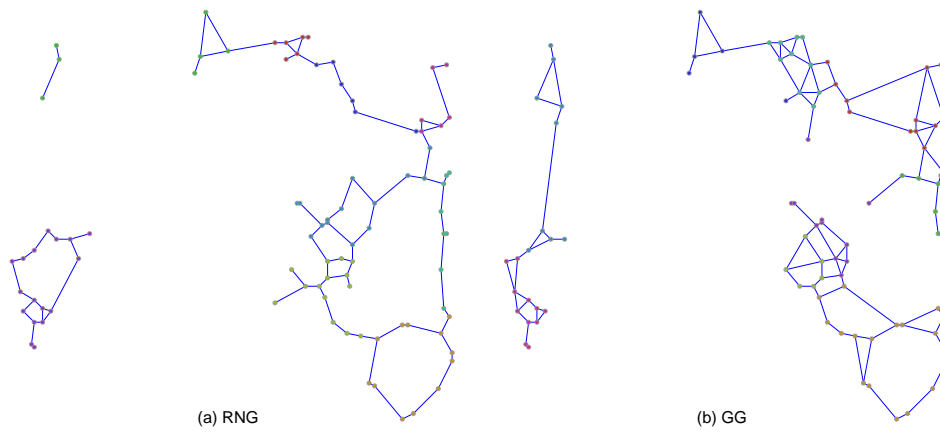


Fig. A70 Fukuoka networks with $N = 100$ nodes after 10% node removals by recalculated betweenness (RB) attacks. The locations of nodes are selected by inverse order of population (Inv.). The fragmentation is observed by removing links between communities which are different as compared to Figure A69.

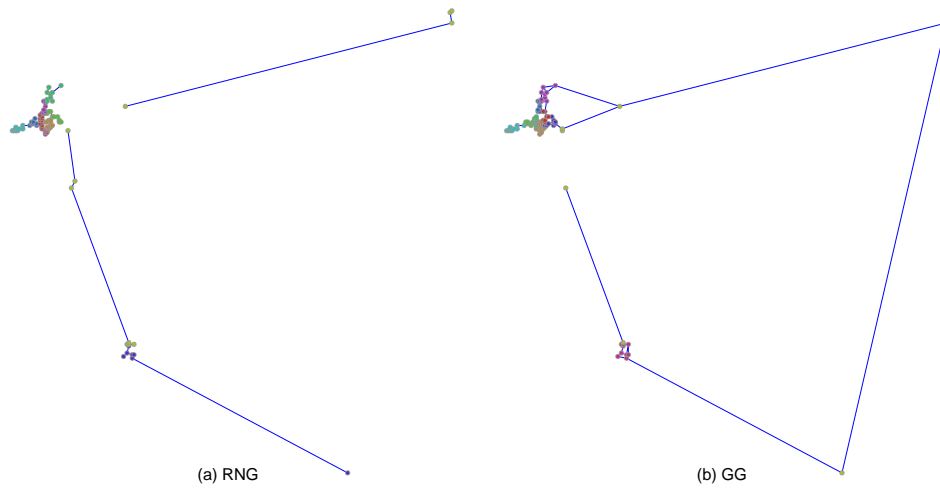


Fig. A71 Hiroshima networks with $N = 100$ nodes after 10% node removals by recalculated betweenness (RB) attacks. The locations of nodes are selected by decreasing order of population (Pop.). The fragmentation is observed by removing links between communities especially in densely populated areas

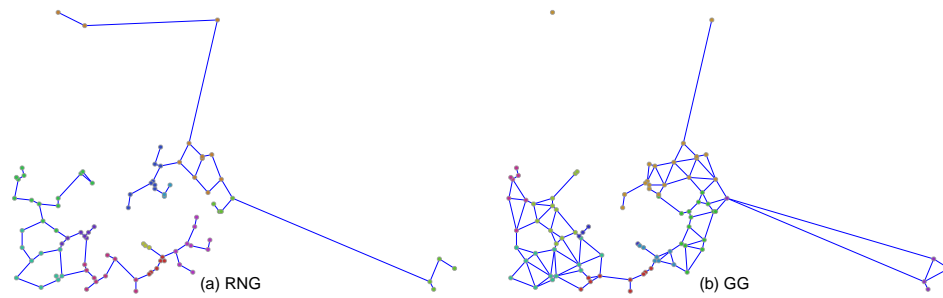


Fig. A72 Hiroshima networks with $N = 100$ nodes after 10% node removals by recalculated betweenness (RB) attacks. The locations of nodes are selected by inverse order of population (Inv.). The fragmentation is observed by removing links between communities which are different as compared to Figure A71.

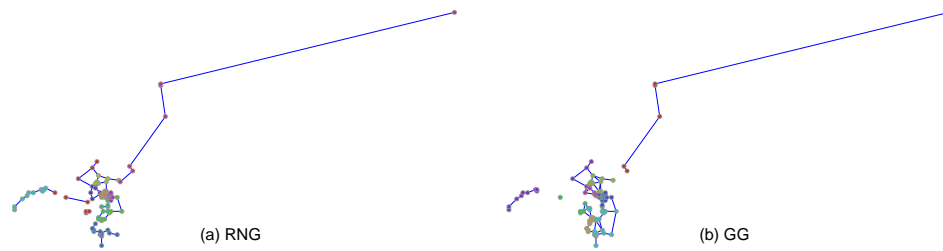


Fig. A73 Keihan networks with $N = 100$ nodes after 10% node removals by recalculated betweenness (RB) attacks. The locations of nodes are selected by decreasing order of population (Pop.). The fragmentation is observed by removing links between communities especially in densely populated areas

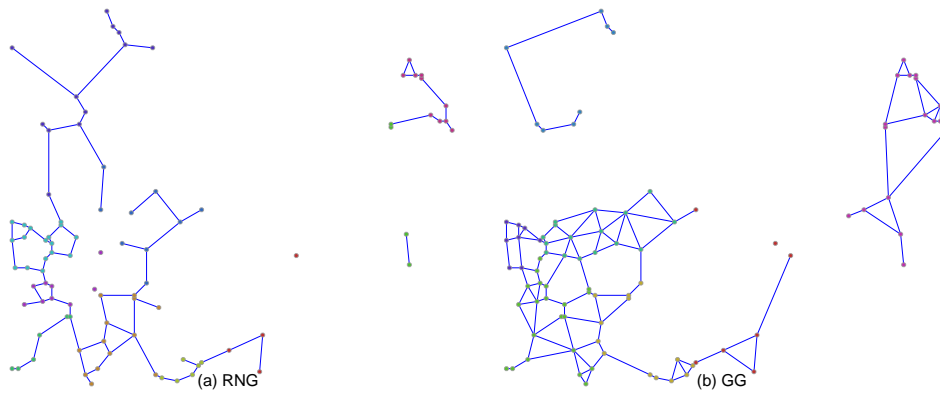


Fig. A74 Keihan networks with $N = 100$ nodes after 10% node removals by recalculated betweenness (RB) attacks. The locations of nodes are selected by inverse order of population (Inv.). The fragmentation is observed by removing links between communities which are different as compared to Figure A73.

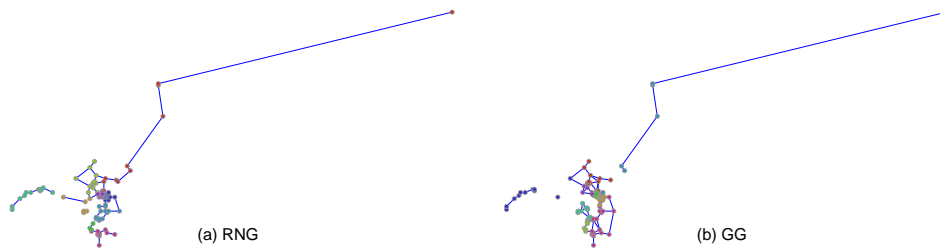


Fig. A75 Nagoya networks with $N = 100$ nodes after 10% node removals by recalculated betweenness (RB) attacks. The locations of nodes are selected by decreasing order of population (Pop.). The fragmentation is observed by removing links between communities especially in densely populated areas

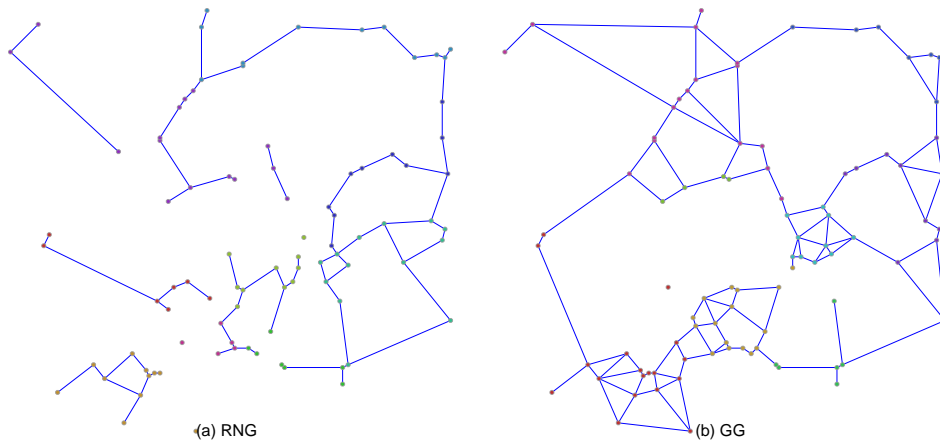


Fig. A76 Nagoya networks with $N = 100$ nodes after 10% node removals by recalculated betweenness (RB) attacks. The locations of nodes are selected by inverse order of population (Inv.). The fragmentation is observed by removing links between communities which are different as compared to Figure A75.

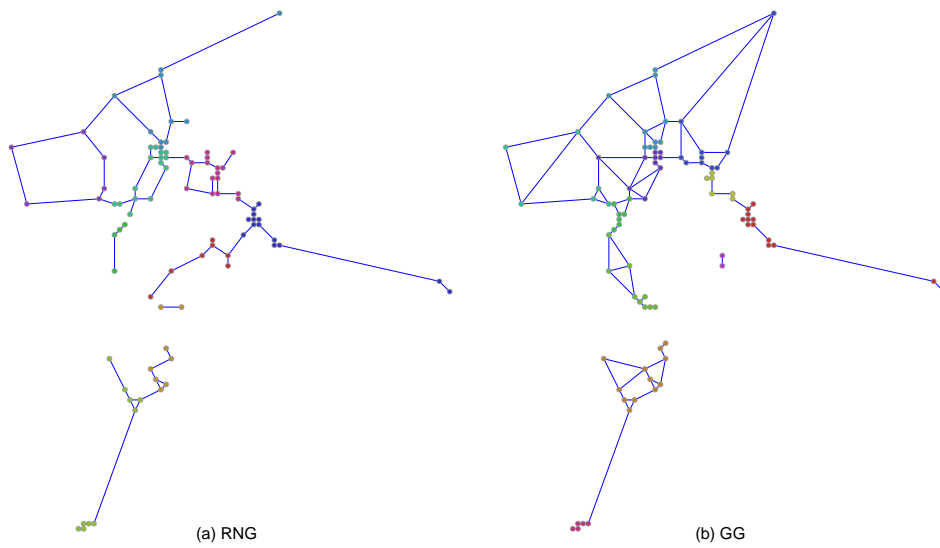


Fig. A77 Tokyo networks with $N = 100$ nodes after 10% node removals by recalculated betweenness (RB) attacks. The locations of nodes are selected by decreasing order of population (Pop.). The fragmentation is observed by removing links between communities especially in densely populated areas

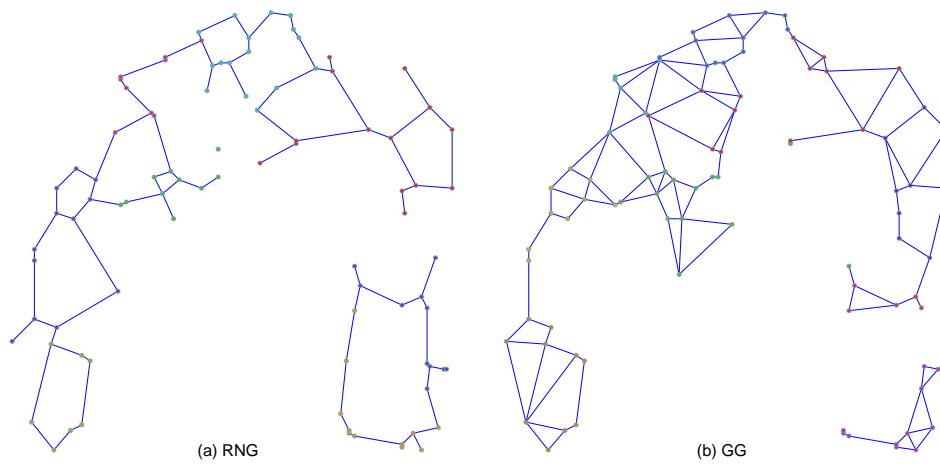


Fig. A78 Tokyo networks with $N = 100$ nodes after 10% node removals by recalculated betweenness (RB) attacks. The locations of nodes are selected by inverse order of population (Inv.). The fragmentation is observed by removing links between communities which are different as compared to Figure A77.



Fig. A79 Sendai networks with $N = 100$ nodes after 10% node removals by recalculated betweenness (RB) attacks. The locations of nodes are selected by decreasing order of population (Pop.). The fragmentation is observed by removing links between communities especially in densely populated areas

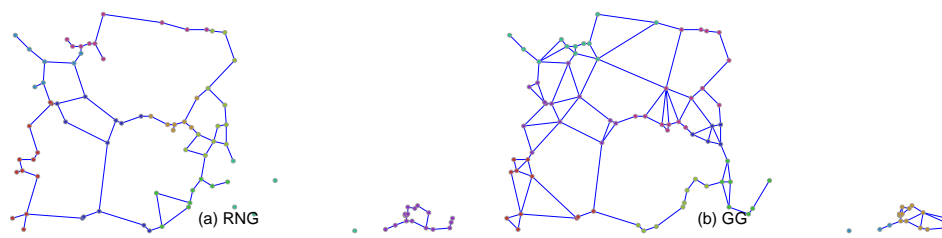


Fig. A80 Sendai networks with $N = 100$ nodes after 10% node removals by recalculated betweenness (RB) attacks. The locations of nodes are selected by inverse order of population (Inv.). The fragmentation is observed by removing links between communities which are different as compared to Figure A79.

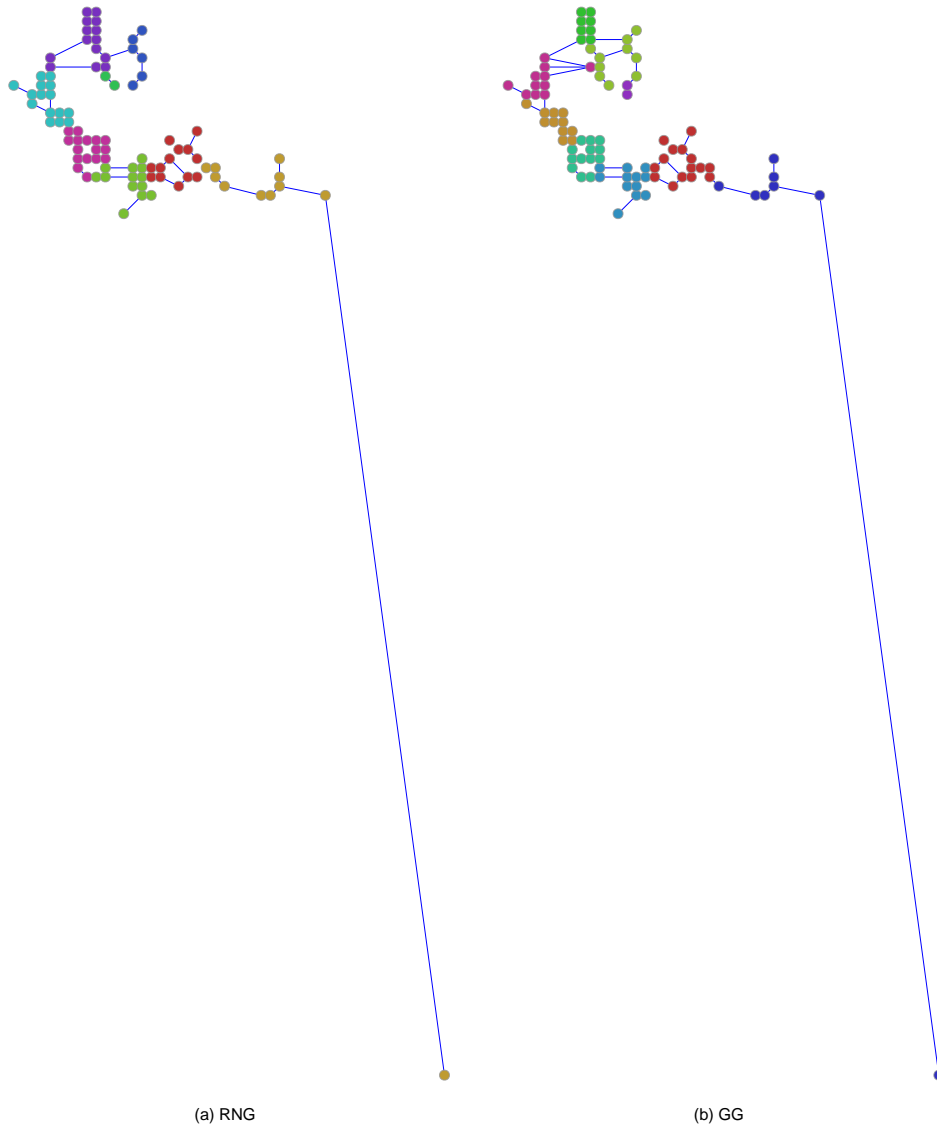


Fig. A81 Sapporo networks with $N = 100$ nodes after 10% node removals by recalculated betweenness (RB) attacks. The locations of nodes are selected by decreasing order of population (Pop.). The fragmentation is observed by removing links between communities especially in densely populated areas

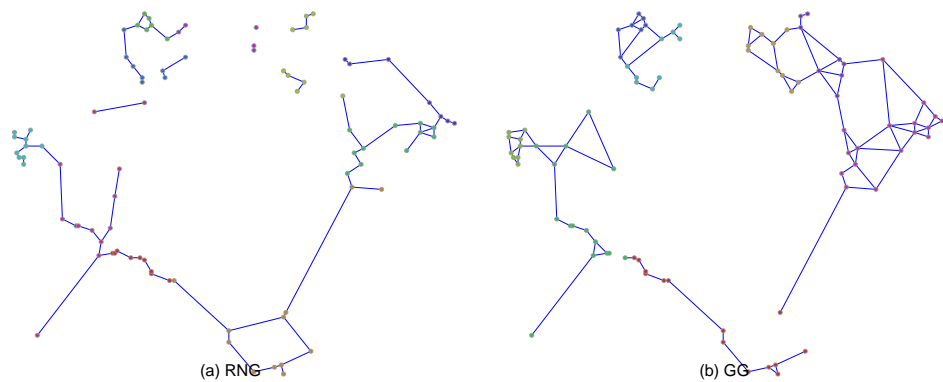


Fig. A82 Sapporo networks with $N = 100$ nodes after 10% node removals by recalculated betweenness (RB) attacks. The locations of nodes are selected by inverse order of population (Inv.). The fragmentation is observed by removing links between communities which are different as compared to Figure A81.

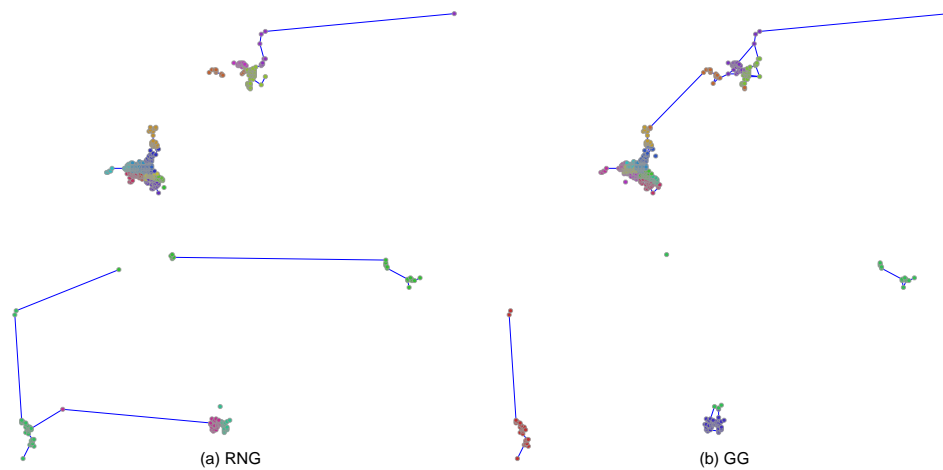


Fig. A83 Fukuoka networks with $N = 484$ nodes after 10% node removals by recalculated betweenness (RB) attacks. The locations of nodes are selected by decreasing order of population (Pop.). The fragmentation is observed by removing links between communities especially in densely populated areas

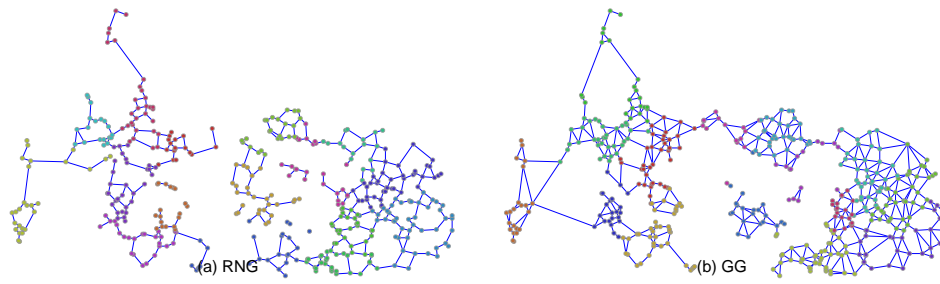


Fig. A84 Fukuoka networks with $N = 484$ nodes after 10% node removals by recalculated betweenness (RB) attacks. The locations of nodes are selected by inverse order of population (Inv.). The fragmentation is observed by removing links between communities which are different as compared to Figure A83.

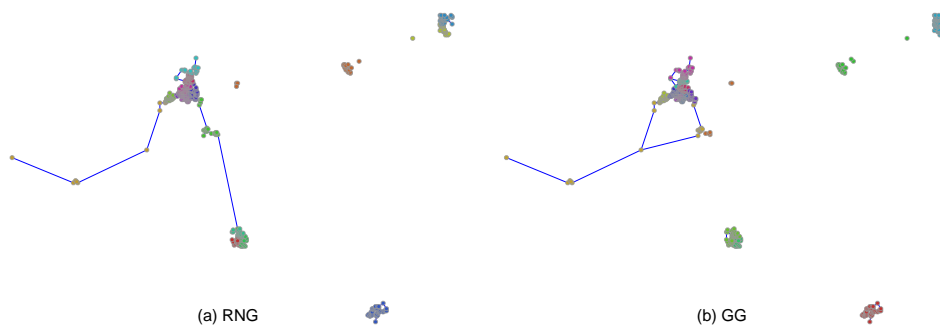


Fig. A85 Hiroshima networks with $N = 484$ nodes after 10% node removals by recalculated betweenness (RB) attacks. The locations of nodes are selected by decreasing order of population (Pop.). The fragmentation is observed by removing links between communities especially in densely populated areas

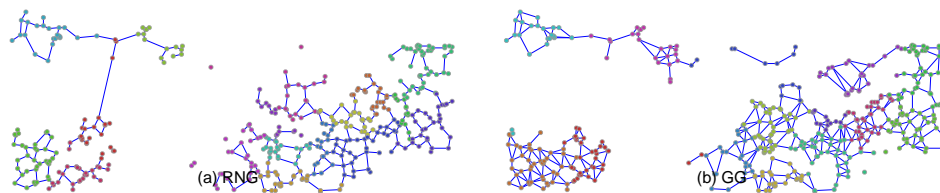


Fig. A86 Hiroshima networks with $N = 484$ nodes after 10% node removals by recalculated betweenness (RB) attacks. The locations of nodes are selected by inverse order of population (Inv.). The fragmentation is observed by removing links between communities which are different as compared to Figure A85.

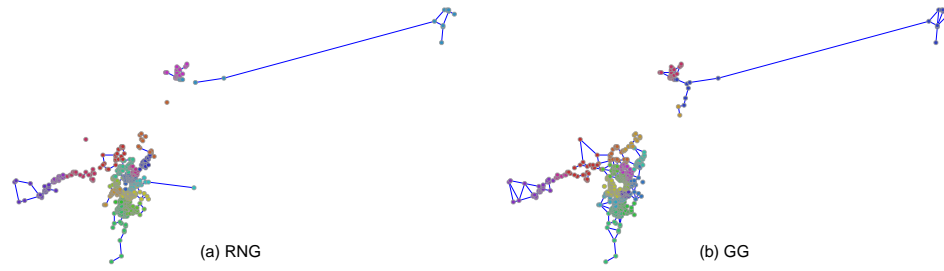


Fig. A87 Keihan networks with $N = 484$ nodes after 10% node removals by recalculated betweenness (RB) attacks. The locations of nodes are selected by decreasing order of population (Pop.). The fragmentation is observed by removing links between communities especially in densely populated areas

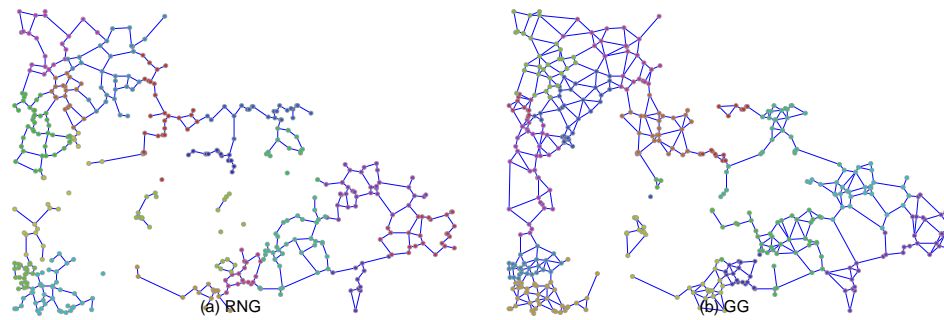


Fig. A88 Keihan networks with $N = 484$ nodes after 10% node removals by recalculated betweenness (RB) attacks. The locations of nodes are selected by inverse order of population (Inv.). The fragmentation is observed by removing links between communities which are different as compared to Figure A87.

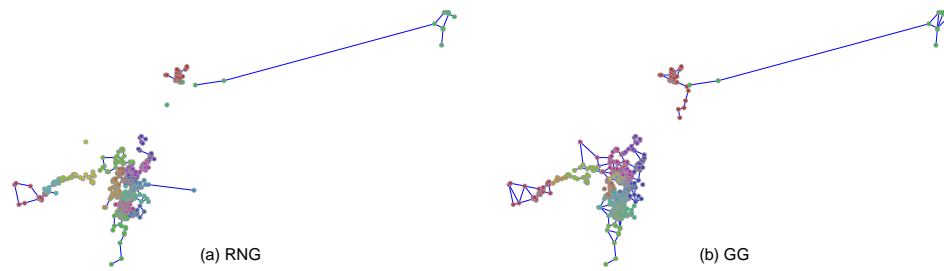


Fig. A89 Nagoya networks with $N = 484$ nodes after 10% node removals by recalculated betweenness (RB) attacks. The locations of nodes are selected by decreasing order of population (Pop.). The fragmentation is observed by removing links between communities especially in densely populated areas

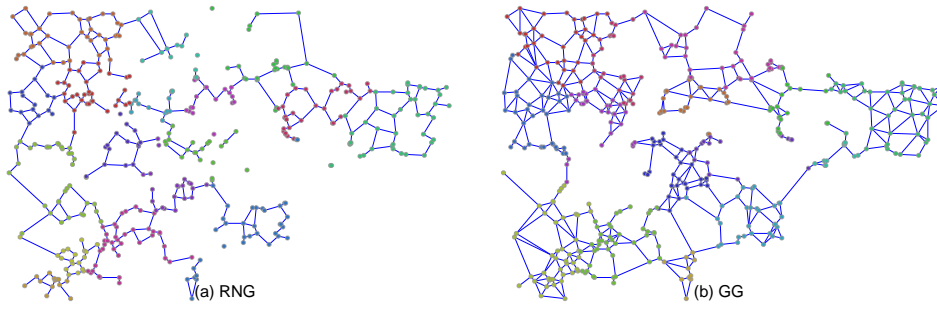


Fig. A90 Nagoya networks with $N = 484$ nodes after 10% node removals by recalculated betweenness (RB) attacks. The locations of nodes are selected by inverse order of population (Inv.). The fragmentation is observed by removing links between communities which are different as compared to Figure A89.

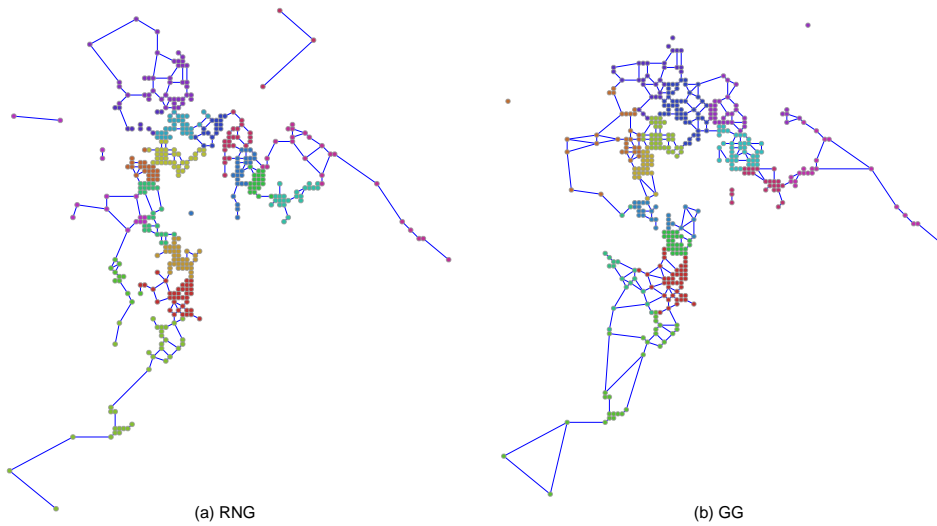


Fig. A91 Tokyo networks with $N = 484$ nodes after 10% node removals by recalculated betweenness (RB) attacks. The locations of nodes are selected by decreasing order of population (Pop.). The fragmentation is observed by removing links between communities especially in densely populated areas

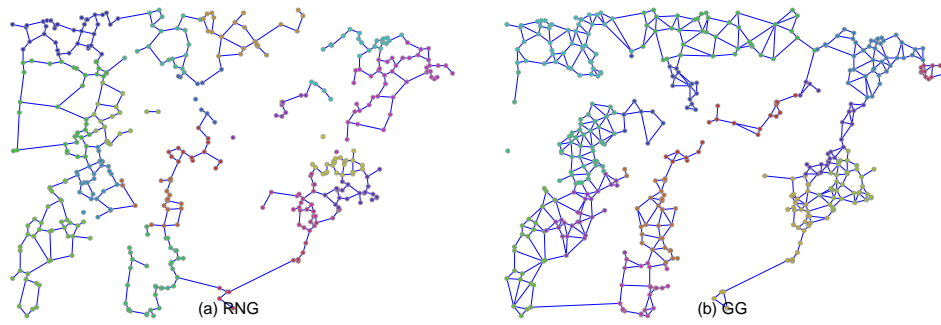


Fig. A92 Tokyo networks with $N = 484$ nodes after 10% node removals by recalculated betweenness (RB) attacks. The locations of nodes are selected by inverse order of population (Inv.). The fragmentation is observed by removing links between communities which are different as compared to Figure A91.

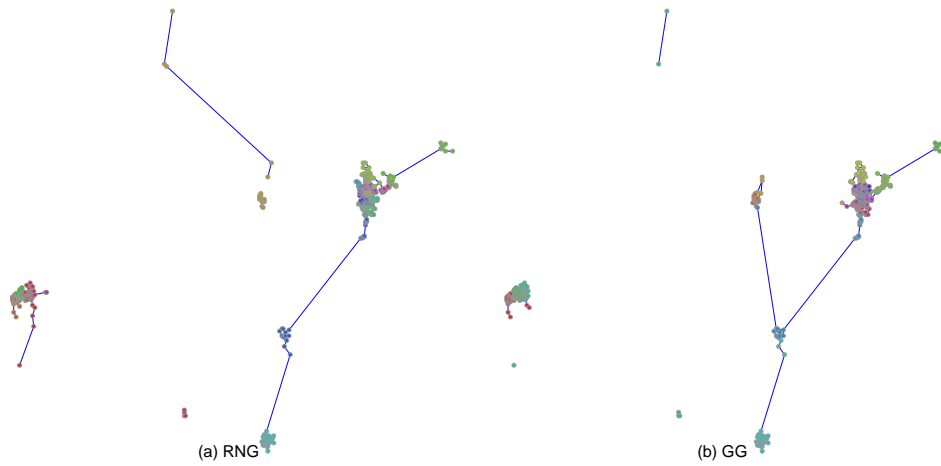


Fig. A93 Sendai networks with $N = 484$ nodes after 10% node removals by recalculated betweenness (RB) attacks. The locations of nodes are selected by decreasing order of population (Pop.). The fragmentation is observed by removing links between communities especially in densely populated areas

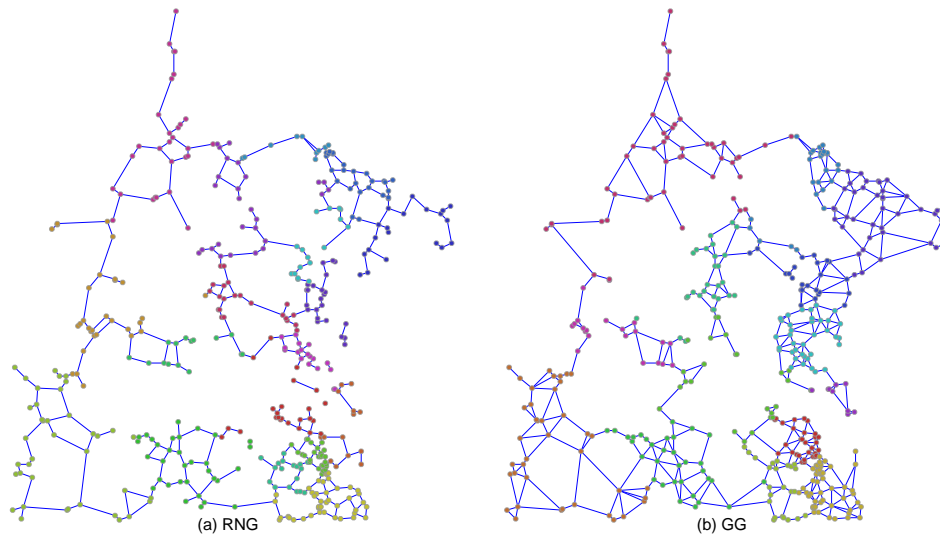


Fig. A94 Sendai networks with $N = 484$ nodes after 10% node removals by recalculated betweenness (RB) attacks. The locations of nodes are selected by inverse order of population (Inv.). The fragmentation is observed by removing links between communities which are different as compared to Figure A93.

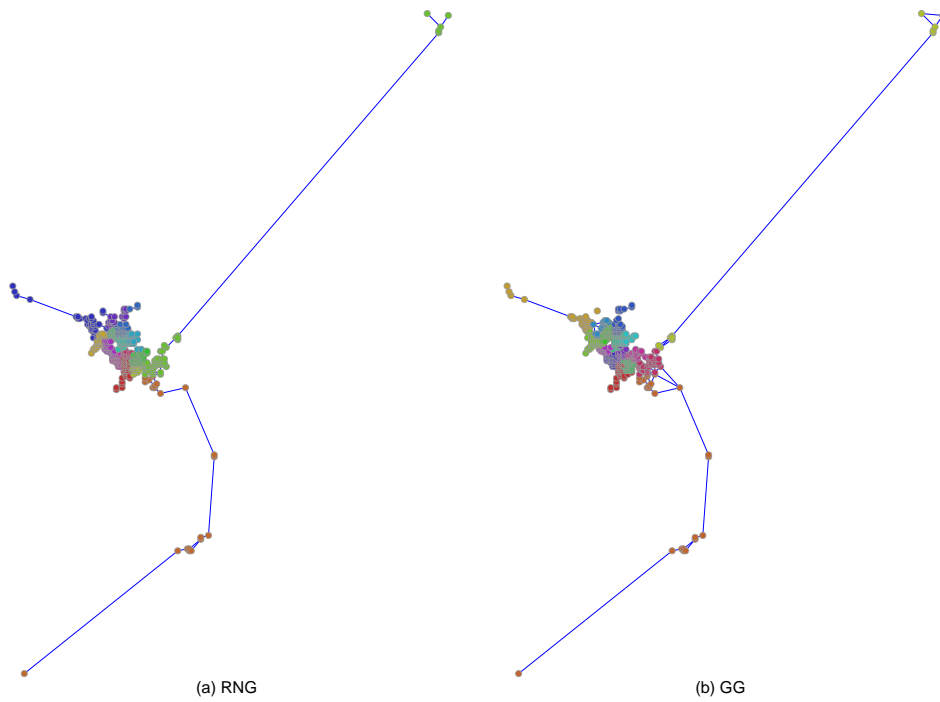


Fig. A95 Sapporo networks with $N = 484$ nodes after 10% node removals by recalculated betweenness (RB) attacks. The locations of nodes are selected by decreasing order of population (Pop.). The fragmentation is observed by removing links between communities especially in densely populated areas

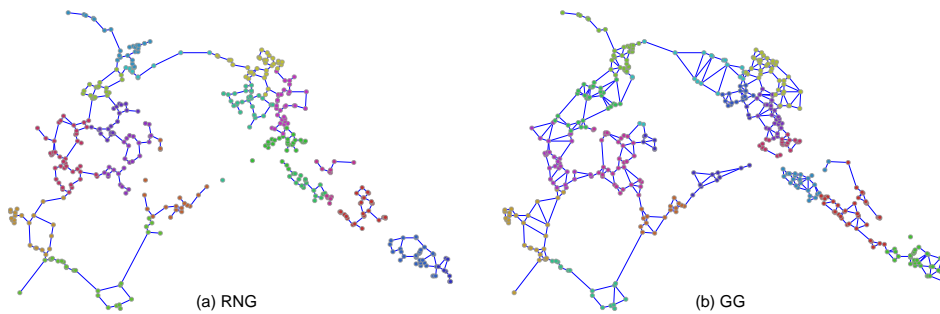


Fig. A96 Sapporo networks with $N = 484$ nodes after 10% node removals by recalculated betweenness (RB) attacks. The locations of nodes are selected by inverse order of population (Inv.). The fragmentation is observed by removing links between communities which are different as compared to Figure A95.

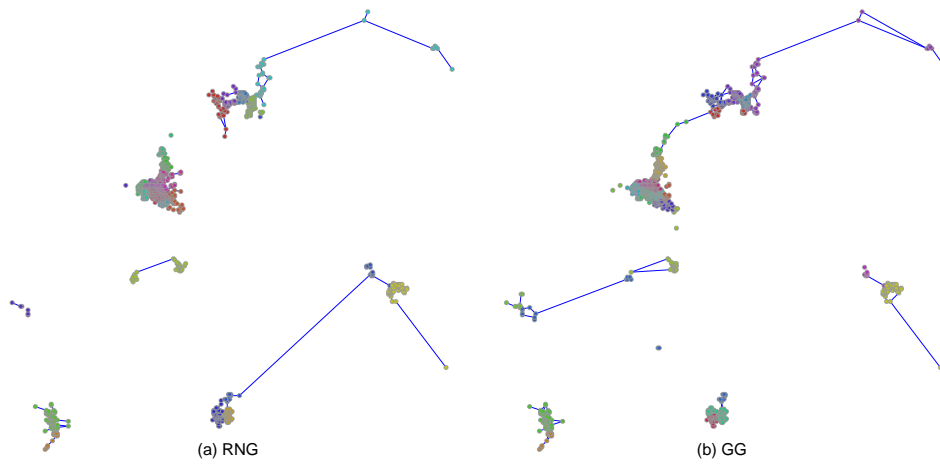


Fig. A97 Fukuoka networks with $N = 1024$ nodes after 10% node removals by recalculated betweenness (RB) attacks. The locations of nodes are selected by decreasing order of population (Pop.). The fragmentation is observed by removing links between communities especially in densely populated areas

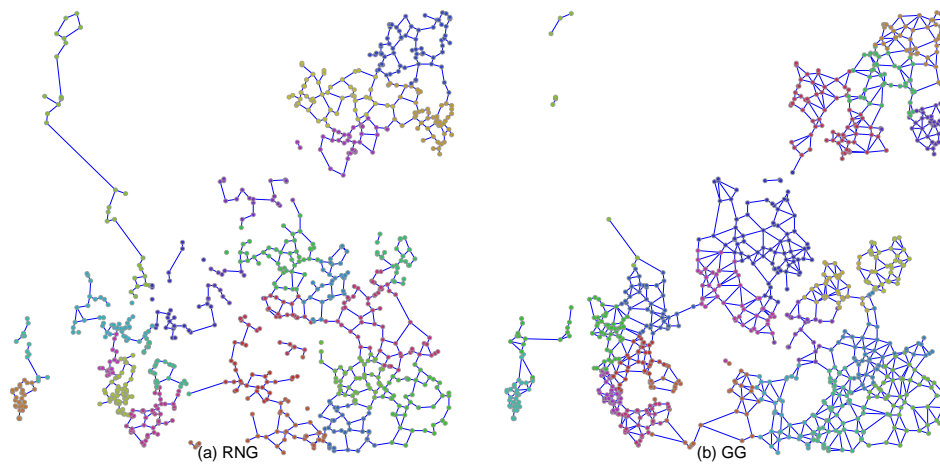


Fig. A98 Fukuoka networks with $N = 1024$ nodes after 10% node removals by recalculated betweenness (RB) attacks. The locations of nodes are selected by inverse order of population (Inv.). The fragmentation is observed by removing links between communities which are different as compared to Figure A97.

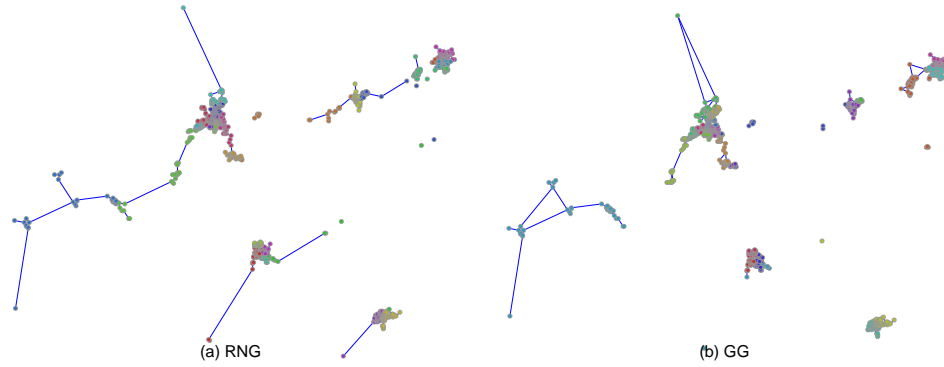


Fig. A99 Hiroshima networks with $N = 1024$ nodes after 10% node removals by recalculated betweenness (RB) attacks. The locations of nodes are selected by decreasing order of population (Pop.). The fragmentation is observed by removing links between communities especially in densely populated areas

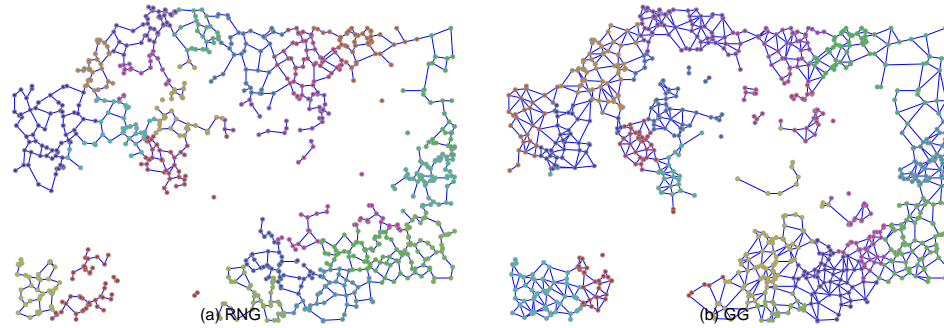


Fig. A100 Hiroshima networks with $N = 1024$ nodes after 10% node removals by recalculated betweenness (RB) attacks. The locations of nodes are selected by inverse order of population (Inv.). The fragmentation is observed by removing links between communities which are different as compared to Figure A99.

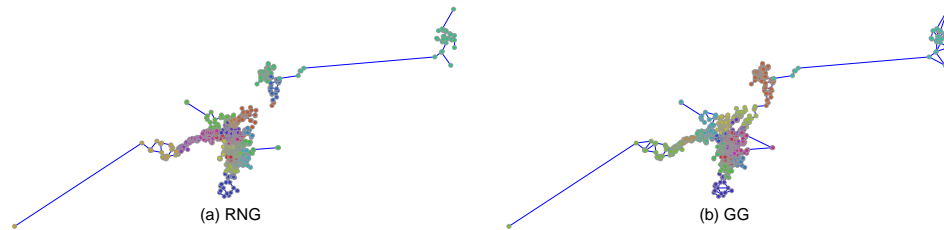


Fig. A101 Keihan networks with $N = 1024$ nodes after 10% node removals by recalculated betweenness (RB) attacks. The locations of nodes are selected by decreasing order of population (Pop.). The fragmentation is observed by removing links between communities especially in densely populated areas

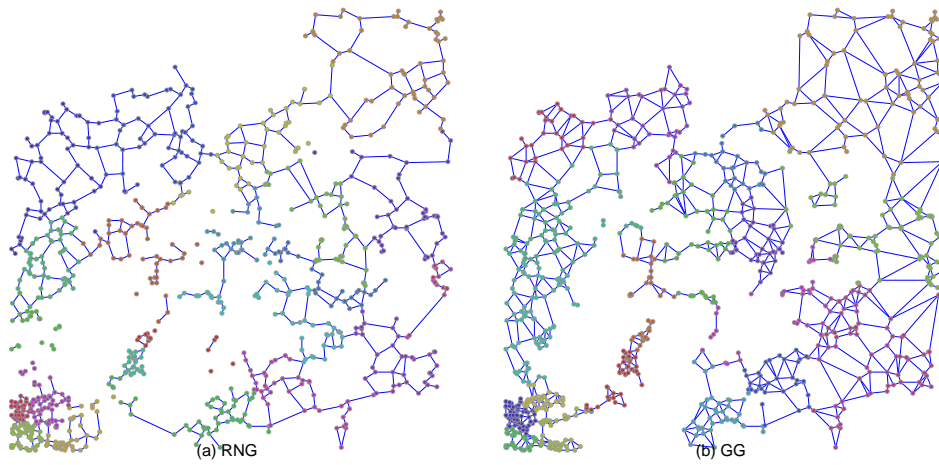


Fig. A102 Keihan networks with $N = 1024$ nodes after 10% node removals by recalculated betweenness (RB) attacks. The locations of nodes are selected by inverse order of population (Inv.). The fragmentation is observed by removing links between communities which are different as compared to Figure A101.

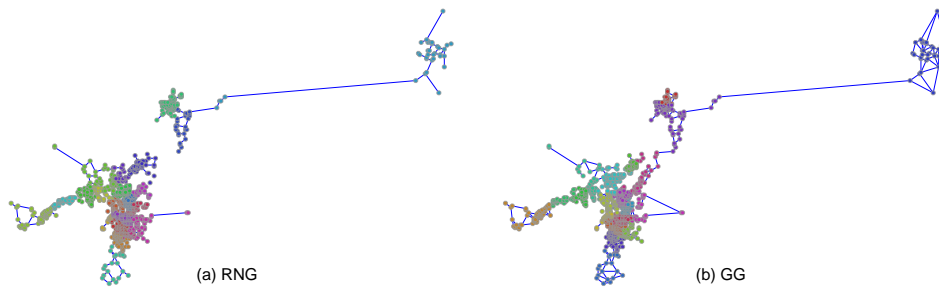


Fig. A103 Nagoya networks with $N = 1024$ nodes after 10% node removals by recalculated betweenness (RB) attacks. The locations of nodes are selected by decreasing order of population (Pop.). The fragmentation is observed by removing links between communities especially in densely populated areas

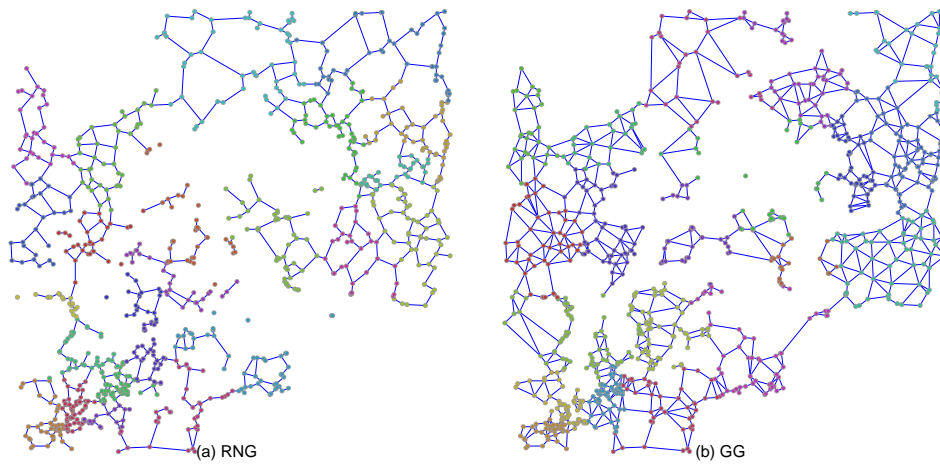


Fig. A104 Nagoya networks with $N = 1024$ nodes after 10% node removals by recalculated betweenness (RB) attacks. The locations of nodes are selected by inverse order of population (Inv.). The fragmentation is observed by removing links between communities which are different as compared to Figure A103.

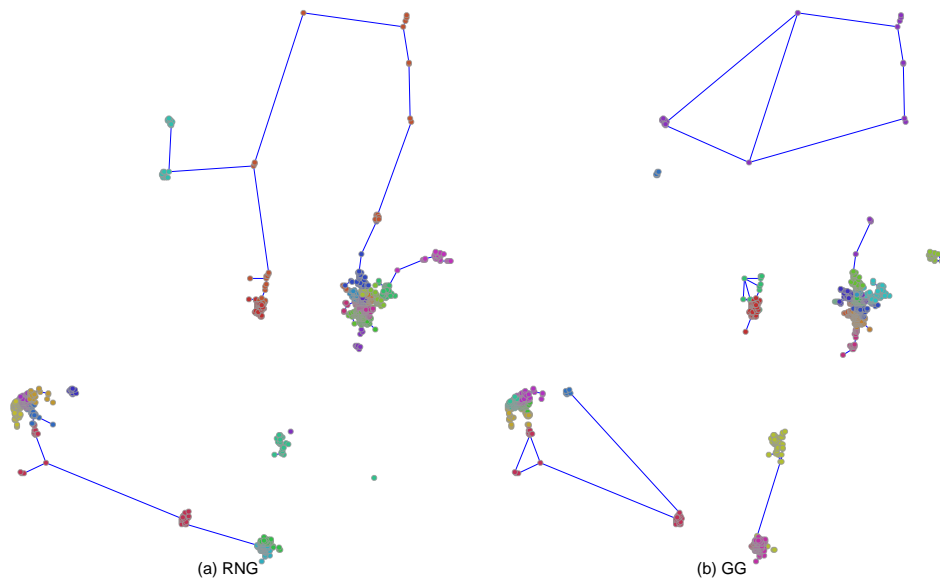


Fig. A105 Sendai networks with $N = 1024$ nodes after 10% node removals by recalculated betweenness (RB) attacks. The locations of nodes are selected by decreasing order of population (Pop.). The fragmentation is observed by removing links between communities especially in densely populated areas

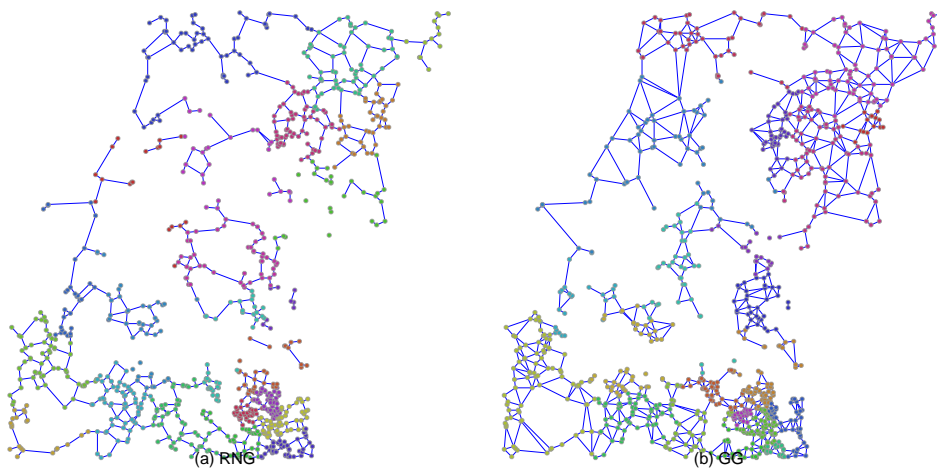


Fig. A106 Sendai networks with $N = 1024$ nodes after 10% node removals by recalculated betweenness (RB) attacks. The locations of nodes are selected by inverse order of population (Inv.). The fragmentation is observed by removing links between communities which are different as compared to Figure A105.

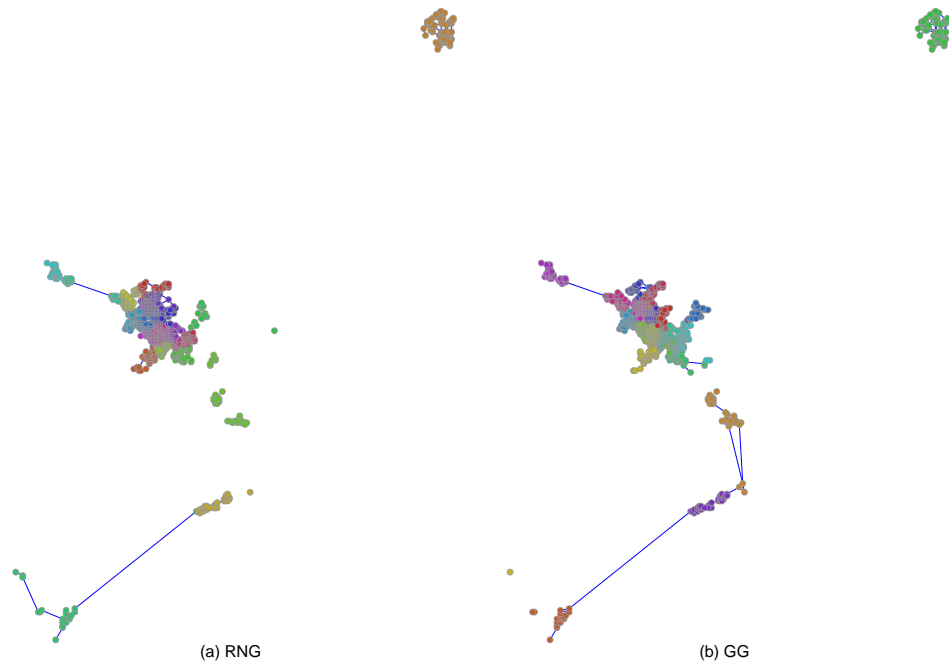


Fig. A107 Sapporo networks with $N = 1024$ nodes after 10% node removals by recalculated betweenness (RB) attacks. The locations of nodes are selected by decreasing order of population (Pop.). The fragmentation is observed by removing links between communities especially in densely populated areas

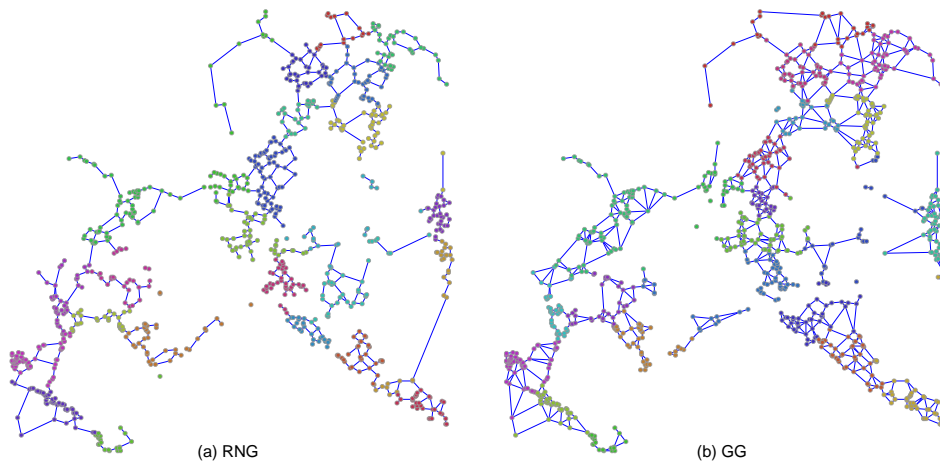


Fig. A108 Sapporo networks with $N = 1024$ nodes after 10% node removals by recalculated betweenness (RB) attacks. The locations of nodes are selected by inverse order of population (Inv.). The fragmentation is observed by removing links between communities which are different as compared to Figure A107.

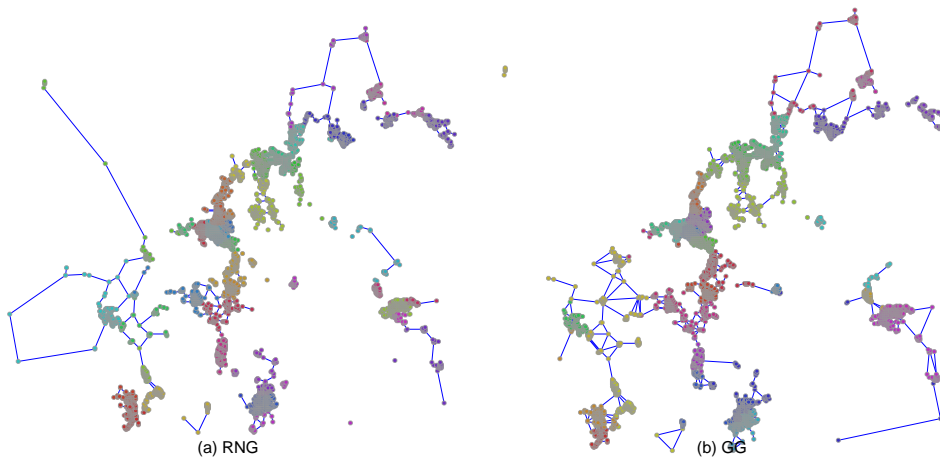


Fig. A109 Fukuoka networks with $N = 5041$ nodes after 10% node removals by recalculated betweenness (RB) attacks. The locations of nodes are selected by decreasing order of population (Pop.). The fragmentation is observed by removing links between communities especially in densely populated areas

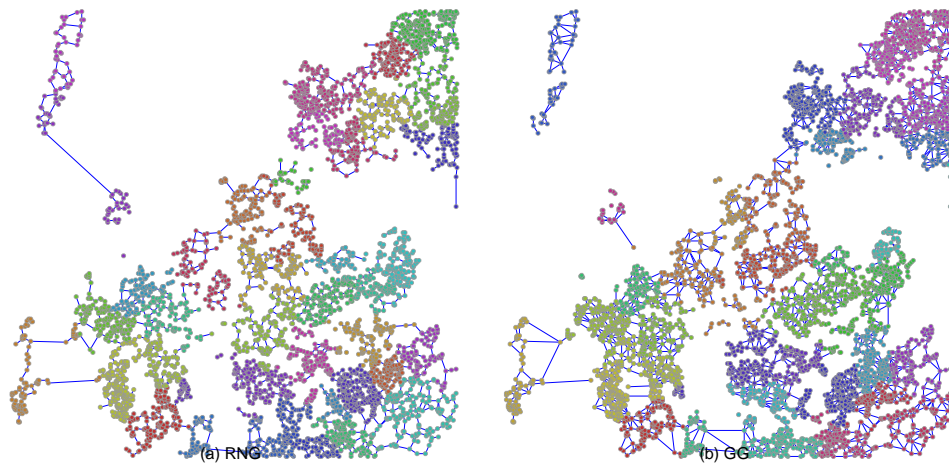


Fig. A110 Fukuoka networks with $N = 5041$ nodes after 10% node removals by recalculated betweenness (RB) attacks. The locations of nodes are selected by inverse order of population (Inv.). The fragmentation is observed by removing links between communities which are different as compared to Figure A109.

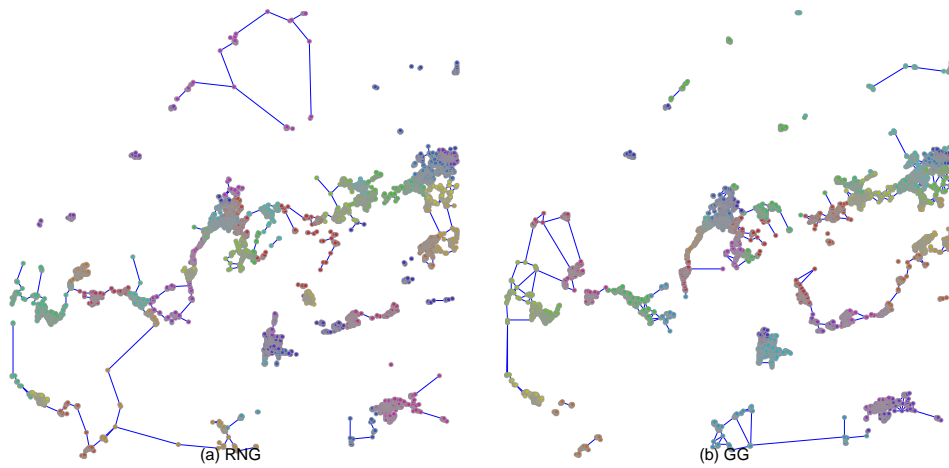


Fig. A111 Hiroshima networks with $N = 5041$ nodes after 10% node removals by recalculated betweenness (RB) attacks. The locations of nodes are selected by decreasing order of population (Pop.). The fragmentation is observed by removing links between communities especially in densely populated areas

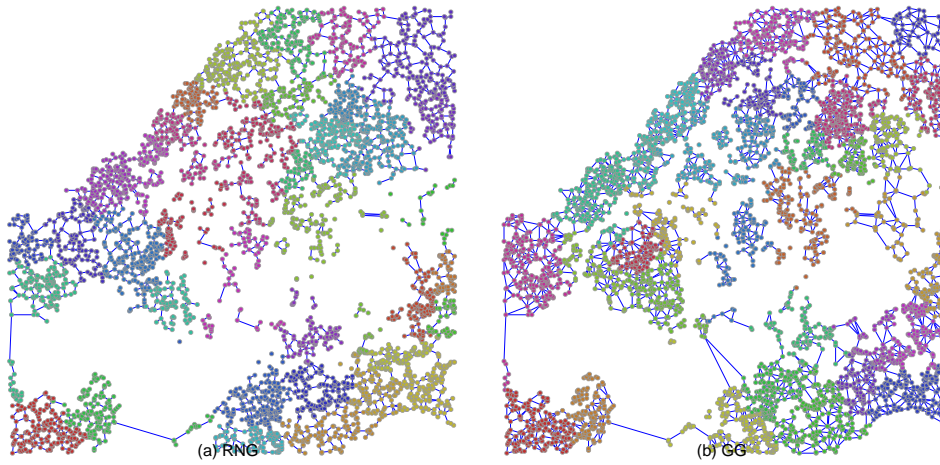


Fig. A112 Hiroshima networks with $N = 5041$ nodes after 10% node removals by recalculated betweenness (RB) attacks. The locations of nodes are selected by inverse order of population (Inv.). The fragmentation is observed by removing links between communities which are different as compared to Figure A111.

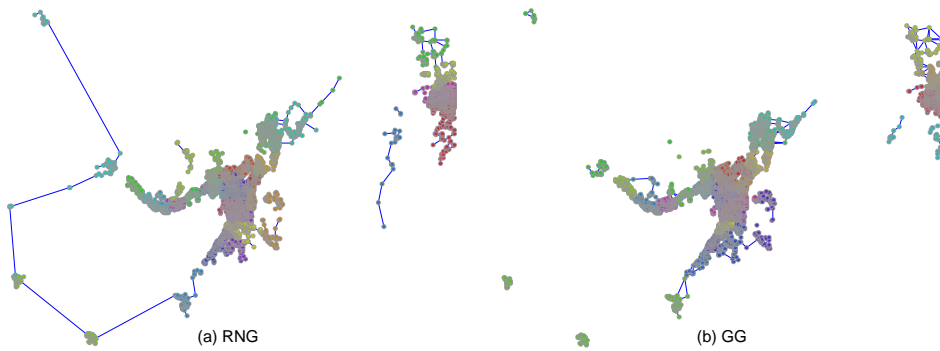


Fig. A113 Keihan networks with $N = 5041$ nodes after 10% node removals by recalculated betweenness (RB) attacks. The locations of nodes are selected by decreasing order of population (Pop.). The fragmentation is observed by removing links between communities especially in densely populated areas

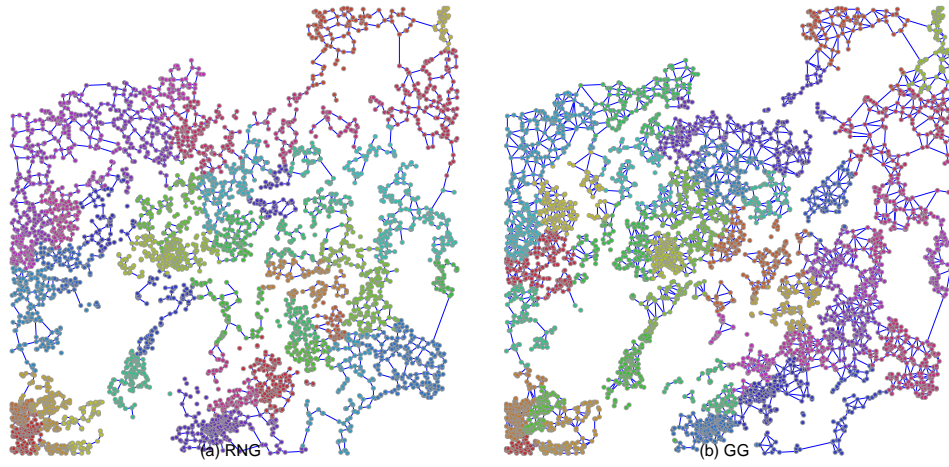


Fig. A114 Keihan networks with $N = 5041$ nodes after 10% node removals by recalculated betweenness (RB) attacks. The locations of nodes are selected by inverse order of population (Inv.). The fragmentation is observed by removing links between communities which are different as compared to Figure A113.



Fig. A115 Nagoya networks with $N = 5041$ nodes after 10% node removals by recalculated betweenness (RB) attacks. The locations of nodes are selected by decreasing order of population (Pop.). The fragmentation is observed by removing links between communities especially in densely populated areas

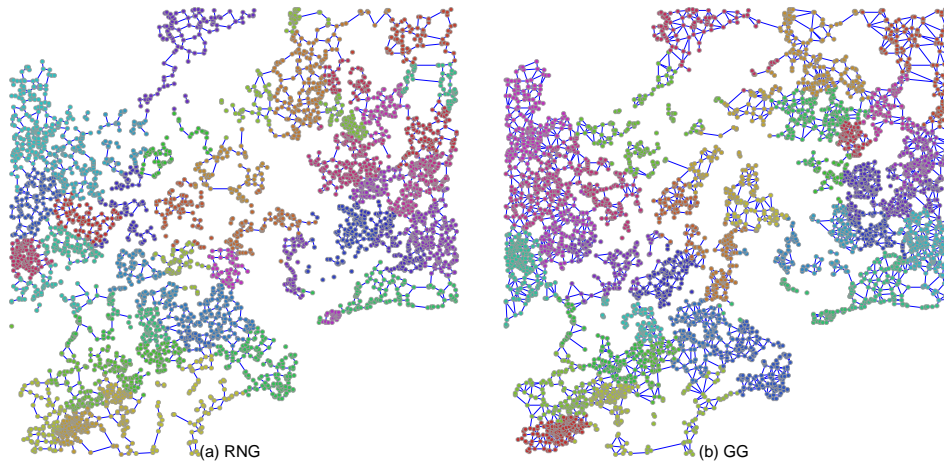


Fig. A116 Nagoya networks with $N = 5041$ nodes after 10% node removals by recalculated betweenness (RB) attacks. The locations of nodes are selected by inverse order of population (Inv.). The fragmentation is observed by removing links between communities which are different as compared to Figure A115.

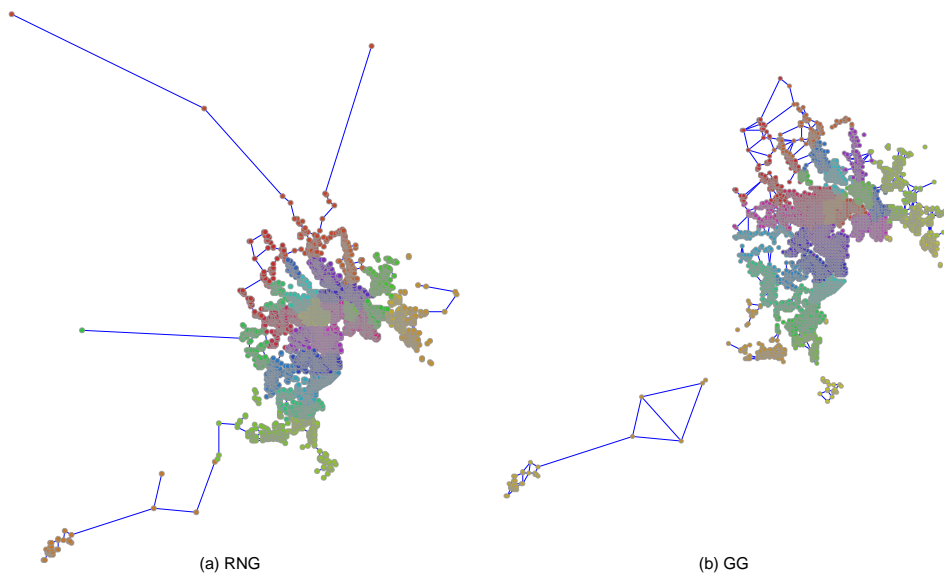


Fig. A117 Tokyo networks with $N = 5041$ nodes after 10% node removals by recalculated betweenness (RB) attacks. The locations of nodes are selected by decreasing order of population (Pop.). The fragmentation is observed by removing links between communities especially in densely populated areas

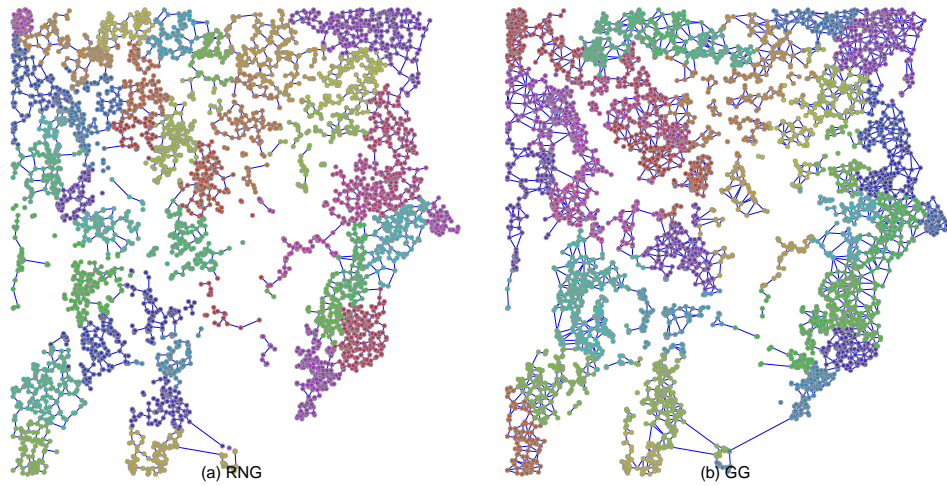


Fig. A118 Tokyo networks with $N = 5041$ nodes after 10% node removals by recalculated betweenness (RB) attacks. The locations of nodes are selected by inverse order of population (Inv.). The fragmentation is observed by removing links between communities which are different as compared to Figure A117.

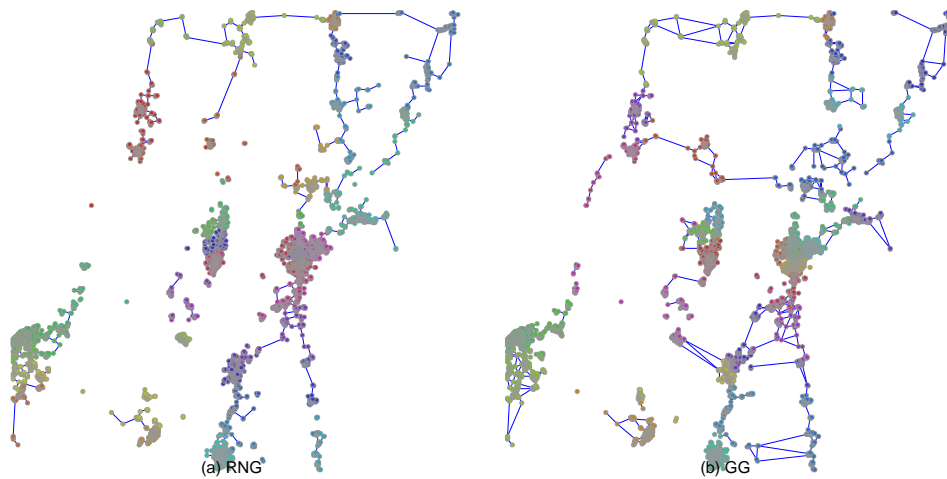


Fig. A119 Sendai networks with $N = 5041$ nodes after 10% node removals by recalculated betweenness (RB) attacks. The locations of nodes are selected by decreasing order of population (Pop.). The fragmentation is observed by removing links between communities especially in densely populated areas

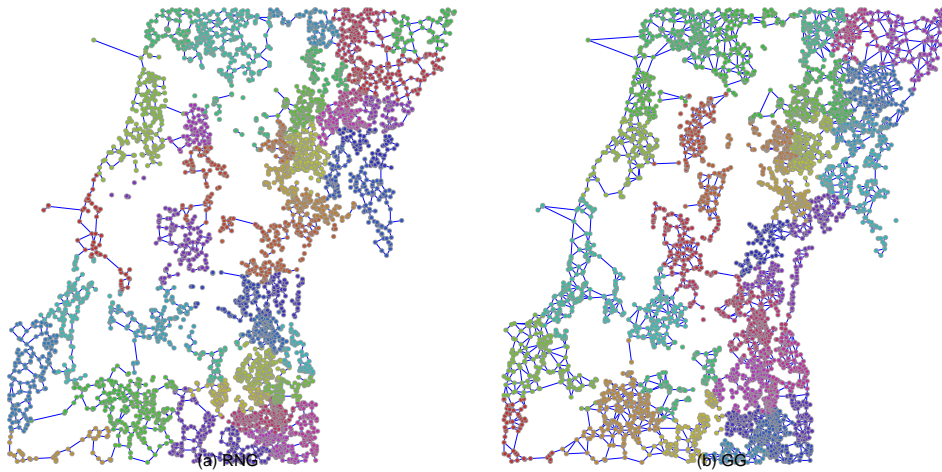


Fig. A120 Sendai networks with $N = 5041$ nodes after 10% node removals by recalculated betweenness (RB) attacks. The locations of nodes are selected by inverse order of population (Inv.). The fragmentation is observed by removing links between communities which are different as compared to Figure A119.

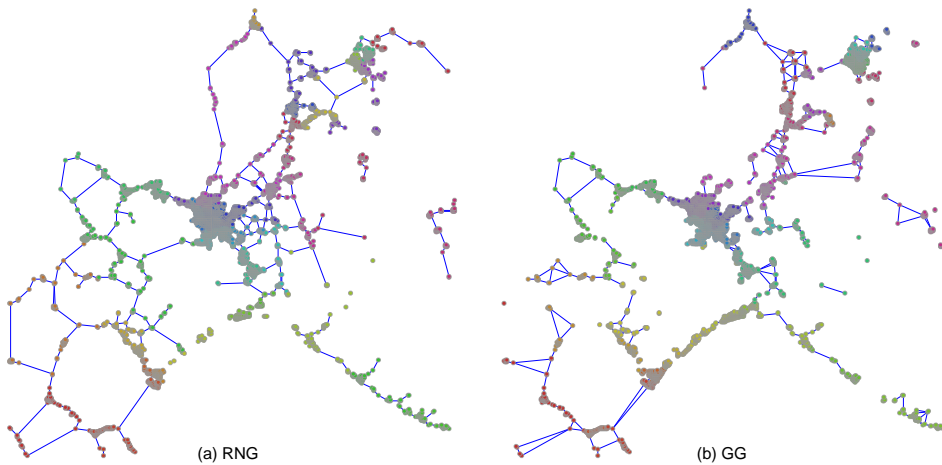


Fig. A121 Sapporo networks with $N = 5041$ nodes after 10% node removals by recalculated betweenness (RB) attacks. The locations of nodes are selected by decreasing order of population (Pop.). The fragmentation is observed by removing links between communities especially in densely populated areas

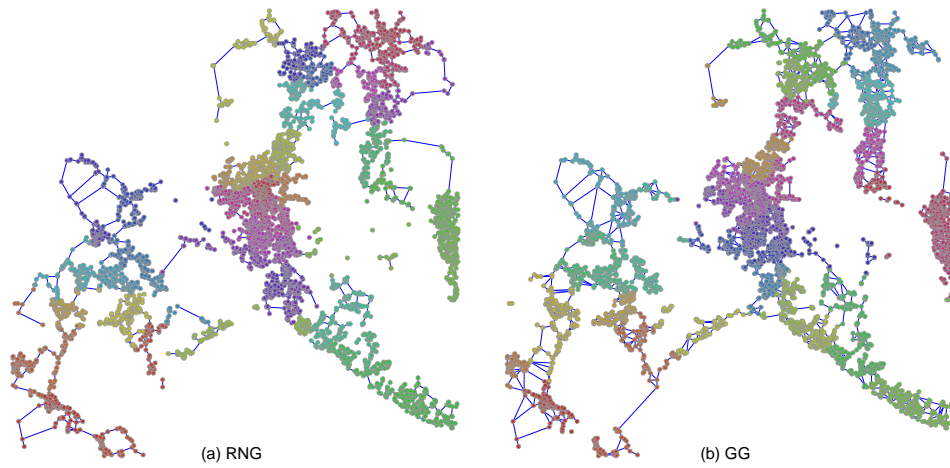


Fig. A122 Sapporo networks with $N = 5041$ nodes after 10% node removals by recalculated betweenness (RB) attacks. The locations of nodes are selected by inverse order of population (Inv.). The fragmentation is observed by removing links between communities which are different as compared to Figure A121.

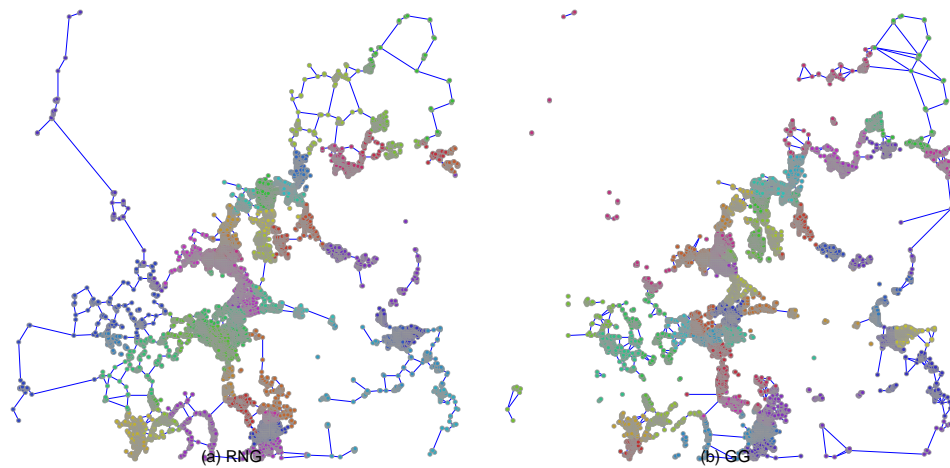


Fig. A123 Fukuoka networks with $N = 10000$ nodes after 10% node removals by recalculated betweenness (RB) attacks. The locations of nodes are selected by decreasing order of population (Pop.). The fragmentation is observed by removing links between communities especially in densely populated areas

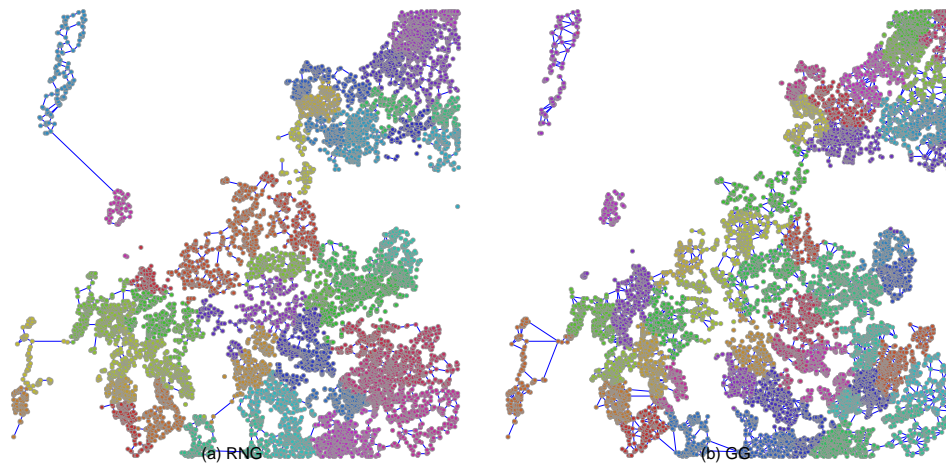


Fig. A124 Fukuoka networks with $N = 10000$ nodes after 10% node removals by recalculated betweenness (RB) attacks. The locations of nodes are selected by inverse order of population (Inv.). The fragmentation is observed by removing links between communities which are different as compared to Figure A123.

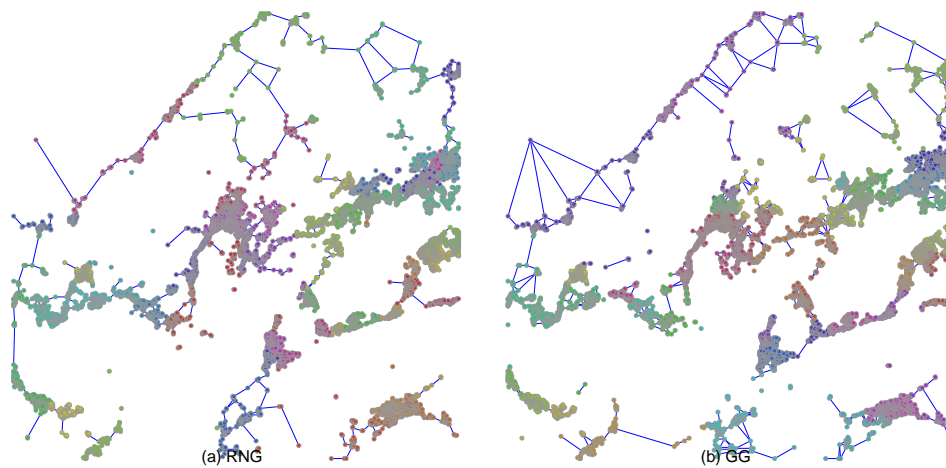


Fig. A125 Hiroshima networks with $N = 10000$ nodes after 10% node removals by recalculated betweenness (RB) attacks. The locations of nodes are selected by decreasing order of population (Pop.). The fragmentation is observed by removing links between communities especially in densely populated areas

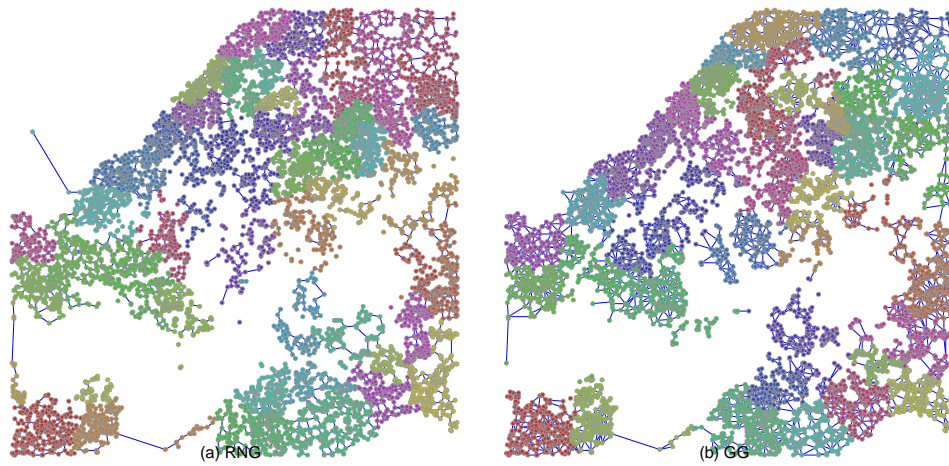


Fig. A126 Hiroshima networks with $N = 10000$ nodes after 10% node removals by recalculated betweenness (RB) attacks. The locations of nodes are selected by inverse order of population (Inv.). The fragmentation is observed by removing links between communities which are different as compared to Figure A125.

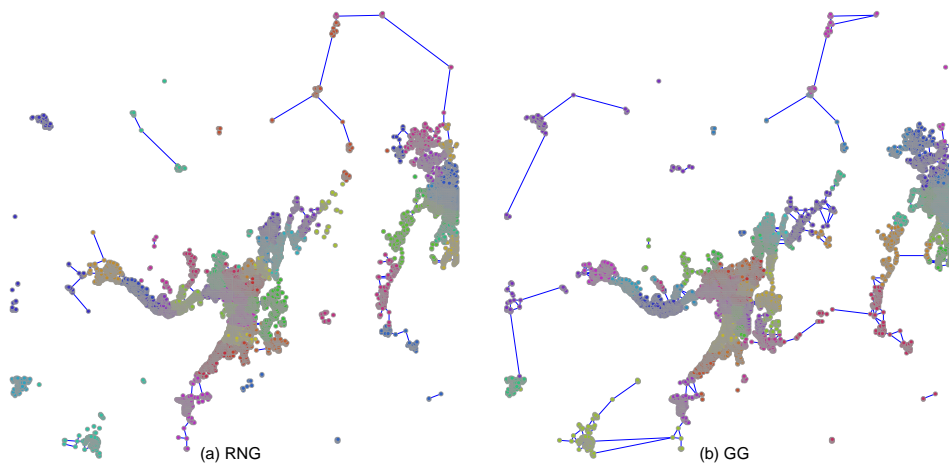


Fig. A127 Keihan networks with $N = 10000$ nodes after 10% node removals by recalculated betweenness (RB) attacks. The locations of nodes are selected by decreasing order of population (Pop.). The fragmentation is observed by removing links between communities especially in densely populated areas

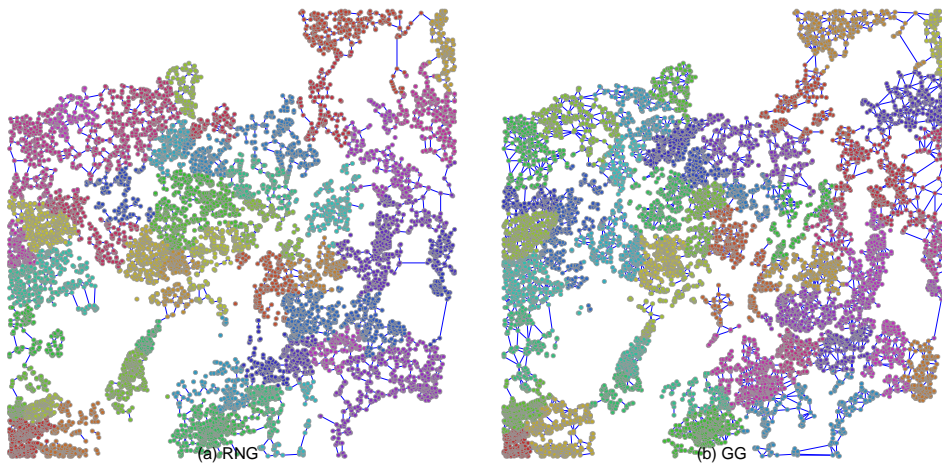


Fig. A128 Keihan networks with $N = 10000$ nodes after 10% node removals by recalculated betweenness (RB) attacks. The locations of nodes are selected by inverse order of population (Inv.). The fragmentation is observed by removing links between communities which are different as compared to Figure A127.

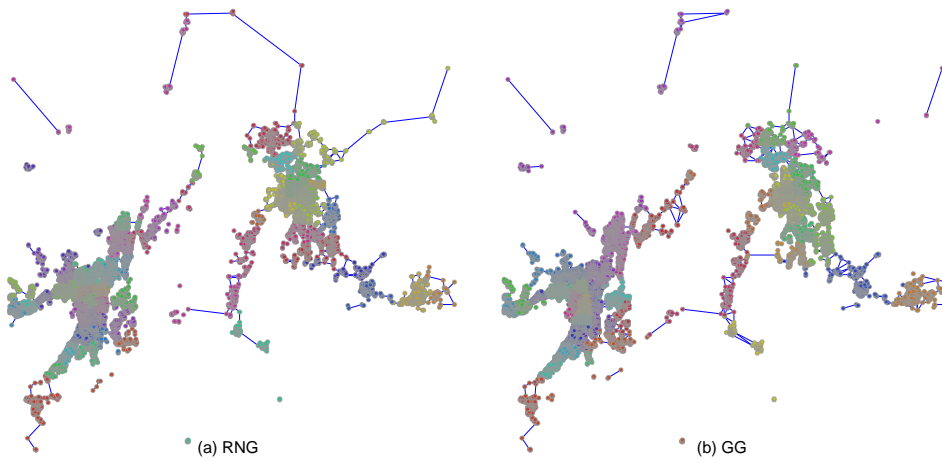


Fig. A129 Nagoya networks with $N = 10000$ nodes after 10% node removals by recalculated betweenness (RB) attacks. The locations of nodes are selected by decreasing order of population (Pop.). The fragmentation is observed by removing links between communities especially in densely populated areas

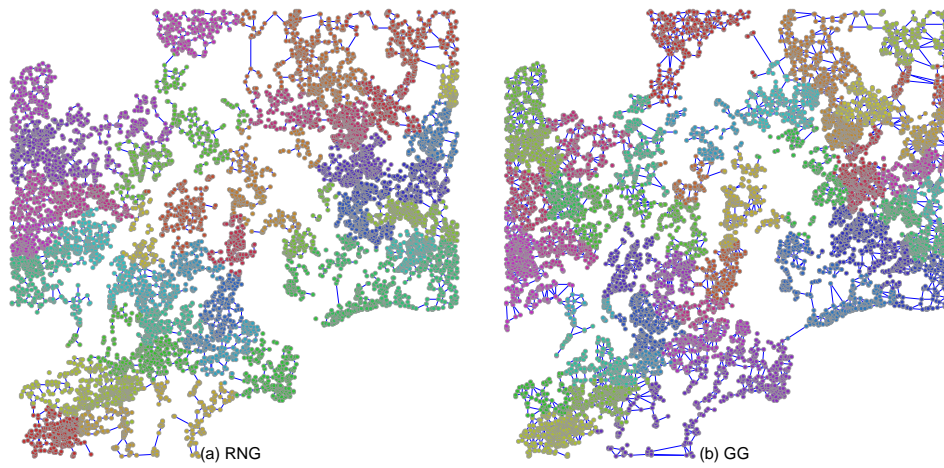


Fig. A130 Nagoya networks with $N = 10000$ nodes after 10% node removals by recalculated betweenness (RB) attacks. The locations of nodes are selected by inverse order of population (Inv.). The fragmentation is observed by removing links between communities which are different as compared to Figure A129.

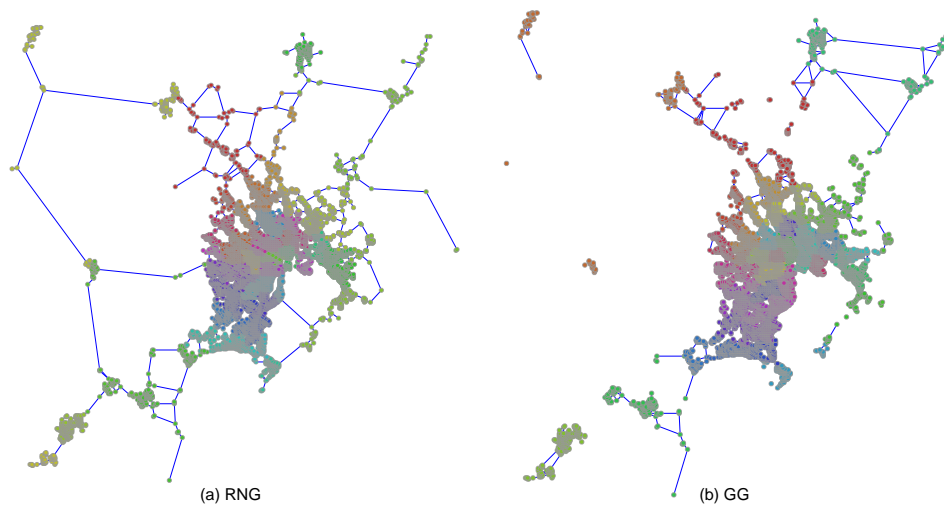


Fig. A131 Tokyo networks with $N = 10000$ nodes after 10% node removals by recalculated betweenness (RB) attacks. The locations of nodes are selected by decreasing order of population (Pop.). The fragmentation is observed by removing links between communities especially in densely populated areas

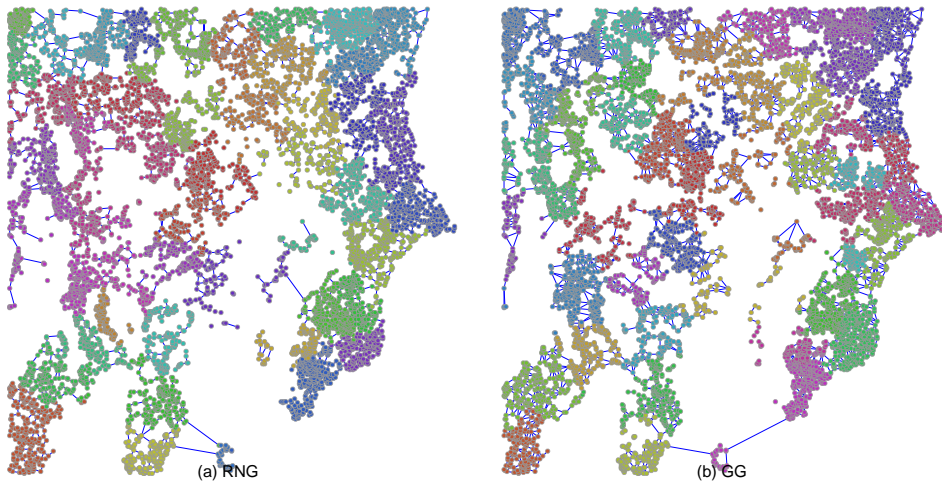


Fig. A132 Tokyo networks with $N = 10000$ nodes after 10% node removals by recalculated betweenness (RB) attacks. The locations of nodes are selected by inverse order of population (Inv.). The fragmentation is observed by removing links between communities which are different as compared to Figure A131.

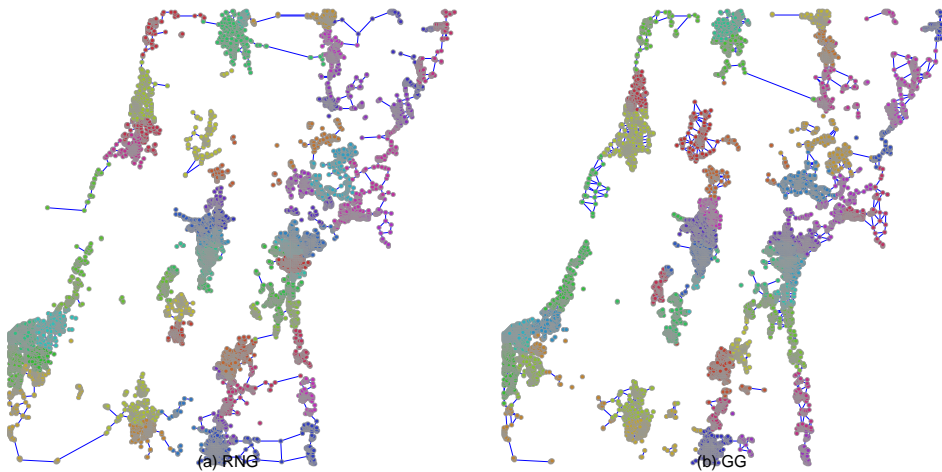


Fig. A133 Sendai networks with $N = 10000$ nodes after 10% node removals by recalculated betweenness (RB) attacks. The locations of nodes are selected by decreasing order of population (Pop.). The fragmentation is observed by removing links between communities especially in densely populated areas

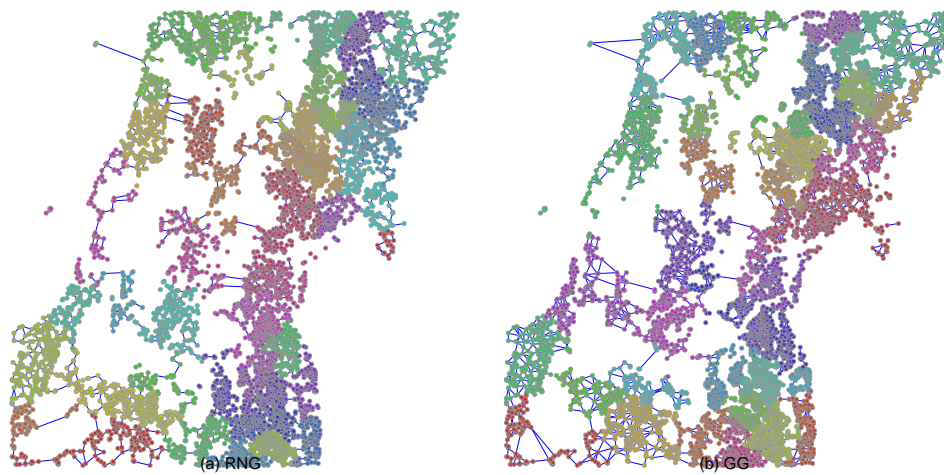


Fig. A134 Sendai networks with $N = 10000$ nodes after 10% node removals by recalculated betweenness (RB) attacks. The locations of nodes are selected by inverse order of population (Inv.). The fragmentation is observed by removing links between communities which are different as compared to Figure A133.

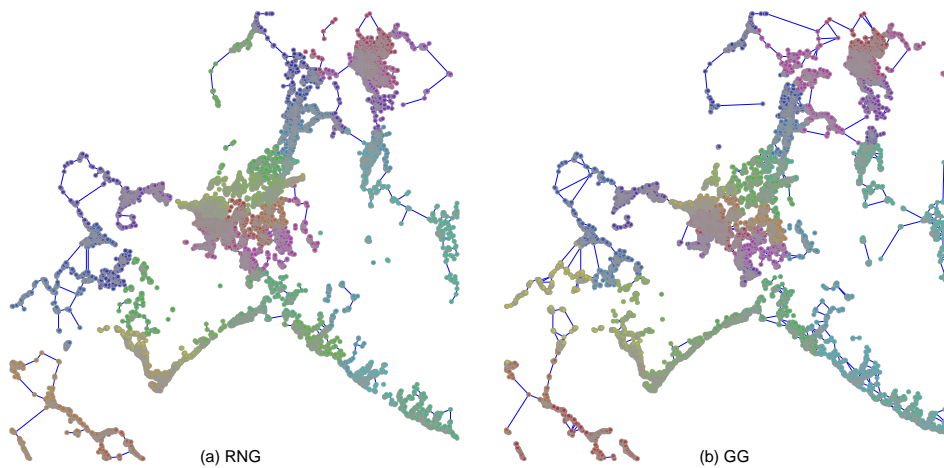


Fig. A135 Sapporo networks with $N = 10000$ nodes after 10% node removals by recalculated betweenness (RB) attacks. The locations of nodes are selected by decreasing order of population (Pop.). The fragmentation is observed by removing links between communities especially in densely populated areas

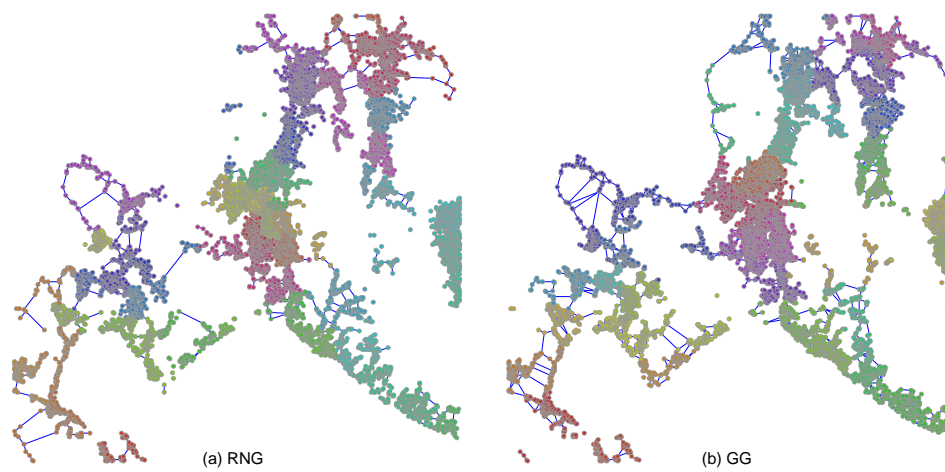


Fig. A136 Sapporo networks with $N = 10000$ nodes after 10% node removals by recalculated betweenness (RB) attacks. The locations of nodes are selected by inverse order of population (Inv.). The fragmentation is observed by removing links between communities which are different as compared to Figure A135.

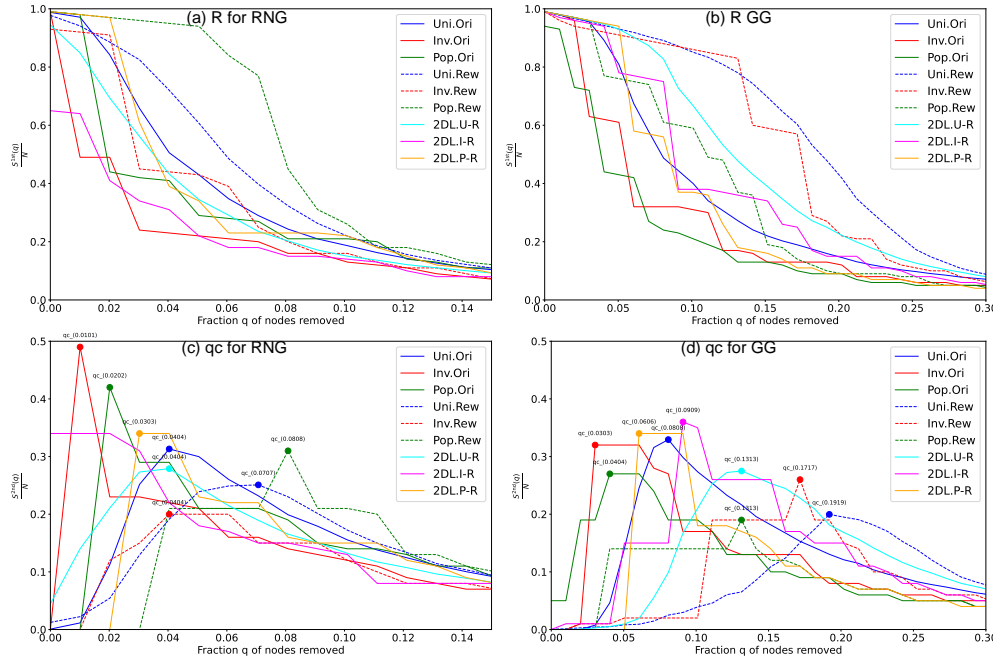


Fig. A137 Robustness against recalculated betweenness (RB) attacks for Fukuoka networks with $N = 100$ nodes. For both Rew (Randomized networks) and 2DL lines, the rewiring process preserves the original degree distributions. Two measures are applied: (a) (b) $S^{1st}(q)/N$ the relative size of largest connected component, and (c) (d) $S^{2nd}(q)/N$ the critical fraction q_c at the peak of the relative size of second largest component.

.3 Robustness against RB attacks

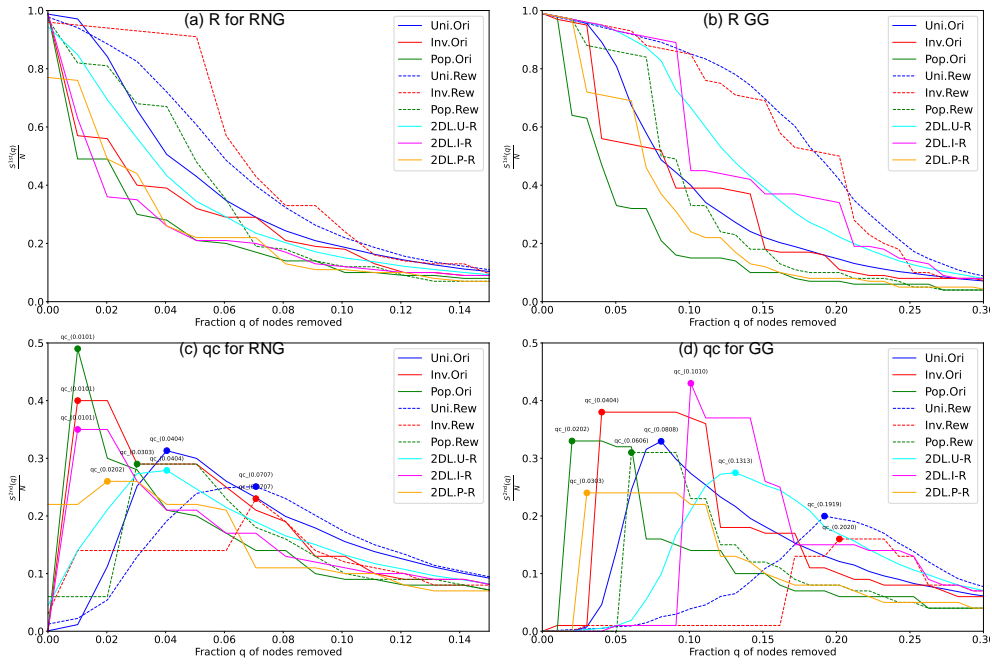


Fig. A138 Robustness against recalculated betweenness (RB) attacks for Hiroshima networks with $N = 100$ nodes. For both Rew (Randomized networks) and 2DL lines, the rewiring process preserves the original degree distributions. Two measures are applied: (a) (b) $S^{1st}(q)/N$ the relative size of largest connected component, and (c) (d) $S^{2nd}(q)/N$ the critical fraction q_c at the peak of the relative size of second largest component.

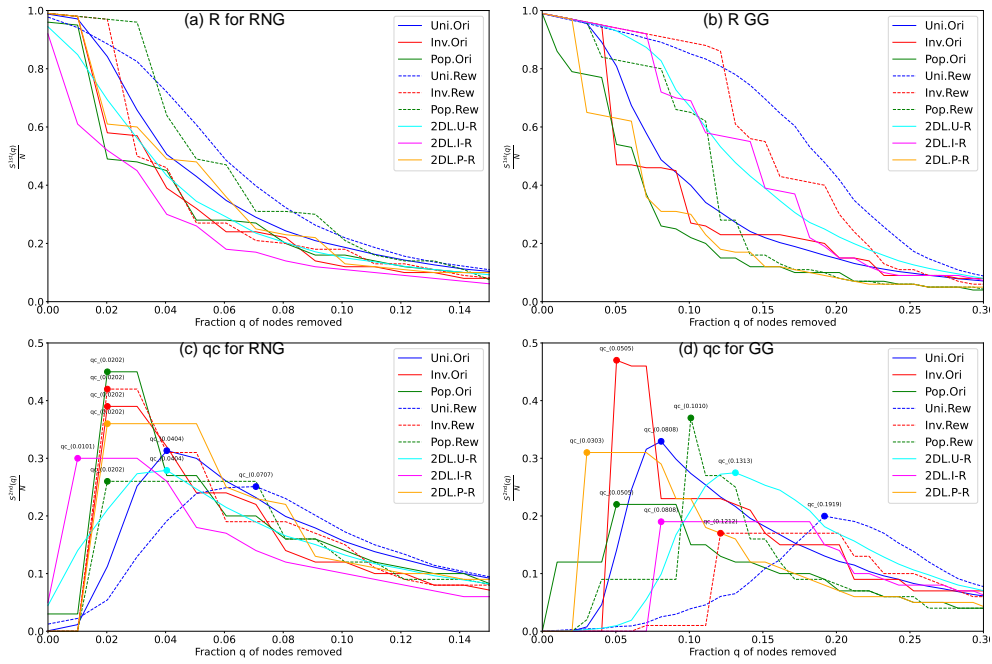


Fig. A140 Robustness against recalculated betweenness (RB) attacks for Nagoya networks with $N = 100$ nodes. For both Rew (Randomized networks) and 2DL lines, the rewiring process preserves the original degree distributions. Two measures are applied: (a) (b) $S^{1st}(q)/N$ the relative size of largest connected component, and (c) (d) $S^{2nd}(q)/N$ the critical fraction q_c at the peak of the relative size of second largest component.

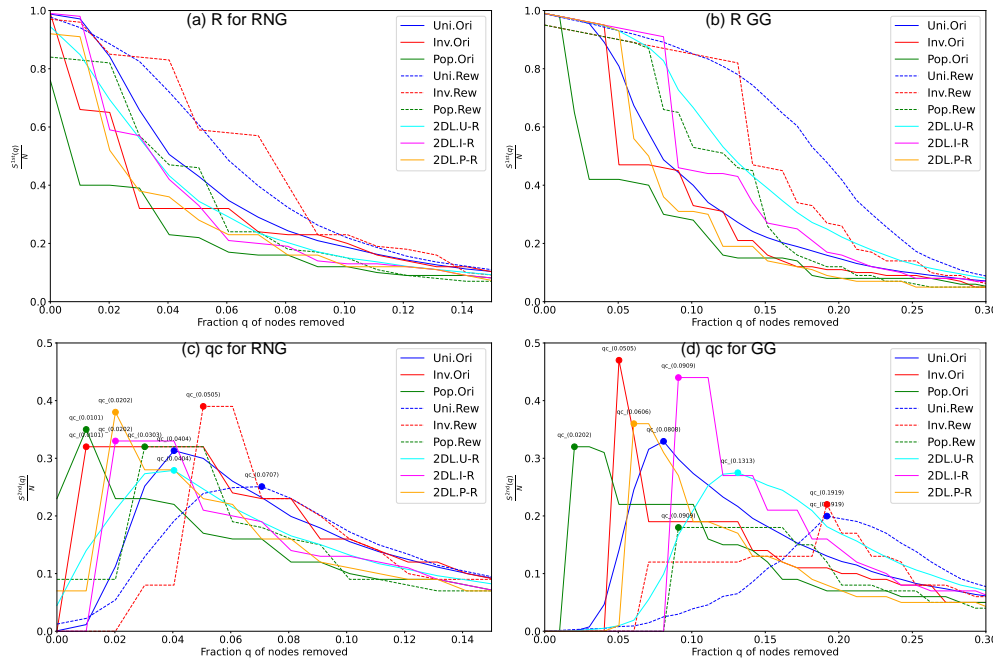


Fig. A141 Robustness against recalculated betweenness (RB) attacks for Tokyo networks with $N = 100$ nodes. For both Rew (Randomized networks) and 2DL lines, the rewiring process preserves the original degree distributions. Two measures are applied: (a) (b) $S^{1st}(q)/N$ the relative size of largest connected component, and (c) (d) $S^{2nd}(q)/N$ the critical fraction q_c at the peak of the relative size of second largest component.

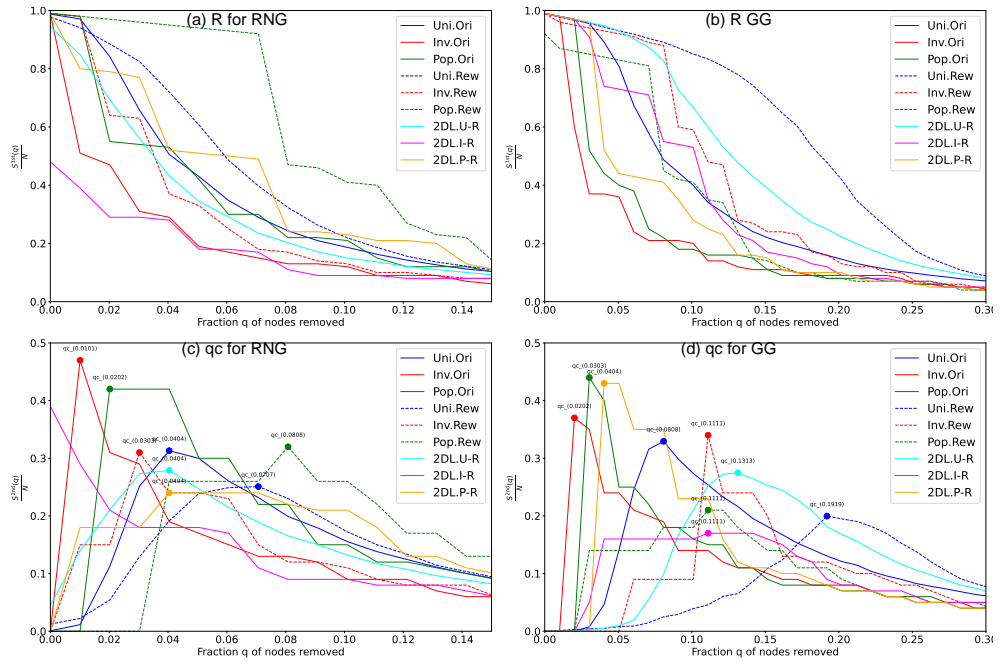


Fig. A143 Robustness against recalculated betweenness (RB) attacks for Sapporo networks with $N = 100$ nodes. For both Rew (Randomized networks) and 2DL lines, the rewiring process preserves the original degree distributions. Two measures are applied: (a) (b) $S^{1st}(q)/N$ the relative size of largest connected component, and (c) (d) $S^{2nd}(q)/N$ the critical fraction q_c at the peak of the relative size of second largest component.

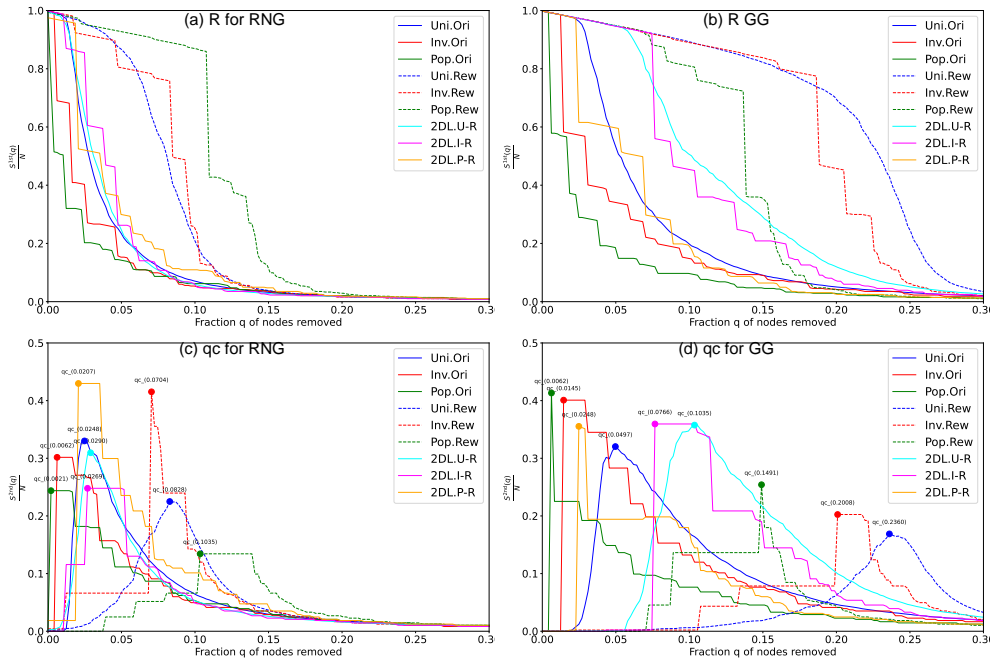


Fig. A144 Robustness against recalculated betweenness (RB) attacks for Fukuoka networks with $N = 484$ nodes. For both Rew (Randomized networks) and 2DL lines, the rewiring process preserves the original degree distributions. Two measures are applied: (a) (b) $S^{1st}(q)/N$ the relative size of largest connected component, and (c) (d) $S^{2nd}(q)/N$ the critical fraction q_c at the peak of the relative size of second largest component.

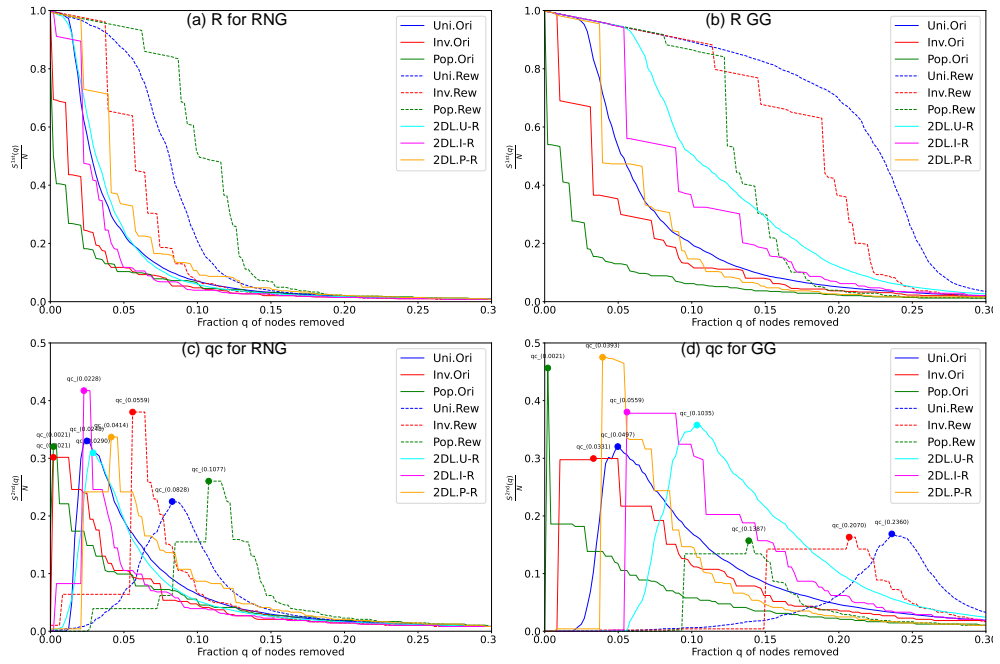


Fig. A145 Robustness against recalculated betweenness (RB) attacks for Hiroshima networks with $N = 484$ nodes. For both Rew (Randomized networks) and 2DL lines, the rewiring process preserves the original degree distributions. Two measures are applied: (a) (b) $S^{1st}(q)/N$ the relative size of largest connected component, and (c) (d) $S^{2nd}(q)/N$ the critical fraction q_c at the peak of the relative size of second largest component.

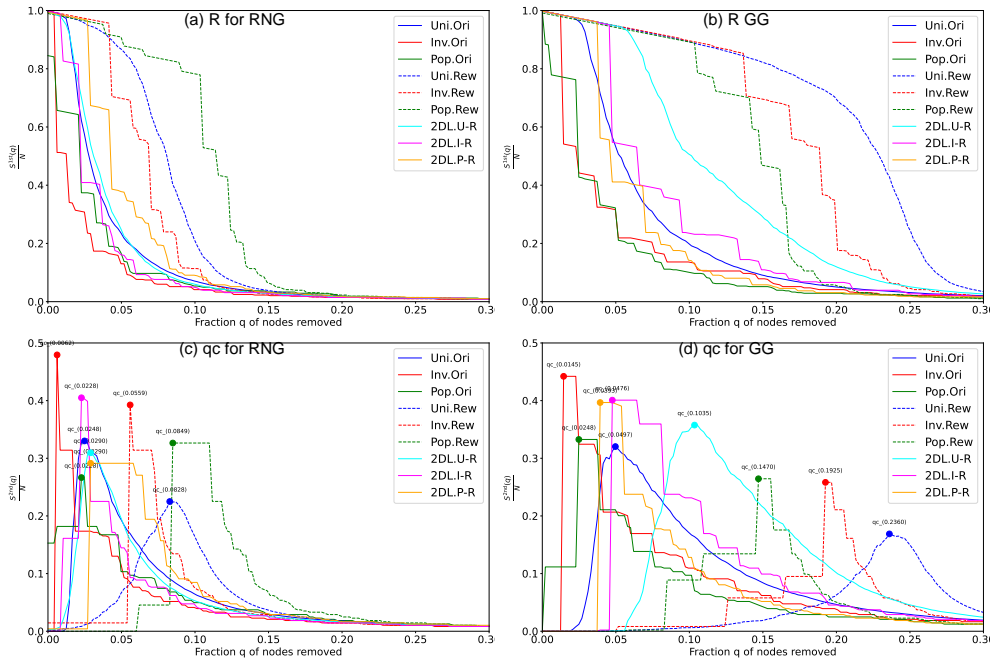


Fig. A146 Robustness against recalculated betweenness (RB) attacks for Keihan networks with $N = 484$ nodes. For both Rew (Randomized networks) and 2DL lines, the rewiring process preserves the original degree distributions. Two measures are applied: (a) (b) $S^{1st}(q)/N$ the relative size of largest connected component, and (c) (d) $S^{2nd}(q)/N$ the critical fraction q_c at the peak of the relative size of second largest component.

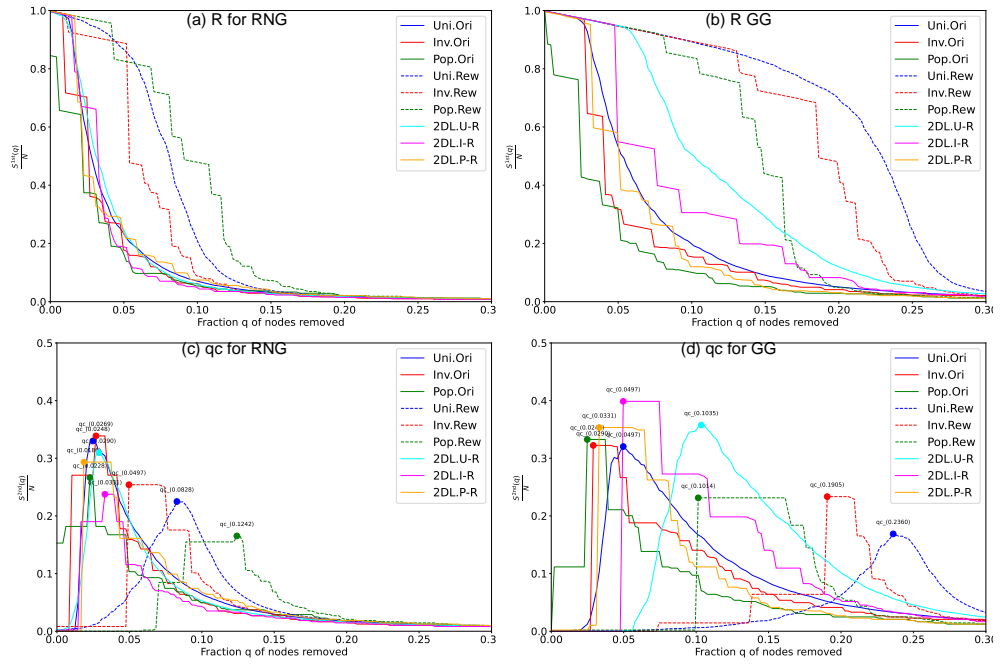


Fig. A147 Robustness against recalculated betweenness (RB) attacks for Nagoya networks with $N = 484$ nodes. For both Rew (Randomized networks) and 2DL lines, the rewiring process preserves the original degree distributions. Two measures are applied: (a) (b) $S^{1st}(q)/N$ the relative size of largest component, and (c) (d) $S^{2nd}(q)/N$ the critical fraction q_c at the peak of the relative size of second largest component.

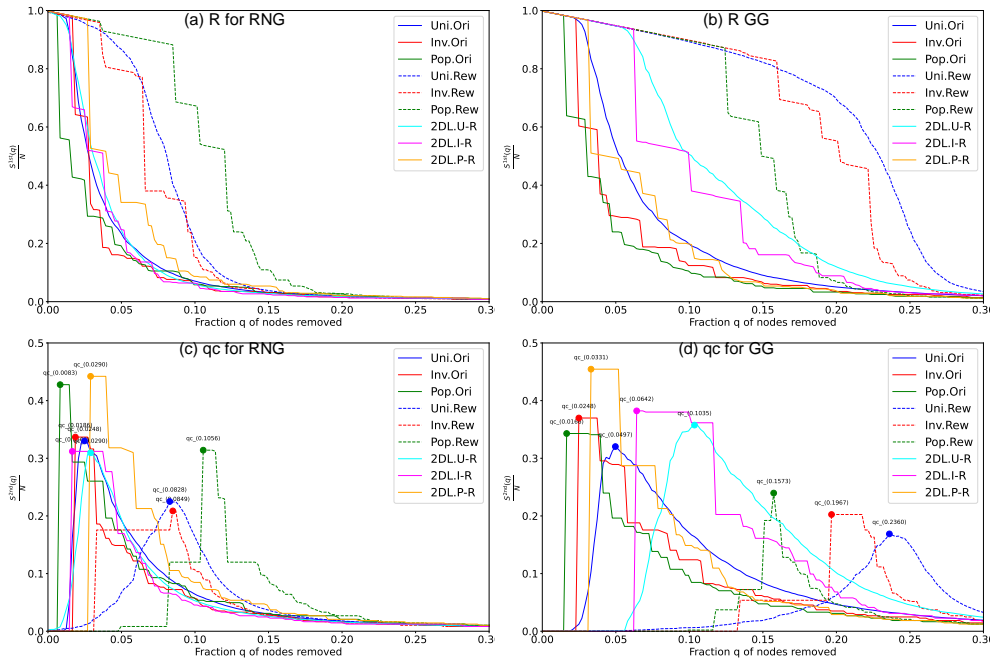


Fig. A148 Robustness against recalculated betweenness (RB) attacks for Tokyo networks with $N = 484$ nodes. For both Rew (Randomized networks) and 2DL lines, the rewiring process preserves the original degree distributions. Two measures are applied: (a) (b) $S^{1st}(q)/N$ the relative size of largest connected component, and (c) (d) $S^{2nd}(q)/N$ the critical fraction q_c at the peak of the relative size of second largest component.

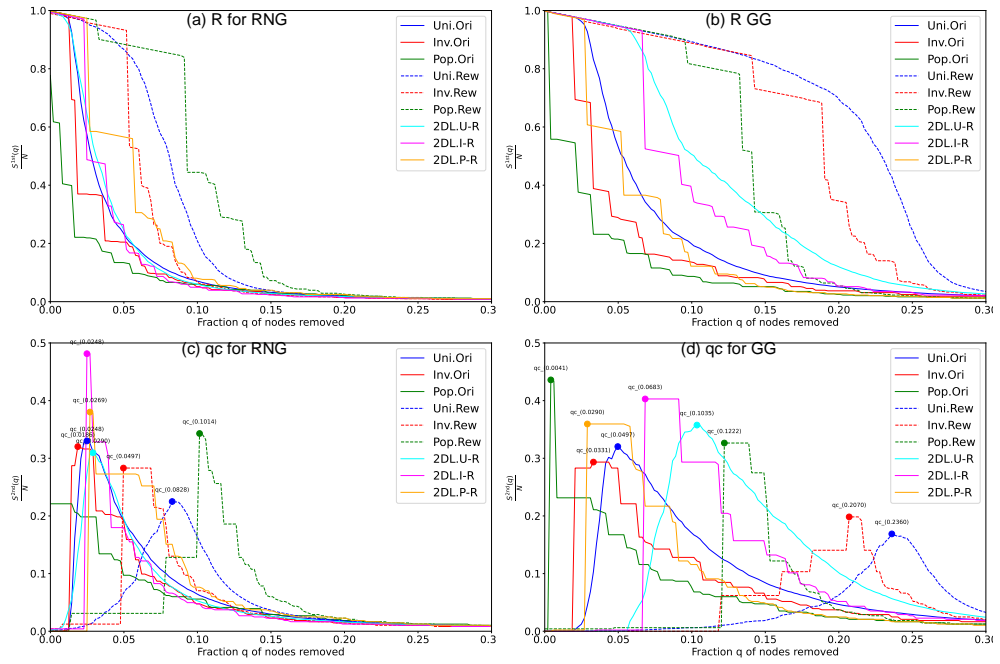


Fig. A149 Robustness against recalculated betweenness (RB) attacks for Sendai networks with $N = 484$ nodes. For both Rew (Randomized networks) and 2DL lines, the rewiring process preserves the original degree distributions. Two measures are applied: (a) (b) $S^{1st}(q)/N$ the relative size of largest connected component, and (c) (d) $S^{2nd}(q)/N$ the critical fraction q_c at the peak of the relative size of second largest component.

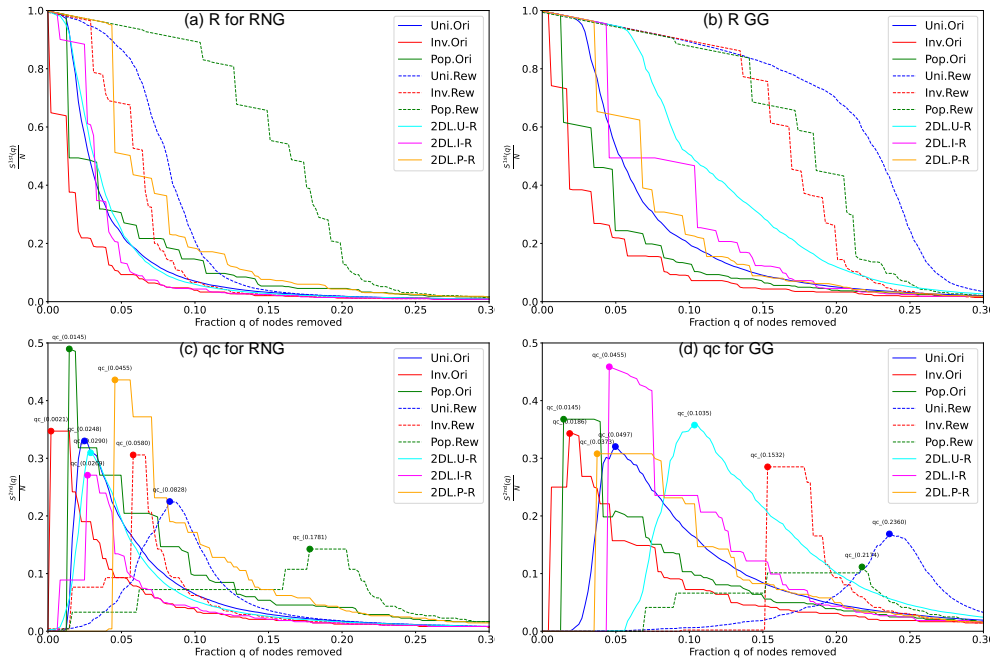


Fig. A150 Robustness against recalculated betweenness (RB) attacks for Sapporo networks with $N = 484$ nodes. For both Rew (Randomized networks) and 2DL lines, the rewiring process preserves the original degree distributions. Two measures are applied: (a) (b) $S^{1st}(q)/N$ the relative size of largest connected component, and (c) (d) $S^{2nd}(q)/N$ the critical fraction q_c at the peak of the relative size of second largest component.

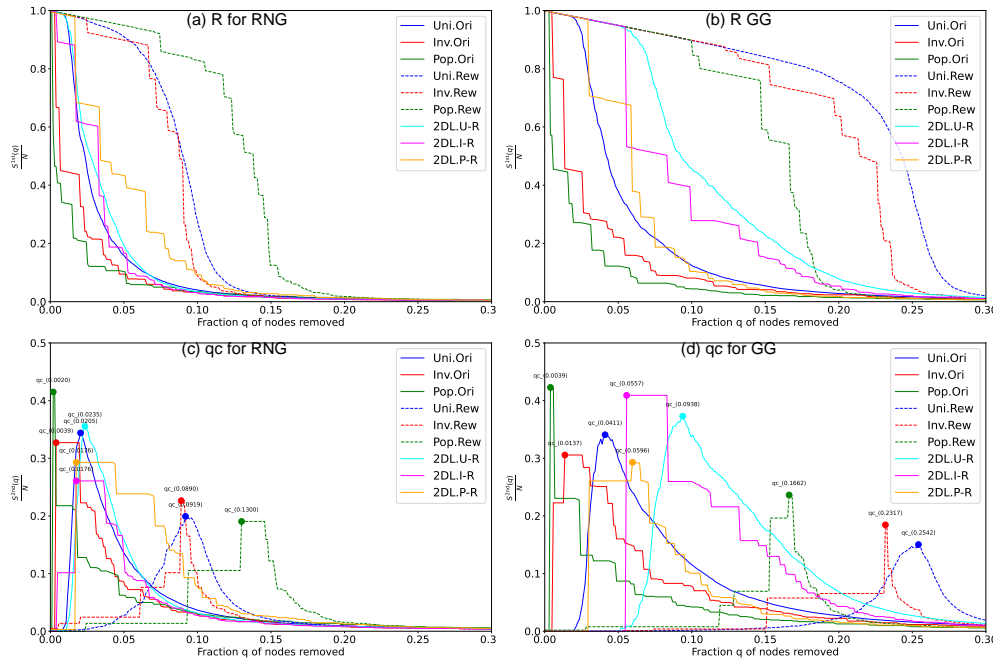


Fig. A151 Robustness against recalculated betweenness (RB) attacks for Fukuoka networks with $N = 1024$ nodes. For both Rew (Randomized networks) and 2DL lines, the rewiring process preserves the original degree distributions. Two measures are applied: (a) (b) $S^{1st}(q)/N$ the relative size of largest component, and (c) (d) $S^{2nd}(q)/N$ the critical fraction q_c at the peak of the relative size of second largest component.

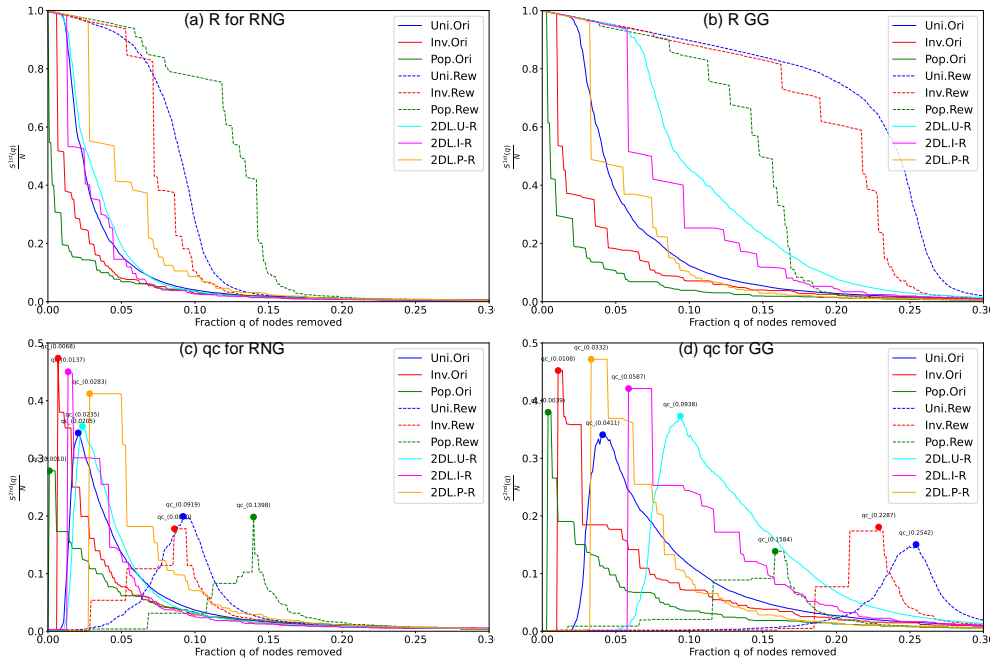


Fig. A152 Robustness against recalculated betweenness (RB) attacks for Hiroshima networks with $N = 1024$ nodes. For both Rew (Randomized networks) and 2DL lines, the rewiring process preserves the original degree distributions. Two measures are applied: (a) (b) $S^{1st}(q)/N$ the relative size of largest connected component, and (c) (d) $S^{2nd}(q)/N$ the critical fraction q_c at the peak of the relative size of second largest component.

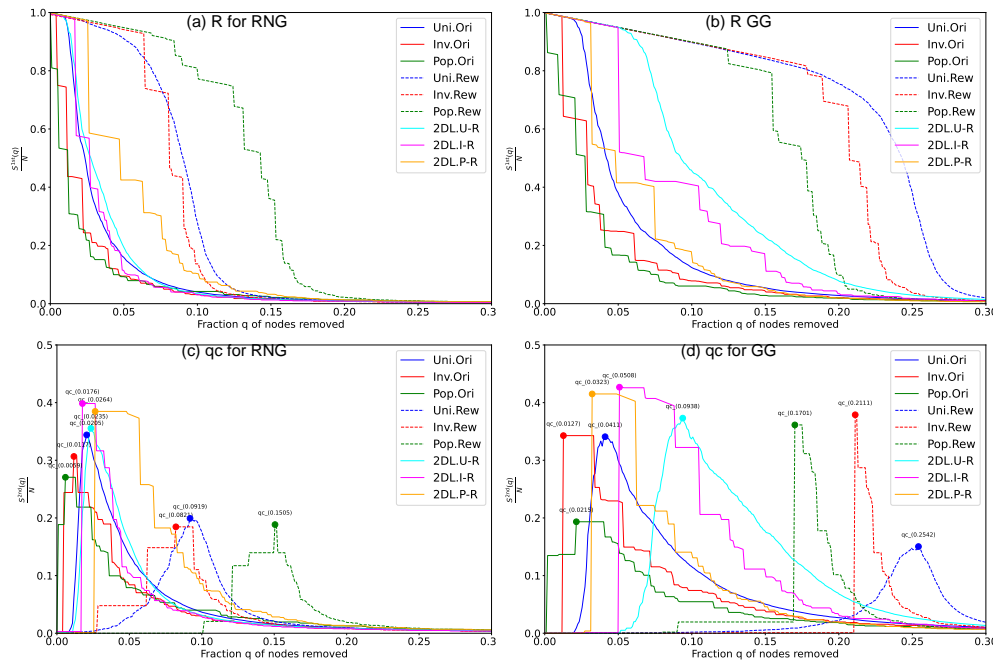


Fig. A153 Robustness against recalculated betweenness (RB) attacks for Keihan networks with $N = 1024$ nodes. For both Rew (Randomized networks) and 2DL lines, the rewiring process preserves the original degree distributions. Two measures are applied: (a) (b) $S^{1st}(q)/N$ the relative size of largest connected component, and (c) (d) $S^{2nd}(q)/N$ the critical fraction q_c at the peak of the relative size of second largest component.

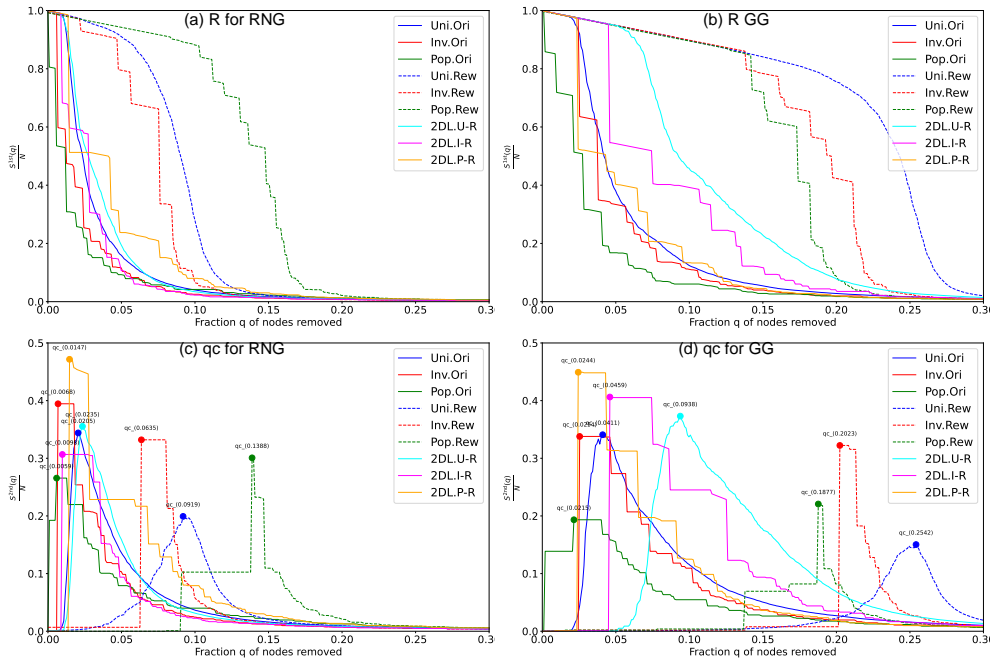


Fig. A154 Robustness against recalculated betweenness (RB) attacks for Nagoya networks with $N = 1024$ nodes. For both Rew (Randomized networks) and 2DL lines, the rewiring process preserves the original degree distributions. Two measures are applied: (a) (b) $S^{1st}(q)/N$ the relative size of largest connected component, and (c) (d) $S^{2nd}(q)/N$ the critical fraction q_c at the peak of the relative size of second largest component.

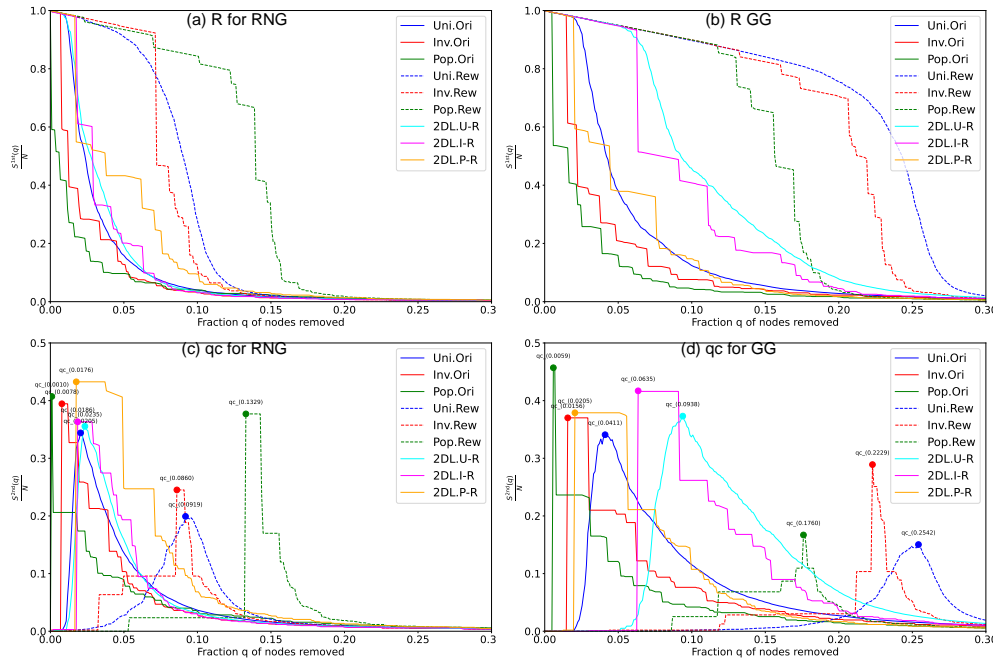


Fig. A155 Robustness against recalculated betweenness (RB) attacks for Sendai networks with $N = 1024$ nodes. For both Rew (Randomized networks) and 2DL lines, the rewiring process preserves the original degree distributions. Two measures are applied: (a) (b) $S^{1st}(q)/N$ the relative size of largest connected component, and (c) (d) $S^{2nd}(q)/N$ the critical fraction q_c at the peak of the relative size of second largest component.

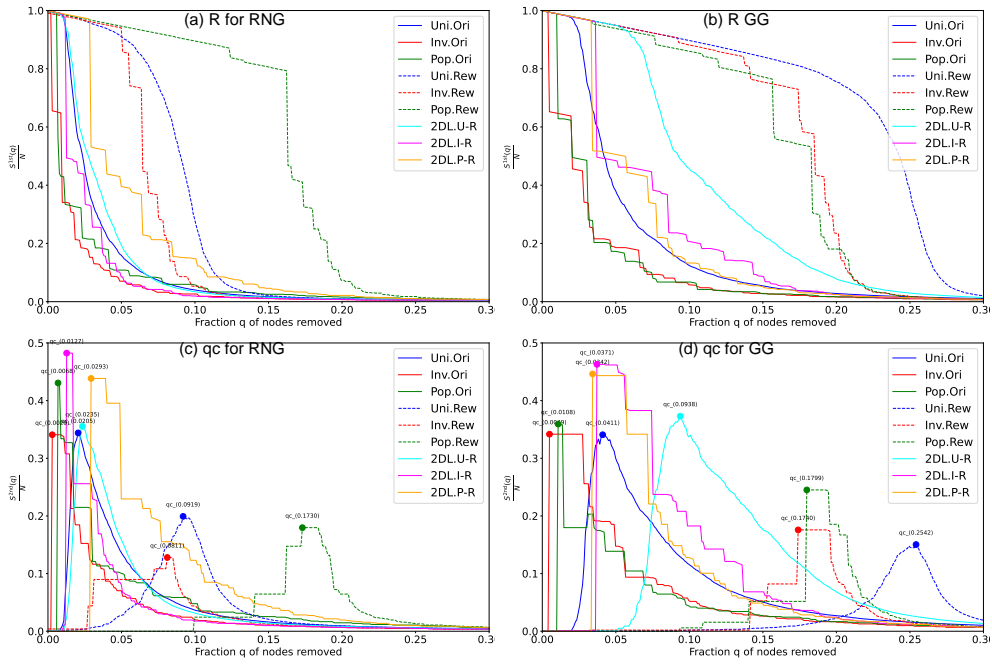


Fig. A156 Robustness against recalculated betweenness (RB) attacks for Sapporo networks with $N = 1024$ nodes. For both Rew (Randomized networks) and 2DL lines, the rewiring process preserves the original degree distributions. Two measures are applied: (a) (b) $S^{1st}(q)/N$ the relative size of largest connected component, and (c) (d) $S^{2nd}(q)/N$ the critical fraction q_c at the peak of the relative size of second largest component.

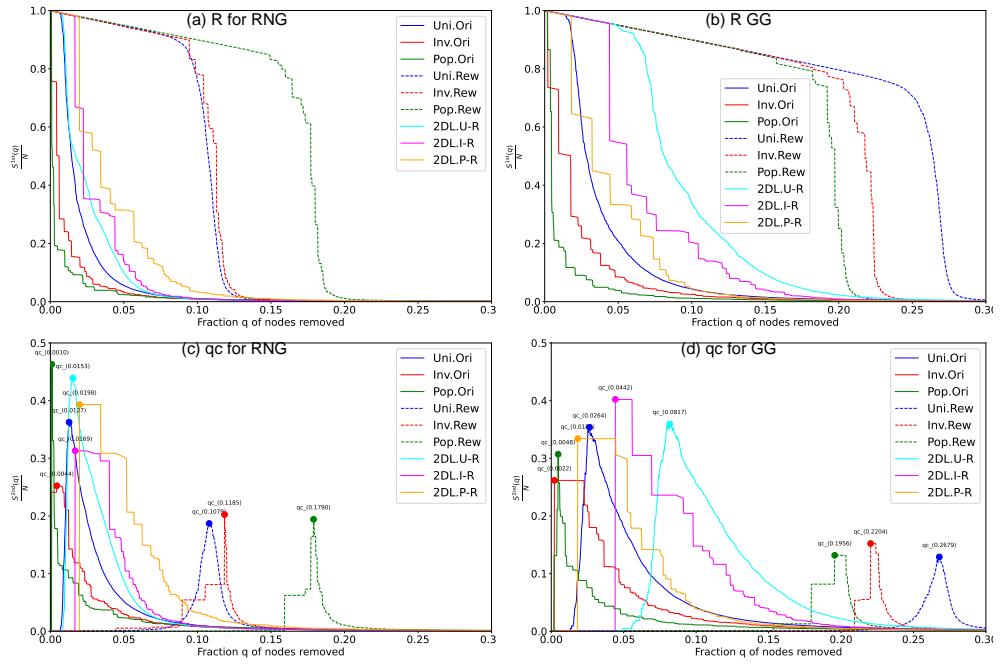


Fig. A157 Robustness against recalculated betweenness (RB) attacks for Fukuoka networks with $N = 5041$ nodes. For both Rew (Randomized networks) and 2DL lines, the rewiring process preserves the original degree distributions. Two measures are applied: (a) (b) $S^{1st}(q)/N$ the relative size of largest connected component, and (c) (d) $S^{2nd}(q)/N$ the critical fraction q_c at the peak of the relative size of second largest component.

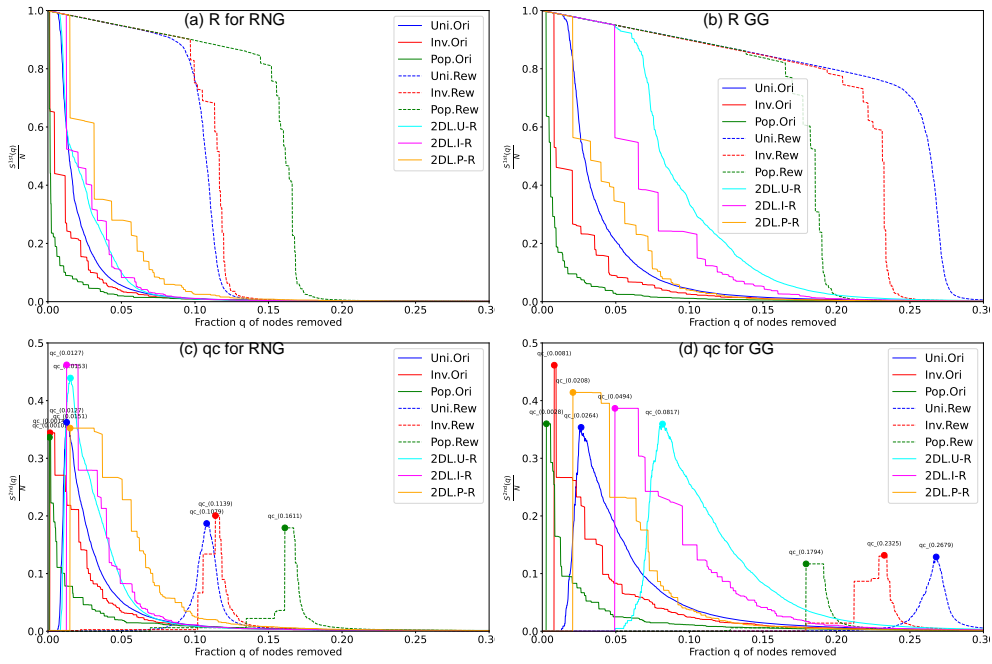


Fig. A158 Robustness against recalculated betweenness (RB) attacks for Hiroshima networks with $N = 5041$ nodes. For both Rew (Randomized networks) and 2DL lines, the rewiring process preserves the original degree distributions. Two measures are applied: (a) (b) $S^{1st}(q)/N$ the relative size of largest connected component, and (c) (d) $S^{2nd}(q)/N$ the critical fraction q_c at the peak of the relative size of second largest component.

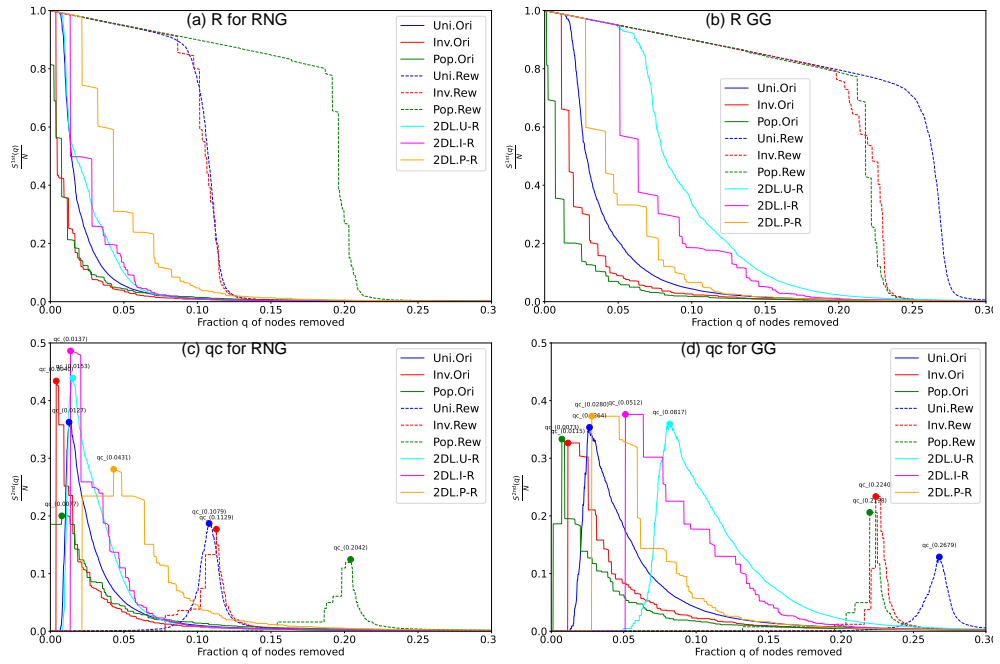


Fig. A159 Robustness against recalculated betweenness (RB) attacks for Keihan networks with $N = 5041$ nodes. For both Rew (Randomized networks) and 2DL lines, the rewiring process preserves the original degree distributions. Two measures are applied: (a) (b) $S^{1st}(q)/N$ the relative size of largest connected component, and (c) (d) $S^{2nd}(q)/N$ the critical fraction q_c at the peak of the relative size of second largest component.

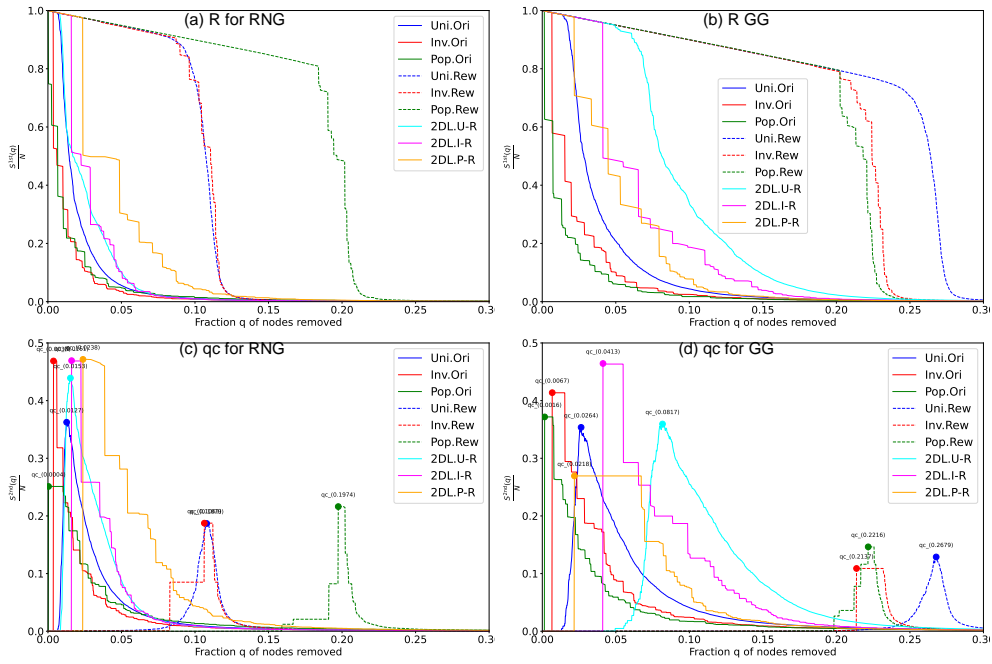


Fig. A160 Robustness against recalculated betweenness (RB) attacks for Nagoya networks with $N = 5041$ nodes. For both Rew (Randomized networks) and 2DL lines, the rewiring process preserves the original degree distributions. Two measures are applied: (a) (b) $S^{1st}(q)/N$ the relative size of largest connected component, and (c) (d) $S^{2nd}(q)/N$ the critical fraction q_c at the peak of the relative size of second largest component.

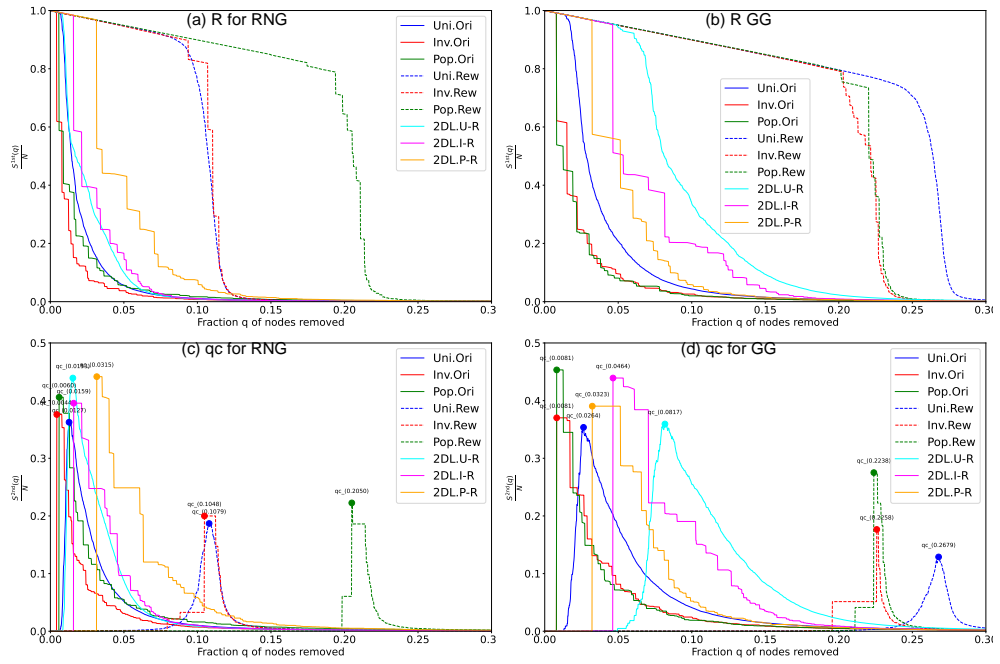


Fig. A161 Robustness against recalculated betweenness (RB) attacks for Tokyo networks with $N = 5041$ nodes. For both Rew (Randomized networks) and 2DL lines, the rewiring process preserves the original degree distributions. Two measures are applied: (a) (b) $S^{1st}(q)/N$ the relative size of largest connected component, and (c) (d) $S^{2nd}(q)/N$ the critical fraction q_c at the peak of the relative size of second largest component.

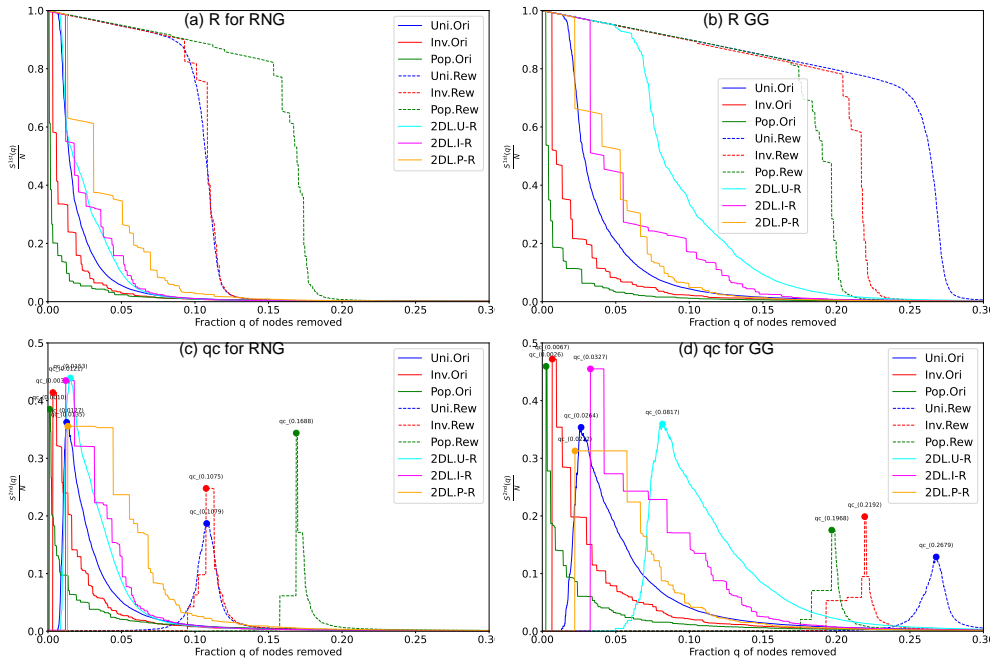


Fig. A162 Robustness against recalculated betweenness (RB) attacks for Sendai networks with $N = 5041$ nodes. For both Rew (Randomized networks) and 2DL lines, the rewiring process preserves the original degree distributions. Two measures are applied: (a) (b) $S^{1st}(q)/N$ the relative size of largest connected component, and (c) (d) $S^{2nd}(q)/N$ the critical fraction q_c at the peak of the relative size of second largest component.

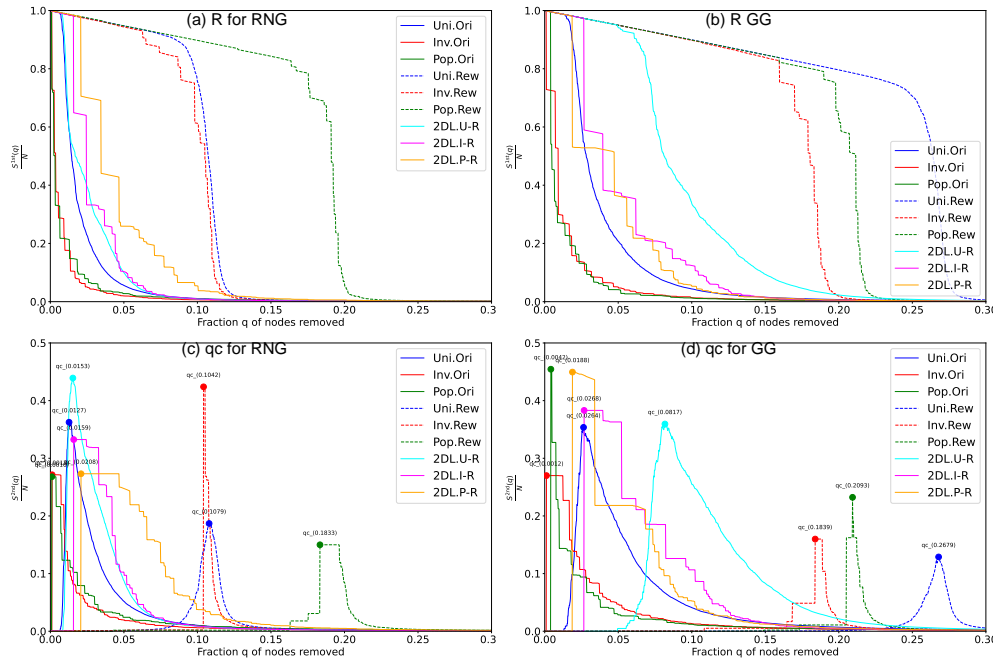


Fig. A163 Robustness against recalculated betweenness (RB) attacks for Sapporo networks with $N = 5041$ nodes. For both Rew (Randomized networks) and 2DL lines, the rewiring process preserves the original degree distributions. Two measures are applied: (a) (b) $S^{1st}(q)/N$ the relative size of largest connected component, and (c) (d) $S^{2nd}(q)/N$ the critical fraction q_c at the peak of the relative size of second largest component.

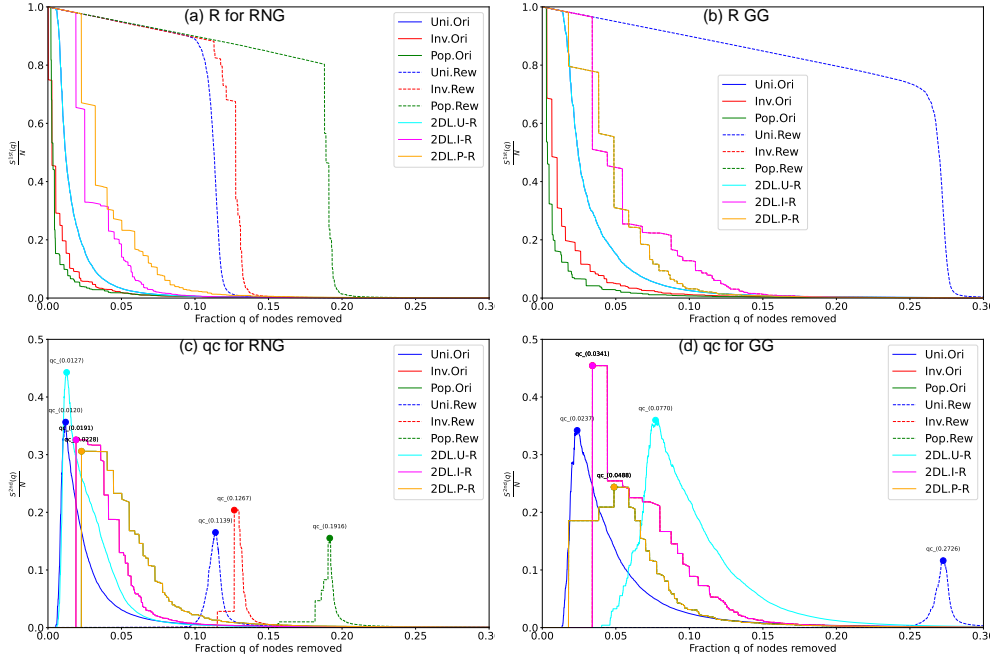


Fig. A164 Robustness against recalculated betweenness (RB) attacks for Fukuoka networks with $N = 10000$ nodes. For both Rew (Randomized networks) and 2DL lines, the rewiring process preserves the original degree distributions. Two measures are applied: (a) (b) $S^{1st}(q)/N$ the relative size of largest connected component, and (c) (d) $S^{2nd}(q)/N$ the critical fraction q_c at the peak of the relative size of second largest component.

Cities	RNG		GG	
	Inv.	Pop.	Inv.	Pop.
Fukuoka	0.087 Δ	0.0754 ∇	0.0975 Δ	0.0837
Hiroshima	0.0779 ∇	0.071 ∇	0.1191 Δ	0.0796 ∇
Keihan	0.0865 Δ	0.0697 ∇	0.1273 Δ	0.0924 Δ
Nagoya	0.0505 ∇	0.0858 Δ	0.1208 Δ	0.0915 Δ
Tokyo	0.0754 ∇	0.0577 ∇	0.117 Δ	0.0907 Δ
Sendai	0.0755 ∇	0.0807	0.0869 Δ	0.0781 ∇
Sapporo	0.0592 ∇	0.0796 ∇	0.0784 ∇	0.0832 ∇
Uniform	0.0807		0.0837	
2D Lattice	0.1636			

Table A1 Robustness index R^{RB} against Recalculated Betweenness (RB) attacks in networks with $(N) = 100$ nodes for seven major Japanese areas. Higher values indicate greater robustness. Values with upper-triangles (Δ) indicate where the cases of Pop. and Inv. have higher robustness of connectivity than the case of Uni., while values with lower-triangles (∇) indicate lower robustness than the case of Uni. for both RNG and GG.

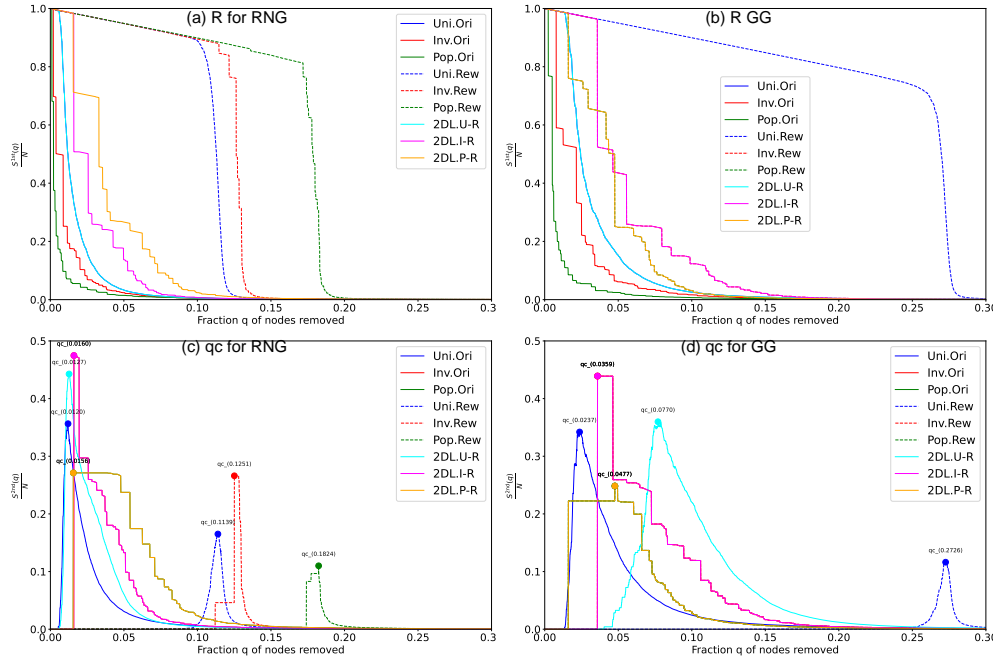


Fig. A165 Robustness against recalculated betweenness (RB) attacks for Hiroshima networks with $N = 10000$ nodes. For both Rew (Randomized networks) and 2DL lines, the rewiring process preserves the original degree distributions. Two measures are applied: (a) (b) $S^{1st}(q)/N$ the relative size of largest connected component, and (c) (d) $S^{2nd}(q)/N$ the critical fraction q_c at the peak of the relative size of second largest component.

Cities	RNG		GG	
	Inv.	Pop.	Inv.	Pop.
Fukuoka	0.0101 ∇	0.0202 ∇	0.0303 ∇	0.0404 ∇
Hiroshima	0.0101 ∇	0.0101 ∇	0.0404 ∇	0.0202 ∇
Keihan	0.0303 ∇	0.0202 ∇	0.0505 ∇	0.0505 ∇
Nagoya	0.0202 ∇	0.0202 ∇	0.0505 ∇	0.0505 ∇
Tokyo	0.0101 ∇	0.0101 ∇	0.0505 ∇	0.0202 ∇
Sendai	0.0303 ∇	0 ∇	0.0505 ∇	0.0505 ∇
Sapporo	0.0101 ∇	0.0202 ∇	0.0202 ∇	0.0303 ∇
Uniform	0.0404		0.0808	
2D Lattice	0.0909			

Table A2 Critical fraction q_c^{RB} against Recalculated Betweenness (RB) attacks in networks with $(N) = 100$ nodes for seven major Japanese areas. Until values of q_c^{RB} , the connectivity is remaining without global fragmentation. Higher values indicate greater robustness of connectivity. Values with lower-triangles (∇) indicate where the cases of Pop. and Inv. have lower robustness of connectivity than the cases of Uni. for both RNG and GG.

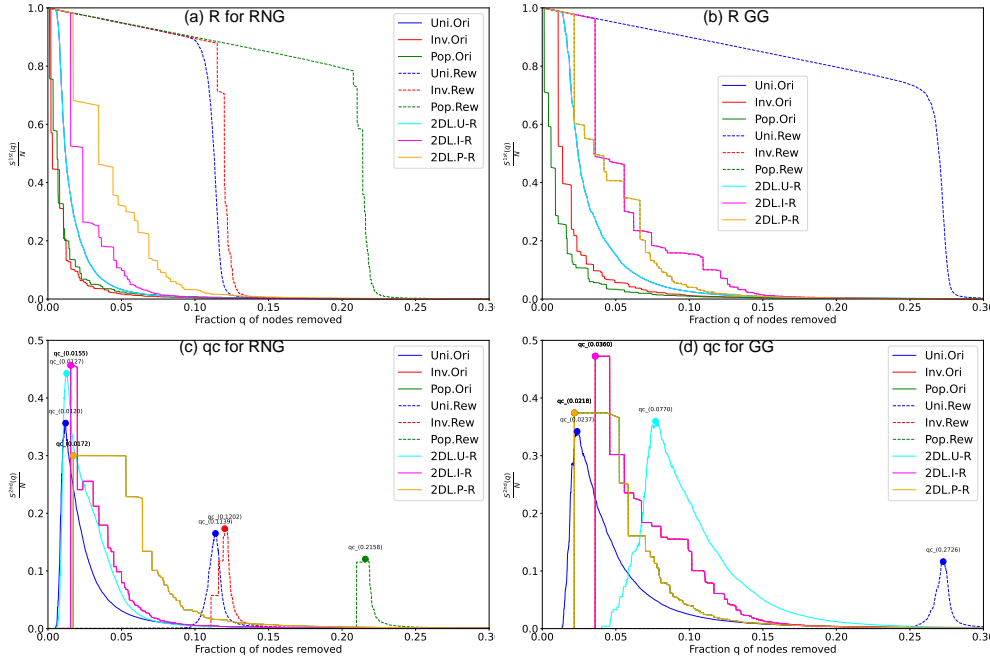


Fig. A166 Robustness against recalculated betweenness (RB) attacks for Keihan networks with $N = 10000$ nodes. For both Rew (Randomized networks) and 2DL lines, the rewiring process preserves the original degree distributions. Two measures are applied: (a) (b) $S^{1st}(q)/N$ the relative size of largest connected component, and (c) (d) $S^{2nd}(q)/N$ the critical fraction q_c at the peak of the relative size of second largest component.

Cities	RNG		GG	
	Inv.	Pop.	Inv.	Pop.
Fukuoka	0.035 ∇	0.0289 ∇	0.0587 ∇	0.0373 ∇
Hiroshima	0.0285 ∇	0.0243 ∇	0.0579 ∇	0.029 ∇
Keihan	0.028 ∇	0.0356 ∇	0.053 ∇	0.0478 ∇
Nagoya	0.0412 ∇	0.0356 ∇	0.0655 ∇	0.0474 ∇
Tokyo	0.0419 ∇	0.0373 ∇	0.0617 ∇	0.0526 ∇
Sendai	0.0383 ∇	0.0269 ∇	0.0588 ∇	0.0389 ∇
Sapporo	0.0273 ∇	0.0521 Δ	0.0436 ∇	0.0562 ∇
Uniform	0.0455		0.0780	
2D Lattice	0.0907			

Table A3 Robustness index R^{RB} against Recalculated Betweenness (RB) attacks in networks with $(N) = 484$ nodes for seven major Japanese areas. Higher values indicate greater robustness of connectivity. Values with upper-triangles (Δ) indicate where the cases of Pop. and Inv. have higher robustness of connectivity than the case of Uni., while values with lower-triangles (∇) indicate lower robustness than the case of Uni. for both RNG and GG.

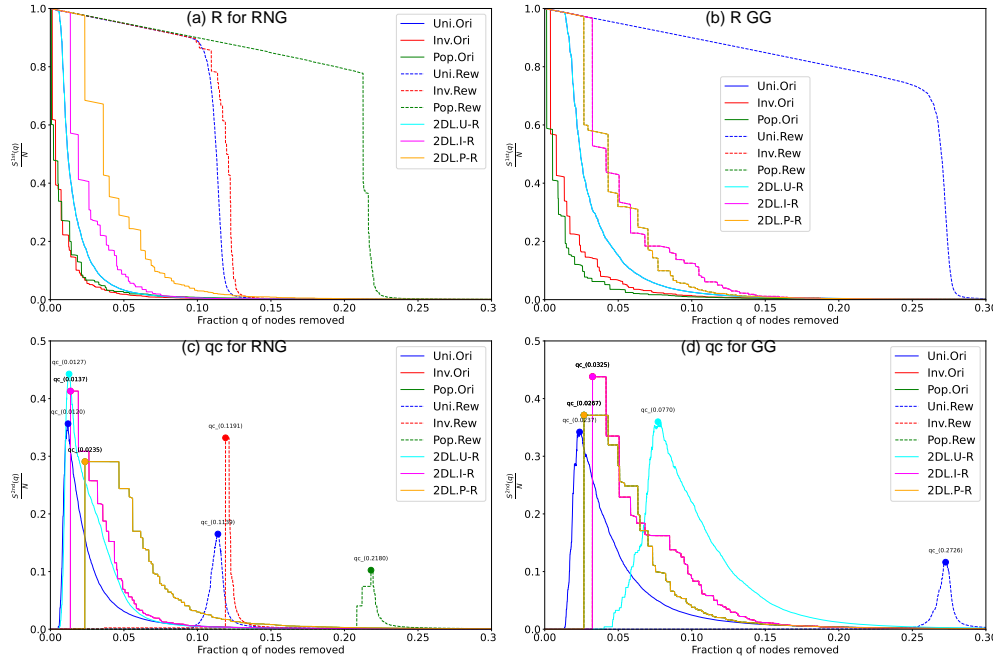


Fig. A167 Robustness against recalculated betweenness (RB) attacks for Nagoya networks with $N = 10000$ nodes. For both Rew (Randomized networks) and 2DL lines, the rewiring process preserves the original degree distributions. Two measures are applied: (a) (b) $S^{1st}(q)/N$ the relative size of largest connected component, and (c) (d) $S^{2nd}(q)/N$ the critical fraction q_c at the peak of the relative size of second largest component.

Cities	RNG		GG	
	Inv.	Pop.	Inv.	Pop.
Fukuoka	0.0062 ∇	0.0021 ∇	0.0145 ∇	0.0062 ∇
Hiroshima	0.0021 ∇	0.0021 ∇	0.0331 ∇	0.0021 ∇
Keihan	0.0062 ∇	0.0228 ∇	0.0145 ∇	0.0248 ∇
Nagoya	0.0269 ∇	0.0228 ∇	0.029 ∇	0.0248 ∇
Tokyo	0.0186 ∇	0.0083 ∇	0.0248 ∇	0.0166 ∇
Sendai	0.0186 ∇	0 ∇	0.0331 ∇	0.0041 ∇
Sapporo	0.0021 ∇	0.0145 ∇	0.0186 ∇	0.0145 ∇
Uniform	0.0269		0.0497	
2D Lattice	0.0435			

Table A4 Critical fraction q_c^{RB} against Recalculated Betweenness (RB) attacks in networks with $(N) = 484$ nodes for seven major Japanese areas. Until values of q_c^{RB} , the connectivity is remaining without global fragmentation. Higher values indicate greater resilience. Values with lower-triangles (∇) indicate where the cases of Pop. and Inv. have lower robustness of connectivity than the cases of Uni. for both RNG and GG.

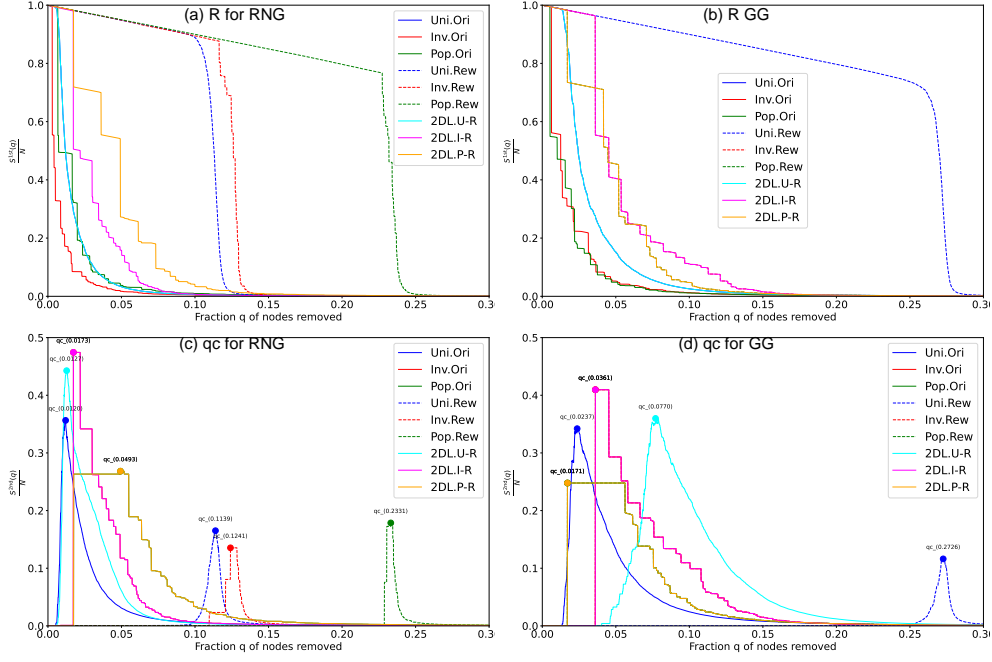


Fig. A168 Robustness against recalculated betweenness (RB) attacks for Tokyo networks with $N = 10000$ nodes. For both Rew (Randomized networks) and 2DL lines, the rewiring process preserves the original degree distributions. Two measures are applied: (a) (b) $S^{1st}(q)/N$ the relative size of largest connected component, and (c) (d) $S^{2nd}(q)/N$ the critical fraction q_c at the peak of the relative size of second largest component.

Cities	RNG		GG	
	Inv.	Pop.	Inv.	Pop.
Fukuoka	0.0237 ∇	0.0188 ∇	0.0379 ∇	0.0253 ∇
Hiroshima	0.0234 ∇	0.0162 ∇	0.0379 ∇	0.0219 ∇
Keihan	0.0258 ∇	0.0232 ∇	0.0448 ∇	0.0375 ∇
Nagoya	0.0262 ∇	0.0233 ∇	0.0548 ∇	0.037 ∇
Tokyo	0.0271 ∇	0.0284 ∇	0.0486 ∇	0.0446 ∇
Sendai	0.0271 ∇	0.0199 ∇	0.0433 ∇	0.0292 ∇
Sapporo	0.02 ∇	0.0264 ∇	0.0356 ∇	0.0369 ∇
Uniform	0.0350		0.0620	
2D Lattice	0.0677			

Table A5 Robustness index R^{RB} against Recalculated Betweenness (RB) attacks in networks with $(N) = 1024$ nodes for seven major Japanese areas. Higher values indicate greater robustness of connectivity. Values with lower-triangles (∇) indicate where the cases of Pop. and Inv. have lower robustness of connectivity than the cases of Uni. for both RNG and GG.

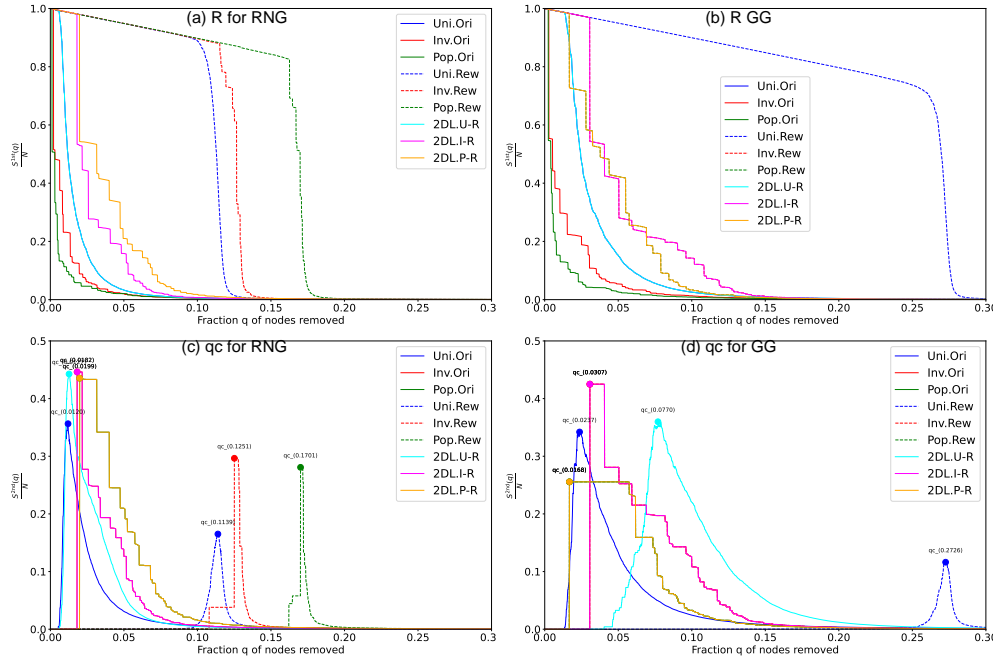


Fig. A169 Robustness against recalculated betweenness (RB) attacks for Sendai networks with $N = 10000$ nodes. For both Rew (Randomized networks) and 2DL lines, the rewiring process preserves the original degree distributions. Two measures are applied: (a) (b) $S^{1st}(q)/N$ the relative size of largest connected component, and (c) (d) $S^{2nd}(q)/N$ the critical fraction q_c at the peak of the relative size of second largest component.

Cities	RNG		GG	
	Inv.	Pop.	Inv.	Pop.
Fukuoka	0.0039 [▽]	0.002 [▽]	0.0137 [▽]	0.0039 [▽]
Hiroshima	0.0068 [▽]	0.001 [▽]	0.0108 [▽]	0.0039 [▽]
Keihan	0.0117 [▽]	0.0059 [▽]	0.0127 [▽]	0.0215 [▽]
Nagoya	0.0068 [▽]	0.0059 [▽]	0.0254 [▽]	0.0215 [▽]
Tokyo	0.0098 [▽]	0.0059 [▽]	0.0235 [▽]	0.0205 [▽]
Sendai	0.0078 [▽]	0.001 [▽]	0.0156 [▽]	0.0059 [▽]
Sapporo	0.0029 [▽]	0.0068 [▽]	0.0049 [▽]	0.0108 [▽]
Uniform	0.0205		0.0411	
2D Lattice	0.0303			

Table A6 Critical fraction q_c^{RB} against Recalculated Betweenness (RB) attacks in networks with $(N) = 1024$ nodes for seven major Japanese areas. Until values of q_c^{RB} , the connectivity is remaining without global fragmentation. Higher values indicate greater robustness of connectivity. Values with lower-triangles ([▽]) indicate where the cases of Pop. and Inv. have lower robustness of connectivity than the cases of Uni. for both RNG and GG.

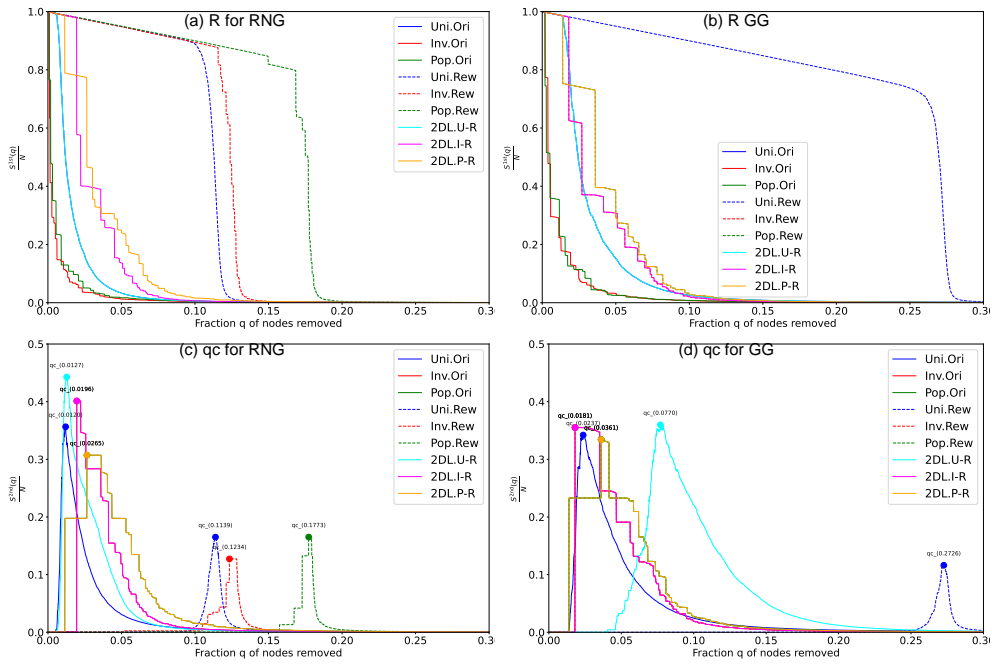


Fig. A170 Robustness against recalculated betweenness (RB) attacks for Sapporo networks with $N = 10000$ nodes. For both Rew (Randomized networks) and 2DL lines, the rewiring process preserves the original degree distributions. Two measures are applied: (a) (b) $S^{1st}(q)/N$ the relative size of largest connected component, and (c) (d) $S^{2nd}(q)/N$ the critical fraction q_c at the peak of the relative size of second largest component.

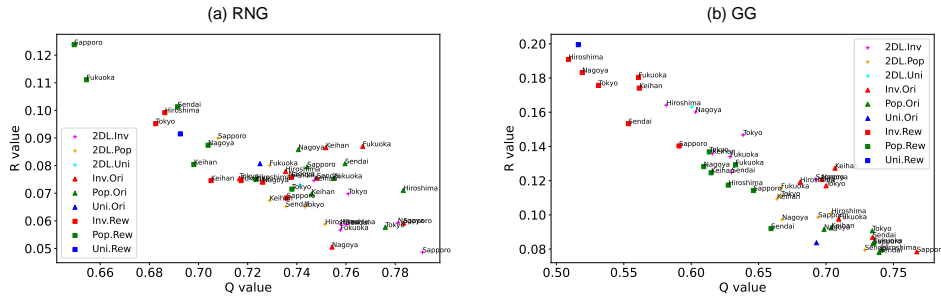


Fig. A171 Relation between robustness index R^{RB} and modularity Q in networks with $N = 100$ nodes

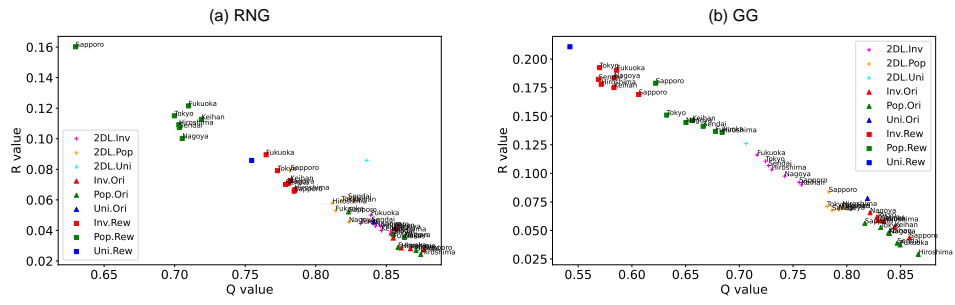


Fig. A172 Relation between robustness index R^{RB} and modularity Q in networks with $N = 484$ nodes

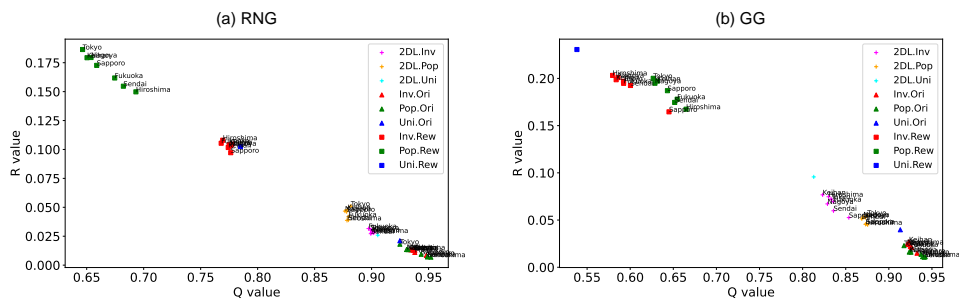


Fig. A173 Relation between robustness index R^{RB} and modularity Q in networks with $N = 5041$ nodes

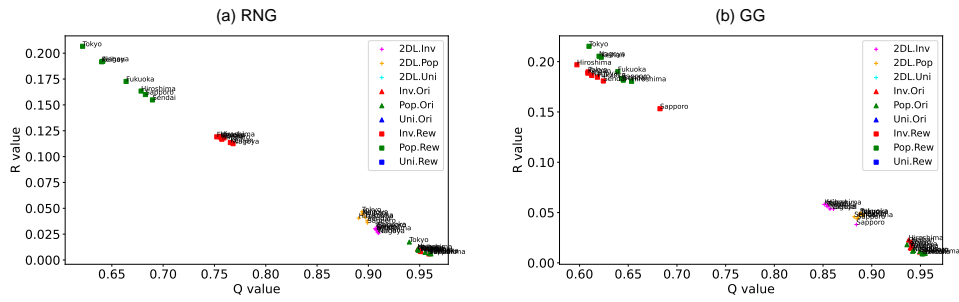


Fig. A174 Relation between robustness index R^{RB} and modularity Q in networks with $N = 10000$ nodes

Cities	RNG		GG	
	Inv.	Pop.	Inv.	Pop.
Fukuoka	0.011 ∇	0.0074 ∇	0.0219 ∇	0.0112 ∇
Hiroshima	0.0133 ∇	0.0069 ∇	0.0242 ∇	0.0111 ∇
Keihan	0.013 ∇	0.0134 ∇	0.0269 ∇	0.0161 ∇
Nagoya	0.0133 ∇	0.0135 ∇	0.0241 ∇	0.016 ∇
Tokyo	0.0132 ∇	0.0181 ∇	0.0238 ∇	0.0229 ∇
Sendai	0.0129 ∇	0.0071 ∇	0.0211 ∇	0.0107 ∇
Sapporo	0.0085 ∇	0.0094 ∇	0.0149 ∇	0.0137 ∇
Uniform	0.0211		0.0397	
2D Lattice	0.0406			

Table A7 Robustness index R^{RB} against Recalculated Betweenness (RB) attacks in networks with $(N) = 5041$ nodes for seven major Japanese areas. Higher values indicate greater robustness of connectivity. Values with lower-triangles (∇) indicate where the cases of Pop. and Inv. have lower robustness of connectivity than the cases of Uni. for both RNG and GG.

Cities	RNG		GG	
	Inv.	Pop.	Inv.	Pop.
Fukuoka	0.0044 ∇	0.001 ∇	0.0022 ∇	0.0048 ∇
Hiroshima	0.0014 ∇	0.001 ∇	0.0081 ∇	0.0028 ∇
Keihan	0.004 ∇	0.0077 ∇	0.0115 ∇	0.0073 ∇
Nagoya	0.0038 ∇	0.0004 ∇	0.0067 ∇	0.0016 ∇
Tokyo	0.0044 ∇	0.006 ∇	0.0081 ∇	0.0081 ∇
Sendai	0.0034 ∇	0.001 ∇	0.0067 ∇	0.0026 ∇
Sapporo	0.0012 ∇	0.001 ∇	0.0012 ∇	0.0042 ∇
Uniform	0.0137		0.0262	
2D Lattice	0.0278			

Table A8 Critical fraction q_c^{RB} against Recalculated Betweenness (RB) attacks in networks with $(N) = 5041$ nodes for seven major Japanese areas. Higher values indicate greater robustness of connectivity. Values with lower-triangles (∇) indicate where the cases of Pop. and Inv. have lower robustness of connectivity than the cases of Uni. for both RNG and GG.

Cities	RNG		GG	
	Inv.	Pop.	Inv.	Pop.
Fukuoka	0.0082 [▽]	0.007 [▽]	0.0149 [▽]	0.0091 [▽]
Hiroshima	0.0106 [▽]	0.0059 [▽]	0.0227 [▽]	0.0095 [▽]
Keihan	0.009 [▽]	0.0105 [▽]	0.0208 [▽]	0.0123 [▽]
Nagoya	0.0086 [▽]	0.0095 [▽]	0.0166 [▽]	0.0116 [▽]
Tokyo	0.0092 [▽]	0.0174 [▽]	0.0189 [▽]	0.018 [▽]
Sendai	0.0094 [▽]	0.0063 [▽]	0.0146 [▽]	0.0089 [▽]
Sapporo	0.0059 [▽]	0.0074 [▽]	0.0108 [▽]	0.0112 [▽]
Uniform	0.0173		0.0334	
2D Lattice	0.0647			

Table A9 Robustness index R^{RB} against Recalculated Betweenness (RB) attacks in networks with $(N) = 10000$ nodes for seven major Japanese areas. Higher values indicate greater robustness of connectivity. Values with lower-triangles (∇) indicate where the cases of Pop. and Inv. have lower robustness of connectivity than the cases of Uni. for both RNG and GG.

Cities	RNG		GG	
	Inv.	Pop.	Inv.	Pop.
Fukuoka	0.0028 [▽]	0.0045 [▽]	0.0032 [▽]	0.0029 [▽]
Hiroshima	0.0021 [▽]	0.0011 [▽]	0.0079 [▽]	0.0052 [▽]
Keihan	0.0021 [▽]	0.0012 [▽]	0.0109 [▽]	0.0014 [▽]
Nagoya	0.0014 [▽]	0.0008 [▽]	0.004 [▽]	0.0014 [▽]
Tokyo	0.003 [▽]	0.0068 [▽]	0.0063 [▽]	0.0053 [▽]
Sendai	0.0022 [▽]	0.0012 [▽]	0.0029 [▽]	0.0025 [▽]
Sapporo	0.0011 [▽]	0.0019 [▽]	0.0039 [▽]	0.0019 [▽]
Uniform	0.0115		0.0229	
2D Lattice	0.0679			

Table A10 Critical fraction q_c^{RB} against Recalculated Betweenness (RB) attacks in networks with $(N) = 10000$ nodes for seven major Japanese areas. Higher values indicate greater robustness of connectivity. Values with lower-triangles (∇) indicate where the cases of Pop. and Inv. have lower robustness of connectivity than the cases of Uni. for both RNG and GG.

Cities	RNG		GG	
	Inv.	Pop.	Inv.	Pop.
Fukuoka	2.28	2.5	3.14	2.72
Hiroshima	2.34	2.24	3.52	2.6
Keihan	2.3	2.34	3.34	2.82
Nagoya	2.26	2.34	3.36	2.82
Tokyo	2.36	2.24	3.38	2.8
Sendai	2.24	2.38 Δ	3.14	2.5
Sapporo	2.18	2.54	2.92	2.62
Uniform	2.37		3.56	
2D Lattice	3.6			

Table A11 Average degree $\langle k \rangle$ in networks with $(N) = 100$ nodes for seven major Japanese areas. Higher average degrees mean more links per node in the network. Values with upper-triangles (Δ) indicate where the cases of Pop. and Inv. have higher $\langle k \rangle$ than the cases of Uni. for both RNG and GG.

Cities	RNG		GG	
	Inv.	Pop.	Inv.	Pop.
Fukuoka	2.4545	2.7231 Δ	3.5579	2.8843
Hiroshima	2.3595	2.6736 Δ	3.4835	2.8058
Keihan	2.3678	2.657 Δ	3.405	2.9545
Nagoya	2.3843	2.657 Δ	3.5083	2.9545
Tokyo	2.4091	2.7149 Δ	3.562	3.0331
Sendai	2.3843	2.6736 Δ	3.5289	2.905
Sapporo	2.343	3.1116 Δ	3.2851	3.2149
Uniform	2.4746		3.8025	
2D Lattice	3.8182			

Table A12 Average degree $\langle k \rangle$ in networks with $(N) = 484$ nodes for seven major Japanese areas. Higher average degrees mean more links per node in the network. Values with upper-triangles (Δ) indicate where the cases of Pop. and Inv. have higher $\langle k \rangle$ than the cases of Uni. for both RNG and GG.

Cities	RNG		GG	
	Inv.	Pop.	Inv.	Pop.
Fukuoka	2.5884 \triangle	3.0121 \triangle	3.5116	3.1367
Hiroshima	2.5824 \triangle	2.9308 \triangle	3.587	3.068
Keihan	2.5725 \triangle	3.1466 \triangle	3.5656	3.2779
Nagoya	2.5606 \triangle	3.1351 \triangle	3.5656	3.2787
Tokyo	2.557 \triangle	3.1922 \triangle	3.5243	3.3045
Sendai	2.5697 \triangle	2.9693 \triangle	3.4596	3.1406
Sapporo	2.5539 \triangle	3.1109 \triangle	3.1883	3.2085
Uniform	2.5319		3.9391	
2D Lattice	3.9437			

Table A13 Average degree $\langle k \rangle$ in networks with $(N) = 5041$ nodes for seven major Japanese areas. Higher average degrees mean more links per node in the network. Values with upper-triangles (\triangle) indicate where the cases of Pop. and Inv. have higher $\langle k \rangle$ than the cases of Uni. for both RNG and GG.

Cities	RNG		GG	
	Inv.	Pop.	Inv.	Pop.
Fukuoka	2.67 \triangle	3.07 \triangle	3.35	3.21
Hiroshima	2.66 \triangle	3.01 \triangle	3.49	3.14
Keihan	2.62 \triangle	3.21 \triangle	3.39	3.32
Nagoya	2.61 \triangle	3.21 \triangle	3.38	3.33
Tokyo	2.65 \triangle	3.32 \triangle	3.42	3.41
Sendai	2.66 \triangle	2.95 \triangle	3.31	3.19
Sapporo	2.66 \triangle	2.99 \triangle	2.99	3.19
Uniform	2.54		3.96	
2D Lattice	3.96			

Table A14 Average degree $\langle k \rangle$ in networks with $(N) = 10000$ nodes for seven major Japanese areas. Higher average degrees mean more links per node in the network. Values with upper-triangles (\triangle) indicate where the cases of Pop. and Inv. have higher $\langle k \rangle$ than the cases of Uni. for both RNG and GG.

Cities	RNG		GG	
	Inv.	Pop.	Inv.	Pop.
Fukuoka	0.7668 Δ	0.7551 Δ	0.7094 Δ	0.7356 Δ
Hiroshima	0.7354 Δ	0.7833 Δ	0.6808 ∇	0.7414 Δ
Keihan	0.7518 Δ	0.746 Δ	0.7067 Δ	0.7039 Δ
Nagoya	0.7543 Δ	0.7406 Δ	0.6968 Δ	0.6985 Δ
Tokyo	0.7167 ∇	0.776 Δ	0.7 Δ	0.7343 Δ
Sendai	0.7481 Δ	0.7596 Δ	0.7345 Δ	0.7393 Δ
Sapporo	0.7834 Δ	0.7442 Δ	0.7673 Δ	0.7348 Δ
Uniform	0.725		0.6929	

Table A15 Modularity Q in networks with 100 nodes for seven major Japanese areas. Higher values indicate stronger community structures. Values with upper-triangles (Δ) or lower-triangles (∇) indicate where the cases of Pop. and Inv. have higher or lower modularity than the case of Uni. for both RNG and GG. Note the generally higher modularity in Pop. and Inv. compared to Uni. networks for both RNG and GG.

Cities	RNG		GG	
	Inv.	Pop.	Inv.	Pop.
Fukuoka	0.8549 Δ	0.8583 Δ	0.8286 Δ	0.8497 Δ
Hiroshima	0.8605 Δ	0.8744 Δ	0.8345 Δ	0.8665 Δ
Keihan	0.8671 Δ	0.8631 Δ	0.8446 Δ	0.8389 Δ
Nagoya	0.8559 Δ	0.8627 Δ	0.8217 Δ	0.8397 Δ
Tokyo	0.8565 Δ	0.8549 Δ	0.8281 Δ	0.8316 Δ
Sendai	0.8535 Δ	0.871 Δ	0.8316 Δ	0.847 Δ
Sapporo	0.8766 Δ	0.8232 ∇	0.8584 Δ	0.8168 ∇
Uniform	0.8412		0.8193	

Table A16 Modularity Q in networks with 484 nodes for seven major Japanese areas. Higher values indicate stronger community structures. Values with upper-triangles (Δ) or lower-triangles (∇) indicate where the cases of Pop. and Inv. have higher or lower modularity than the case of Uni. for both RNG and GG. Note the generally higher modularity in Pop. and Inv. compared to Uni. networks for both RNG and GG.

Cities	RNG		GG	
	Inv.	Pop.	Inv.	Pop.
Fukuoka	0.9379 [△]	0.9491 [△]	0.9249 [△]	0.9392 [△]
Hiroshima	0.9342 [△]	0.952 [△]	0.9234 [△]	0.9422 [△]
Keihan	0.9363 [△]	0.932 [△]	0.9233 [△]	0.9237 [△]
Nagoya	0.9349 [△]	0.9307 [△]	0.9211 [△]	0.9257 [△]
Tokyo	0.9375 [△]	0.9248	0.9246 [△]	0.9176 [△]
Sendai	0.938 [△]	0.949 [△]	0.9264 [△]	0.9411 [△]
Sapporo	0.948 [△]	0.9435 [△]	0.9327 [△]	0.9373 [△]
Uniform	0.9248		0.9133	

Table A17 Modularity Q in networks with 5041 nodes for seven major Japanese areas. Higher values indicate stronger community structures. Values with upper-triangles (Δ) indicate where the cases of Pop. and Inv. have higher modularity than the case of Uni. for both RNG and GG. Note the generally higher modularity in Pop. and Inv. compared to Uni. networks for both RNG and GG.

Cities	RNG		GG	
	Inv.	Pop.	Inv.	Pop.
Fukuoka	0.9514 [△]	0.9603 [△]	0.9395 [△]	0.9516 [△]
Hiroshima	0.948 [△]	0.9609 [△]	0.9379 [△]	0.9549 [△]
Keihan	0.9509 [△]	0.9481 [△]	0.9406 [△]	0.9429 [△]
Nagoya	0.9506 [△]	0.9485 [△]	0.9406 [△]	0.942 [△]
Tokyo	0.9499 [△]	0.9399 [△]	0.9411 [△]	0.9361 [△]
Sendai	0.9508 [△]	0.9594 [△]	0.9406 [△]	0.9525 [△]
Sapporo	0.9589 [△]	0.9553 [△]	0.9492 [△]	0.9495 [△]
Uniform	0.9397		0.9303	

Table A18 Modularity Q in networks with 10000 nodes for seven major Japanese areas. Higher values indicate stronger community structures. Values with upper-triangles (Δ) indicate where the cases of Pop. and Inv. have higher modularity than the case of Uni. for both RNG and GG. Note the generally higher modularity in Pop. and Inv. compared to Uni. networks for both RNG and GG.